NCAT Report 06-01

Material Properties of the 2003 NCAT Test Track Structural Study

By

David H. Timm
Angela L. Priest

April 2006

MATERIAL PROPERTIES OF THE 2003 TEST TRACK STRUCTURAL STUDY

by

David H. Timm, PhD, P.E., Gottlieb Assistant Professor of Civil Engineering
Angela L. Priest, Graduate Research Assistant
National Center for Asphalt Technology
Auburn University, Alabama

NCAT Report 06-01

April 2006

ACKNOWLEDGEMENTS

The authors wish to thank the Alabama Department of Transportation, the Indiana Department of Transportation and the Federal Highway Administration for their support and cooperation with this research. A special thanks is given to Dr. Terhi Pellinen of Purdue University for conducting the laboratory dynamic modulus testing of the asphalt mixtures. Also, the authors wish to thank Vulcan Materials Company for providing supplemental testing of the granular base material.

TABLE OF CONTENTS

LIST OF TABLES

LIST OF FIGURES

CHAPTER 1 – INTRODUCTION

BACKGROUND

Mechanistic-empirical (M-E) pavement design and analysis is generally accepted as a much-needed advancement in pavement engineering as the original AASHO Road Test (Highway Research Board, 1962) becomes more outdated. Advancements in materials and trucking technology make the current AASHTO Design Guide (1993) less applicable to prevailing design conditions. Further, advancements in computing technology and pavement performance prediction models enable designers to consider specific distress modes (i.e., rutting and fatigue cracking), as a function of mechanistic pavement responses, when conducting pavement analysis and design. While there are existing M-E pavement design approaches (Asphalt Institute, 1991; Thompson et al., 1992; Theyse et al., 1996; Timm and Young, 2004), the forthcoming M-E Pavement Design Guide developed under NCHRP 1-37A (2004) has brought national attention to M-E design.

A typical M-E design approach is depicted in Figure 1.1. Most design approaches, whether empirical or mechanistic-based, require some degree of material characterization. For example, the current AASHTO Design Guide (1993) requires resilient modulus of the component pavement layers and subgrade to execute a design. In the case of M-E design, the specific load-response model dictates the required material properties for design. The current state-of-the practice relies upon layered elastic analysis to compute pavement responses under load. Figure 1.1 shows the load response model as the computer program WESLEA (Van Cauwelaert et al., 1989). This model, which stands for Waterways Experiment Station Layered Elastic Analysis, has been shown to be reasonably accurate in its prediction of pavement response (Chadbourn et al, 1997; Barrett and Timm, 2004). The pavement responses are then converted through transfer functions into pavement life predictions (N_f) and damage (D) is computed through Miner's Hypothesis (Miner, 1959). The concept of seasonal changes in material properties is also shown in the Figure 1.1 whereby the design method can accommodate changes in properties as a function of changing temperatures and moisture contents where applicable.

The primary material property inputs for layered elastic analysis are the modulus of elasticity (E) and Poisson's ratio (ν) for each of the component pavement layers. While these are inputs, they are certainly affected by other parameters such as air void content, density, loading frequency, temperature, etc. Therefore, there is a need to quantify relationships between the parameters and material properties for M-E design. Also, the use of various binder grades and modified asphalt binders in hot-mix asphalt (HMA) warrants an investigation of material properties in relation to binder type and grade.

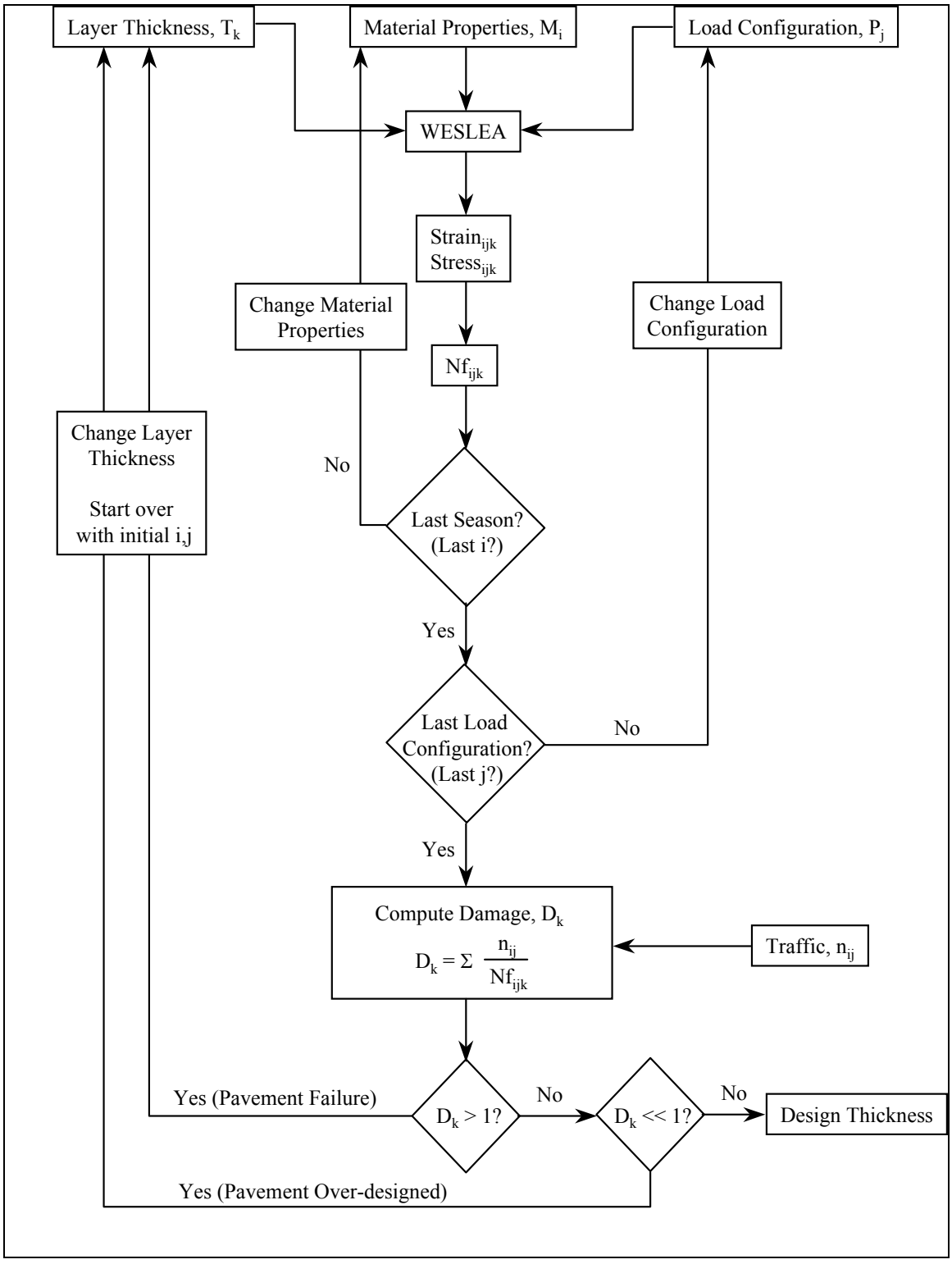

Figure 1.1 Mechanistic-Empirical Design Flowchart (Timm et al., 1998).

The 2003 Structural Study at the National Center for Asphalt Technology (NCAT) Test Track was conducted to address many issues pertaining to M-E design. These included (Timm et al., 2004):

1. Validate mechanistic pavement models.
2. Develop transfer functions for typical asphalt mixtures and pavement cross-sections.
3. Study dynamic effects on pavement deterioration from a mechanistic viewpoint.
4. Evaluate the effect of thickness and polymer modification on structural performance.

To meet the needs listed above, the Structural Study consisted of eight 200 ft test sections as depicted in Figure 1.2. Each section was built on an improved roadbed material, 6 in. of crushed aggregate base course and surfaced with various HMA materials and thicknesses. For the purposes of this report, the improved roadbed material will be referred to as "Fill Material" and the crushed aggregate base course will be referred to as "Granular Base." Another feature of the Structural Study was embedded temperature, strain and pressure gauges in each section. Further details regarding the design, instrumentation and construction of these sections is documented elsewhere (Timm et al., 2004; Powell, 2004).

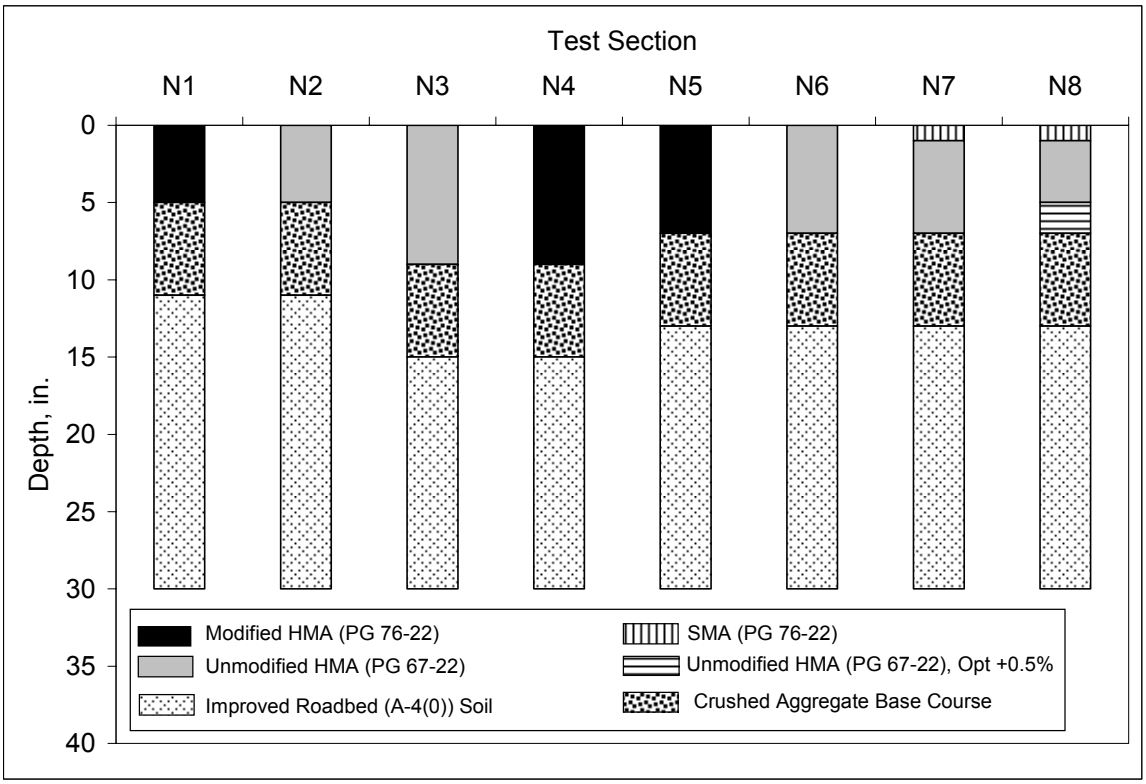

Figure 1.2 Structural Study Pavement Cross Sections.

Central to the main objectives of the Structural Study is the accurate characterization of the material properties. For example, the validation of a mechanistic pavement model requires accurate material properties as inputs to the model. Therefore, there is a need to provide a reference document containing the relevant material property information for the Structural Study. Further, there is a need to simply evaluate the material properties in

the context of M-E design to develop a better understanding of the relevant pavement parameters on the material properties.

OBJECTIVES

The objectives of this report include:

1. Document the material properties of the component pavement layers, to serve as a reference, for the 2003 Structural Study at the NCAT Test Track.
2. Establish relationships between relevant parameters (e.g., temperature) and mechanistic material properties (e.g, HMA stiffness).
3. Characterize differences between laboratory and in situ material properties.
4. Determine the effects of material types on mechanistic material properties.

SCOPE

This report describes the component pavement layers in terms of material composition and mechanistic material properties. Laboratory triaxial resilient and dynamic modulus tests were conducted and are described herein. Further, extensive falling weight deflectometer (FWD) tests were conducted on the pavement sections throughout the two-year study. The data from both laboratory and field were evaluated statistically and models were developed to characterize relationships between relevant pavement parameters and mechanistic material properties. Finally, comparisons were made between laboratory and field properties.

CHAPTER 2 – GENERAL MATERIAL PROPERTIES

INTRODUCTION

Regardless of the pavement design approach, it is important to characterize relevant material properties as they have a direct impact on the mechanistic pavement response of component pavement layers. More specifically, the forthcoming M-E Pavement Design Guide (2004) utilizes some of these parameters to estimate mechanistic properties of the pavement layers. This chapter documents so-called general material properties which will be investigated in later chapters for their influence on mechanistic properties. The component pavement layers are discussed in the order they were constructed (i.e., fill material, granular base and HMA layers).

FILL MATERIAL

The Test Track was reconstructed in 2003 to accommodate the Structural Study. Work began by excavating the existing outside lane down to the subgrade as depicted in Figure 2.1. This subgrade material, originally placed in 2000, was left in place and served as the foundation for the Structural Study. No testing was conducted on the subgrade as part of the Structural Study. However, it can be stated that the existing subgrade and fill material were of similar composition, having been excavated from the same borrow-pit located at the Test Track.

Figure 2.1 Reconstruction of the Test Track.

After the existing pavement had been removed, work began in building the fill layer. The material, classified as an AASHTO A-4(0) soil, was excavated from the west curve of the Test Track (Figure 2.2). Large cobbles were present in the material, but easily broke down under rolling compaction (Figure 2.3). Once the material was compacted and brought to proper elevation and moisture content, a tarp (Figure 2.4) was used to cover the test sections, to protect from rainfall, while other work was occurring elsewhere on the Test Track. Figure 2.5 illustrates the completed fill, prior to base construction.

Figure 2.2 Excavation of Fill Material.

a) Large Cobbles

b) Rolling Compaction

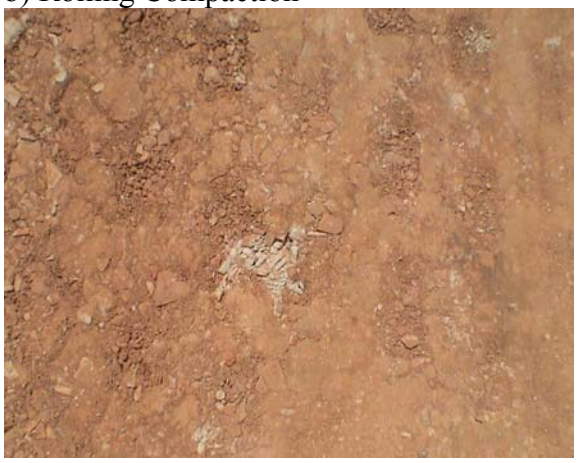

c) Breakage of Cobbles

Figure 2.3 Large Cobbles and Breakage in Fill Material.

Figure 2.4 Tarp Covering Fill Material.

Figure 2.5 Completed Fill Layer.

The gradation of the fill is shown in Figure 2.6. The material had a dry unit weight of 119.6 lb/ft^3 with an optimum moisture content of 8.6%. The as-built moisture contents and densities are shown in Figure 2.7. The data were divided by test section and represent tests conducted at three random locations in the inside and outside wheelpath of each test section.

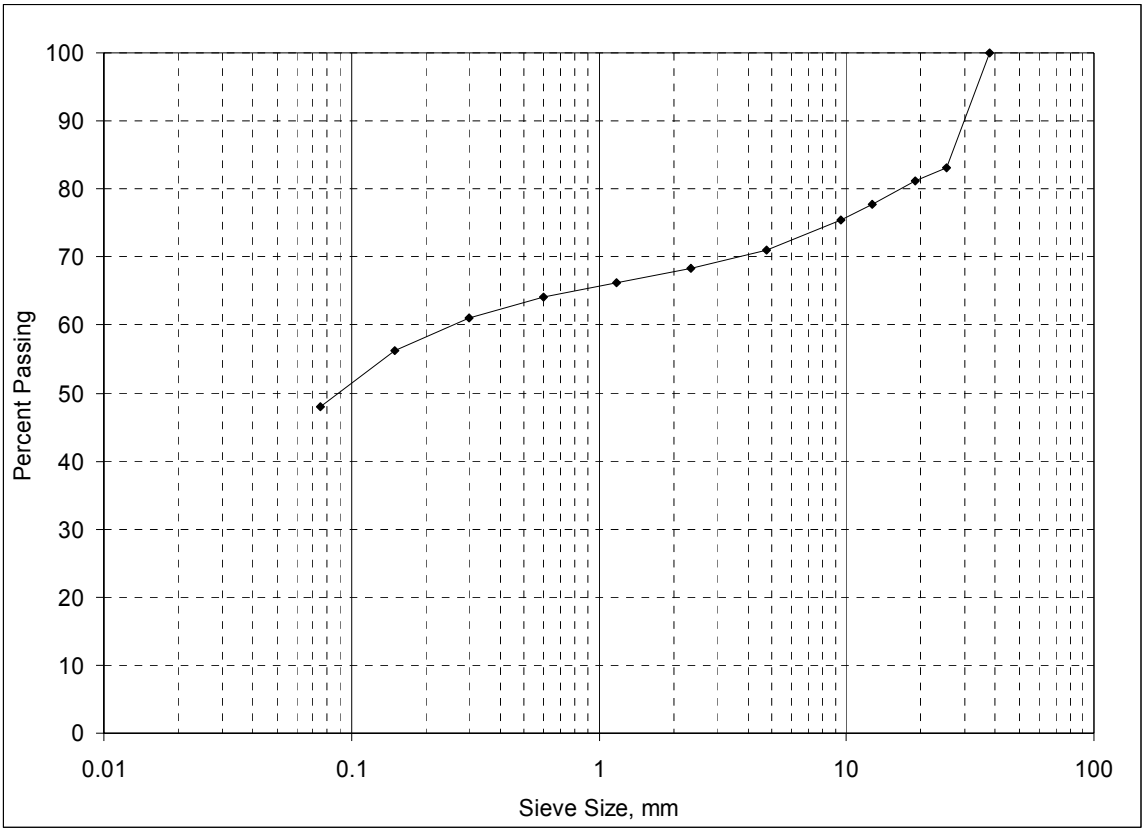

Figure 2.6 Fill Layer Gradation.

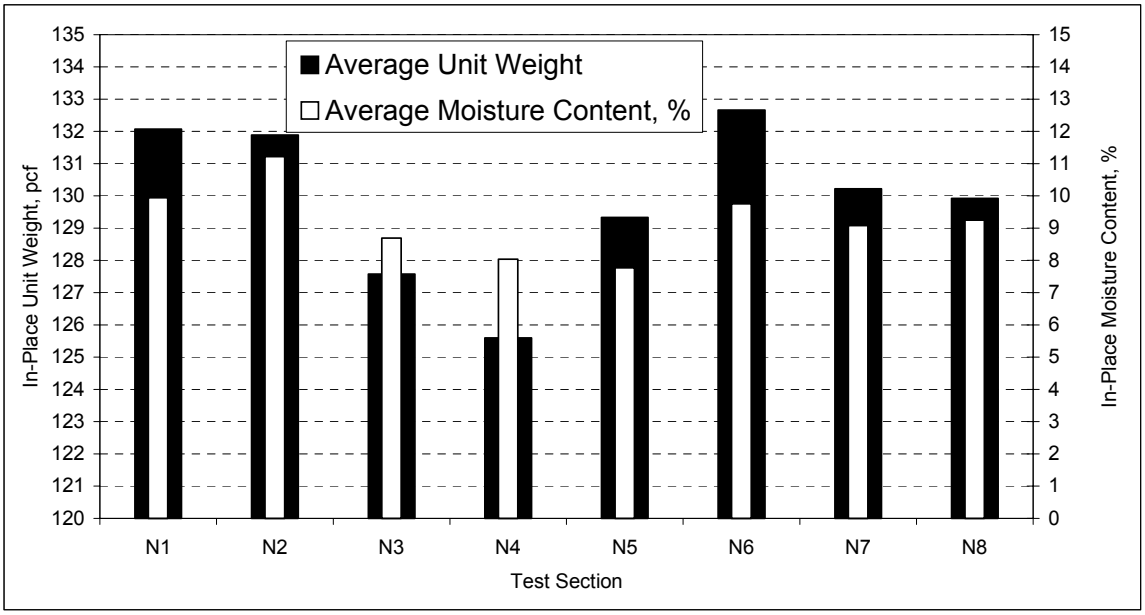

Figure 2.7 Fill Layer As-Built Properties.

GRANULAR BASE LAYER

The granular base layer consisted of a well graded crushed granite material commonly used by the Alabama Department of Transportation (ALDOT) for highway construction. Figure 2.8 shows this material under construction while Figure 2.9 illustrates the material, with markings for instrumentation, just prior to paving with HMA. The dry unit weight of the material was 137.9 lb/ft^3 with an optimum moisture content of 9.2%.

Figure 2.8 Granular Base Under Construction.

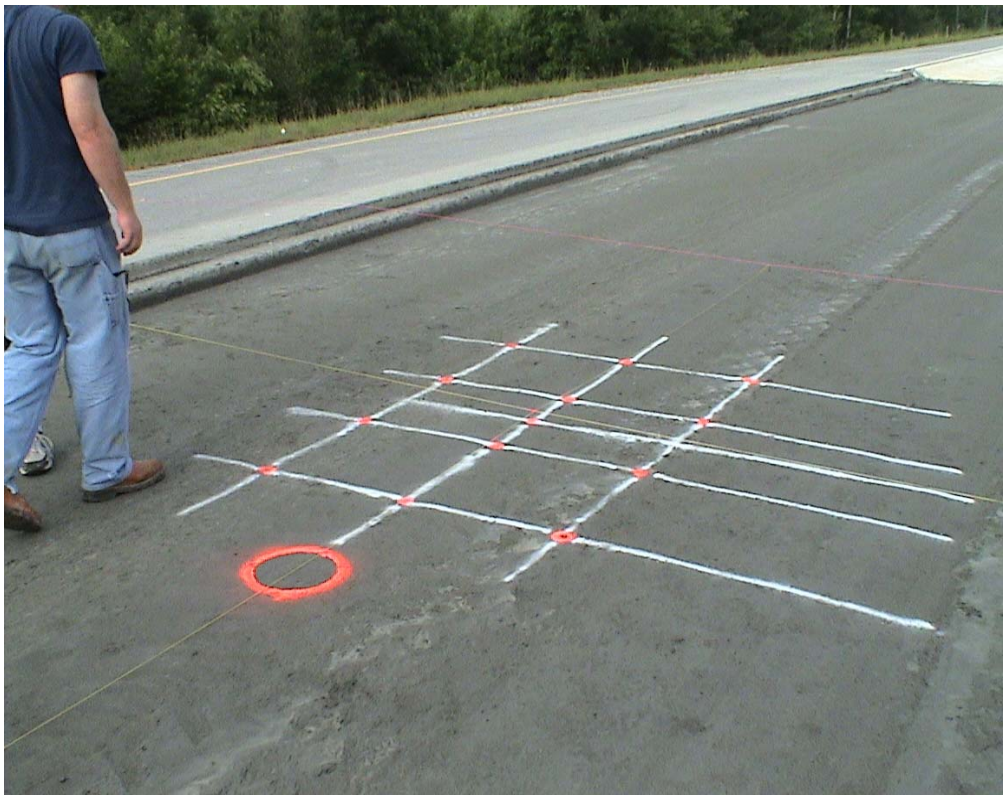

Figure 2.9 Granular Base Ready for Paving.

Figure 2.10 illustrates the granular base gradation, while Figure 2.11 shows the in-place unit weights and moisture contents, by section. As with the fill layer, these data represent averages of three random longitudinal stations and both wheelpaths within individual test sections. In general, the moisture contents and unit weights were fairly uniform throughout the project.

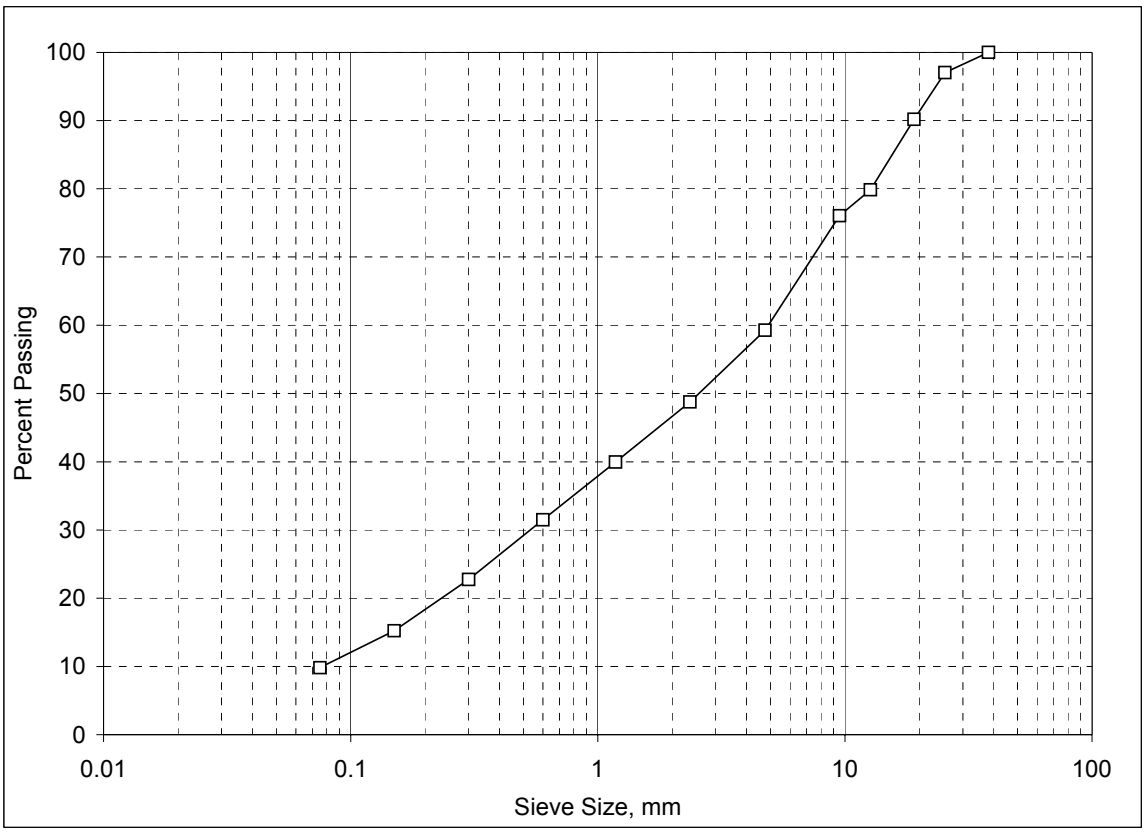

Figure 2.10 Granular Base Gradation.

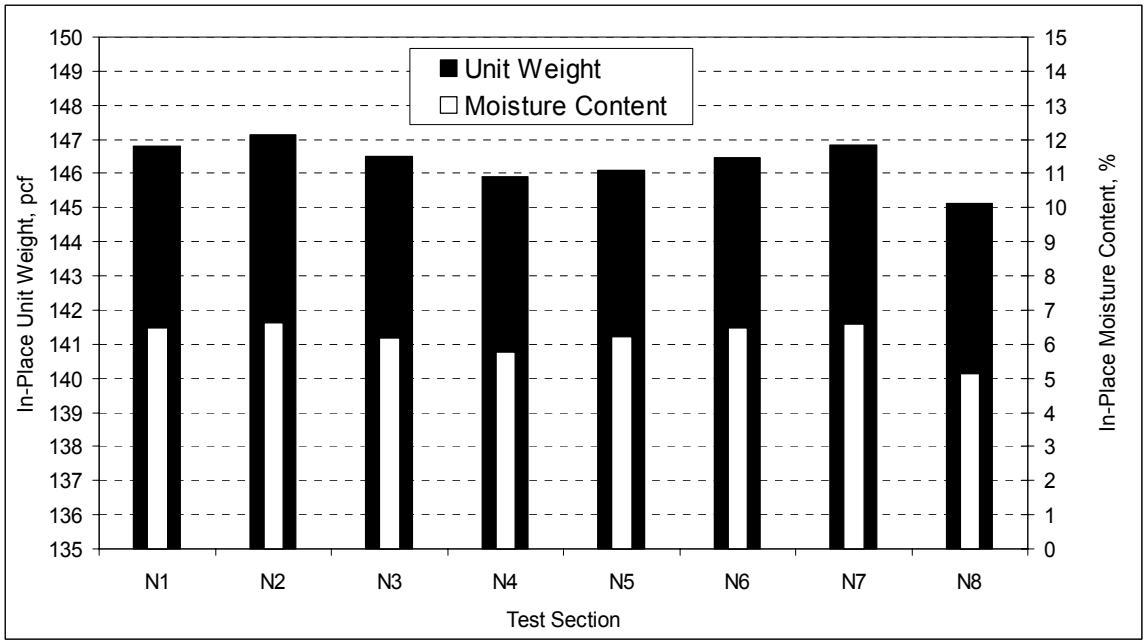

Figure 2.11 Granular Base As-Built Properties.

It must be noted that the granular base layer was not designed with drainage characteristics in mind. However, after the sections were paved, subjected to traffic and had exhibited fatigue cracking, pumping of the base and standing water after rain events were observed (Figure 2.12); therefore, the drainage characteristics were investigated. While permeability tests were not conducted on the material, it was possible to estimate the coefficient of permeability by (Moulton, 1980):

$$k = \frac{6.214 \cdot 10^5 \left(D_{10}\right)^{1.478} \left(n\right)^{6.654}}{P_{200}^{\ 0.597}} \qquad (2.1)$$

where:

k = coefficient of permeability (ft/day)

D_{10} = particle size corresponding to 10% passing (mm)

n = porosity = $1 - \frac{\gamma_d}{\gamma_w G_s}$

γ_d = dry unit weight, lb/ft^3

γ_w = unit weight of water (62.4 lb/ft^3)

G_s = specific gravity of solids (assumed 2.65)

P_{200} = percent passing 0.075 mm (#200) sieve

According to Figure 2.10, D_{10} and P_{200} were 0.078 mm and 9.8% respectively. Using these values in Equation 2.1 yielded a permeability coefficient of 0.0235 ft/day, which is for all practical purposes non-draining. In comparison, the coefficient of permeability for an open graded drainage layer would be at least 6,000 ft/day (Cedergren et al., 1972). Even a slower draining filter layer would approach 2 ft/day (Cedergren et al., 1972). Clearly, based upon field observations and permeability estimates, the granular base can be considered a well graded material with very poor drainage characteristics.

Figure 2.12 Pavement Drainage and Pumping Problems.

HOT-MIX ASPHALT (HMA)

Before considering the HMA as a whole, it is important to describe the component materials and their general properties. The following subsections detail the aggregate, asphalt, mix design and HMA as-built properties.

Aggregate

Three aggregate gradations were developed for the HMA mixtures: Superpave dense-graded wearing, stone-matrix asphalt (SMA) wearing and base course (referred to as a "Binder Layer" according to ALDOT specifications). These same gradations were used throughout the structural experiment test sections and were based on typical ALDOT job-mix formulas. Listed in Table 2.1, the blends consisted of primarily granite and limestone materials. Figure 2.13 illustrates the gradations. It is interesting to note that the percent passing the 4.75 mm sieve were equivalent between the SMA and base course gradations (approximately 52%). This observation will be revisited later when examining mechanistic properties of the HMA mixtures. Other properties are listed in Table 2.2, and it should be noted that the aggregates met the Superpave consensus property requirements.

Table 2.1 Aggregate Stockpile Sources

	Percentage of Solids		
Aggregate Component	Wearing Course	Base Course	SMA Wearing Course
#89 Granite	24	0	77
M10 Granite	29	29	16
#78 Limestone	0	31	0
#8910 Limestone	27	0	0
#57 Limestone	0	20	0
Coarse Sand	19	19	0
Baghouse Fines	1	1	1
Boral Flyash	0	0	6
Cellulose Fibers	0	0	0.3

Figure 2.13 HMA Aggregate Gradations.

Table 2.2 Other HMA Aggregate Properties

Property	Wearing Course	Base Course	SMA Wearing Course
Bulk Specific Gravity of Aggregate	2.720	2.747	2.682
Coarse Aggregate Angularity, %	100	100	100
Fine Aggregate Angularity, %	46	48	47

Asphalt Binder

An important part of the Structural Study was to evaluate differences between two different grades of asphalt binder. The grades were PG 67-22 and PG 76-22, respectively. The PG 67-22 was a neat (unmodified) asphalt, while the PG 76-22 used the same base asphalt as the 67-22 but was modified with Styrene-Butadiene-Styrene (SBS) polymer. Both materials are commonly used by many state DOTs, including ALDOT. It should also be noted that the PG 67-22 is a regional asphalt grade used by many states in the Southeast U.S. According to Superpave, the PG 67-22 asphalt would actually be classified as a PG 64-22. Table 2.3 lists the rheological parameters, as measured according to Superpave specifications, for each binder while Figure 2.14 illustrates the temperature – viscosity relationships.

Table 2.3 Asphalt Rheological Parameters

Asphalt	Unmodified	SBS-Modified
PG Grade	67-22	76-22
Penetration @ 25C, dmm	57	47
Viscosity @ 135C, cP	550	1362
Temperature @ G*/sinδ = 1.0 kPa (Unaged Binder)	70.1	80.9
Temperature @ G*/sinδ = 2.2 kPa (RTFO Binder)	71.7	81
Temperature @ G*sinδ = 5000 kPa (RTFO and PAV Binder)	20.1	20.8
Specific Gravity of Binder	1.03	1.03

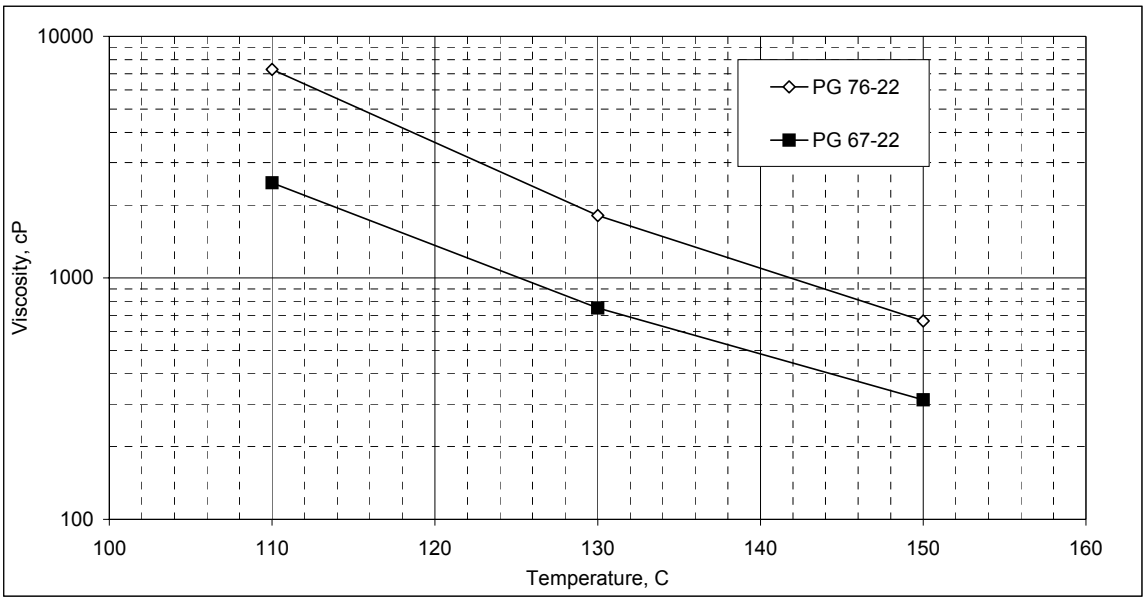

Figure 2.14 Asphalt Temperature-Viscosity Relationship.

HMA Mix Design

The design of the various mixtures used in the Structural Study were performed in accordance with ALDOT specifications. Figure 2.15 illustrates the structural cross-sections, in terms of individual component HMA sub-layers, for each test section. There were six mixtures, as indicated in Figure 2.15, and listed with relevant design parameters in Table 2.4. Mixtures 1 and 3 utilized the wearing course aggregate gradation while mixture 5 was the SMA aggregate. Mixtures 2 and 4 were the base courses, with mixture 6 as another base course mixture with asphalt content 0.5% above optimum. This mixture, which was used as a "rich-bottom" layer, was developed to determine if increased asphalt content (and reduction in air voids for similar levels of compaction) would result in increased fatigue life.

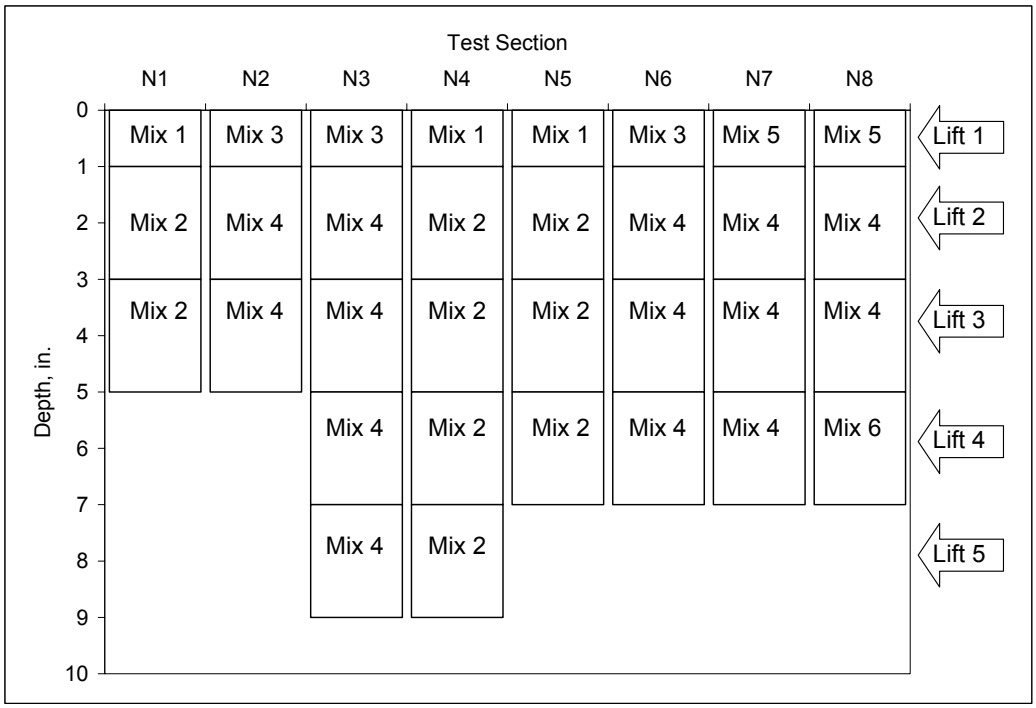

Figure 2.15 HMA Sublayer Mixture Numbering (Corresponds to Table 2.4).

Table 2.4 HMA Mix Design Parameters

Asphalt Mixture	1	2	3	4	5	6
Asphalt PG Grade	76-22	76-22	67-22	67-22	76-22	67-22
Gradation	Wearing	Base	Wearing	Base	SMA	Base
Liquid Antistrip Agent, %	0.5	None	0.5	None	None	None
Design Methodology	Super	Super	Super	Super	Marshall	Super
Compaction Device	Gyratory	Gyratory	Gyratory	Gyratory	Hammer	Gyratory
Compactive Effort, Number of Gyrations	80	80	80	80	50	80
Mixing Temperature, F	345	345	325	325	345	325
Effective Asphalt Content, %	6.13	4.27	6.13	4.27	6.05	4.77
Dust to Asphalt Ratio	0.88	1.10	0.88	1.10	1.50	0.99
Maximum Specific Gravity of Mix	2.474	2.571	2.474	2.571	2.447	2.536
Effective Specific Gravity of Aggregate Blend	2.729	2.766	2.729	2.766	2.687	2.747
Bulk Unit Weight of Compacted Pills, pcf	147.8	153.6	147.8	153.6	145.9	155.5
Tensile Strength Ratio	0.83	0.83	0.83	0.83	0.87	Unknown
Computed Air Voids in Total Mix, %	4.3	4.3	4.3	4.3	4.1	2.5
Voids in Mineral Aggregate, %	17.9	14.5	17.9	14.5	17.9	13.5

HMA As-Built Properties

Paving of the Structural Study test sections began in July, 2003. A material transfer vehicle (MTV), pictured in Figure 2.16, was used to mitigate temperature and aggregate segregation problems. It should also be noted that the only construction equipment positioned on the unpaved surface was the asphalt paver itself. The other equipment (MTV, dump trucks) used the existing inside lane as a construction platform. Construction was performed in accordance with ALDOT specifications and compaction was accomplished with steel wheel static rolling, vibratory compaction and pneumatic-tire rollers. Figure 2.17 shows a steel-wheel roller and a technician checking density after the roller pass.

Figure 2.16 Use of Material Transfer Vehicle During Paving.

Figure 2.17 Steel-Wheel Compaction and Density Check.

The average as-built thickness of individual lifts, surveyed during construction for each test section, are shown in Figure 2.18. In the figure, the wearing course is listed as the

first lift, with underlying lifts increasing in numerical order. Figure 2.19 shows the corresponding asphalt contents, while Figure 2.20 shows the air voids for each test section and individual lifts. These individual layers need to be represented by composite properties for the entire thickness of HMA since it is difficult to distinguish HMA sublayers in backcalculation. This was accomplished by determining a weighted average, according to sub-layer thicknesses, for asphalt and air void content. Figures 2.21 and 2.22 indicate the weighted average asphalt content and air void content, respectively. The averages were computed according to:

$$\overline{X} = \frac{\sum_{i=1}^{k}(h_i \cdot X_i)}{\sum_{i=1}^{k} h_i} \tag{2.2}$$

Where:

$\overline{X}$ = average asphalt or air void content (%)
X_i = asphalt or air void content (%) in sublayer, i
i = HMA sub-layer
k = total number of HMA sub-layers
h_i = thickness (in.) of sublayer, i

Of particular importance were sections N1 and N2, which were meant to be a direct comparison between the two binder grades, but had 0.18% difference in average asphalt content due to a thicker surface course relative to section N1. Sections N3 through N7 were all very similar, with section N8 slightly higher due to the increased asphalt content in the lowest layer. According to Figure 2.22, the average density of the entire structural study was approximately 93% of theoretical maximum density with air voids ranging from 5.75% to 7.11%.

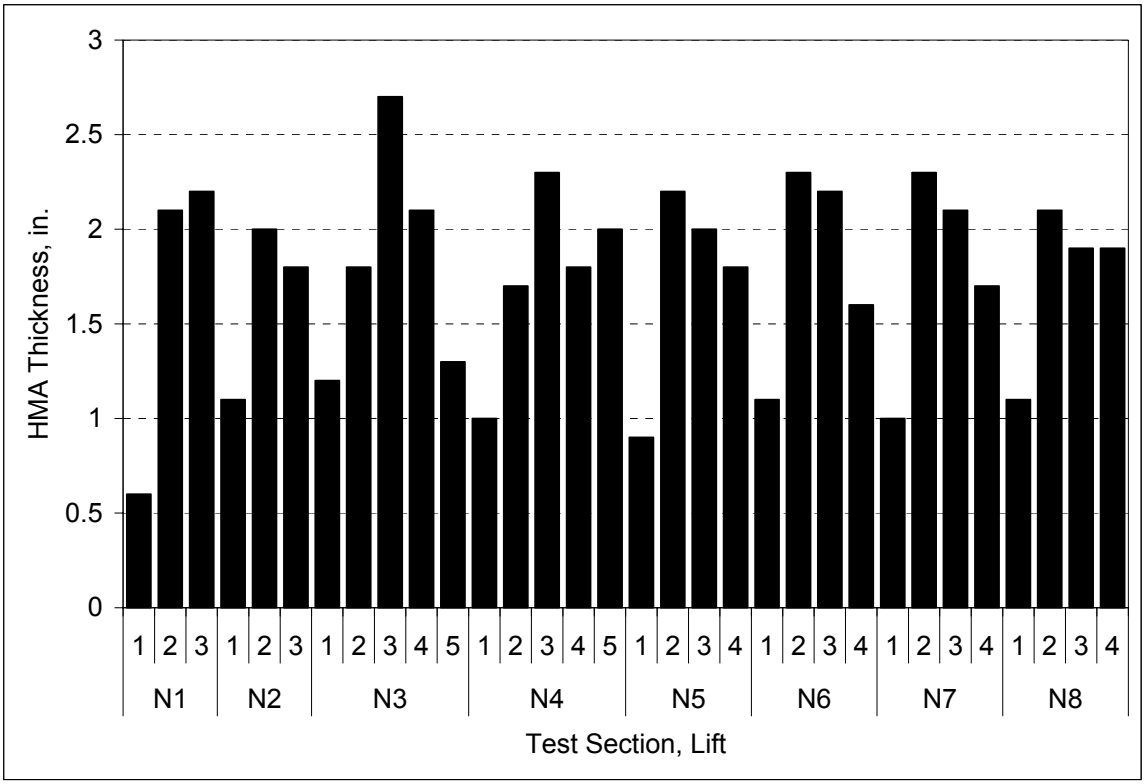

Figure 2.18 As-Built HMA Sub-Layer Thickness.

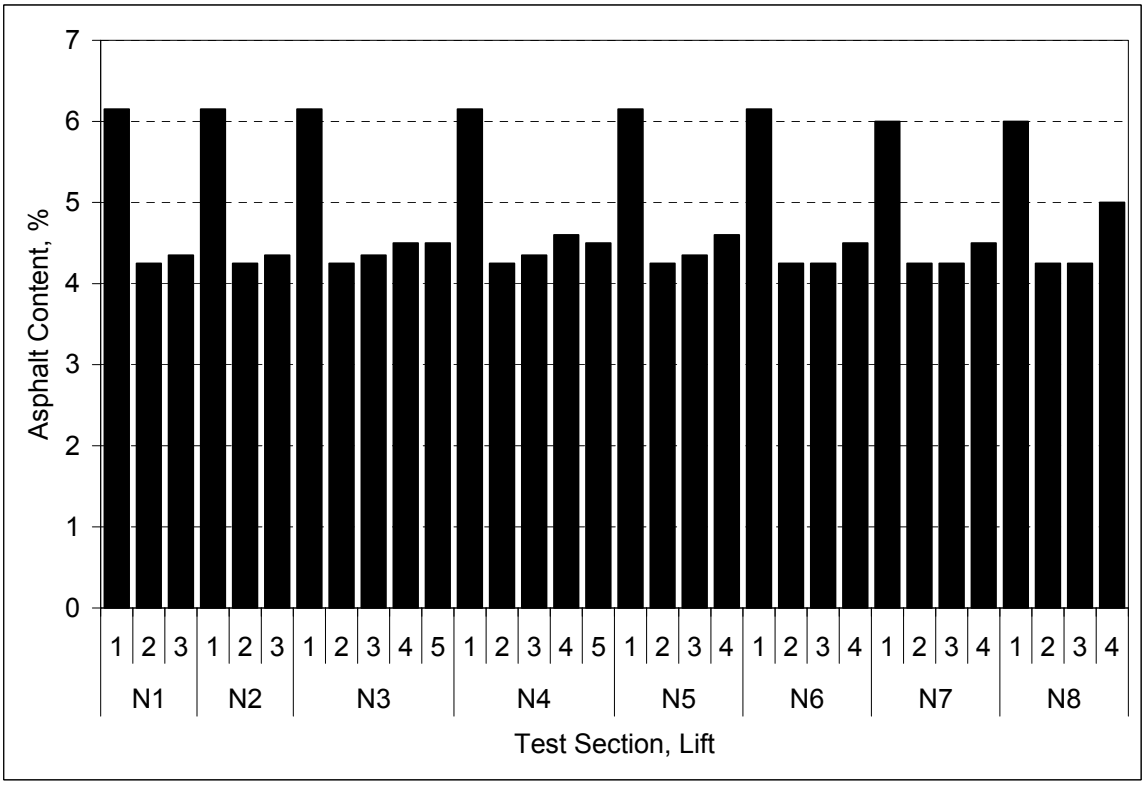

Figure 2.19 As-Built HMA Sub-Layer Asphalt Content.

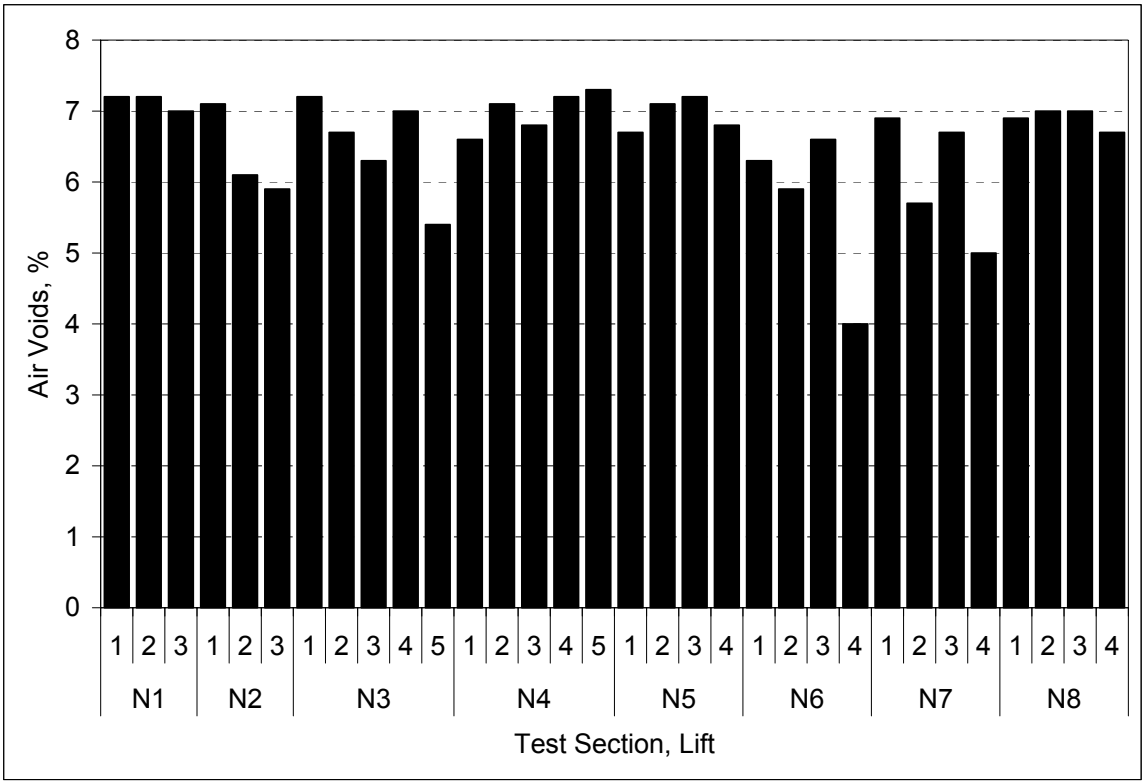

Figure 2.20 As-Built HMA Sub-Layer Air Void Content.

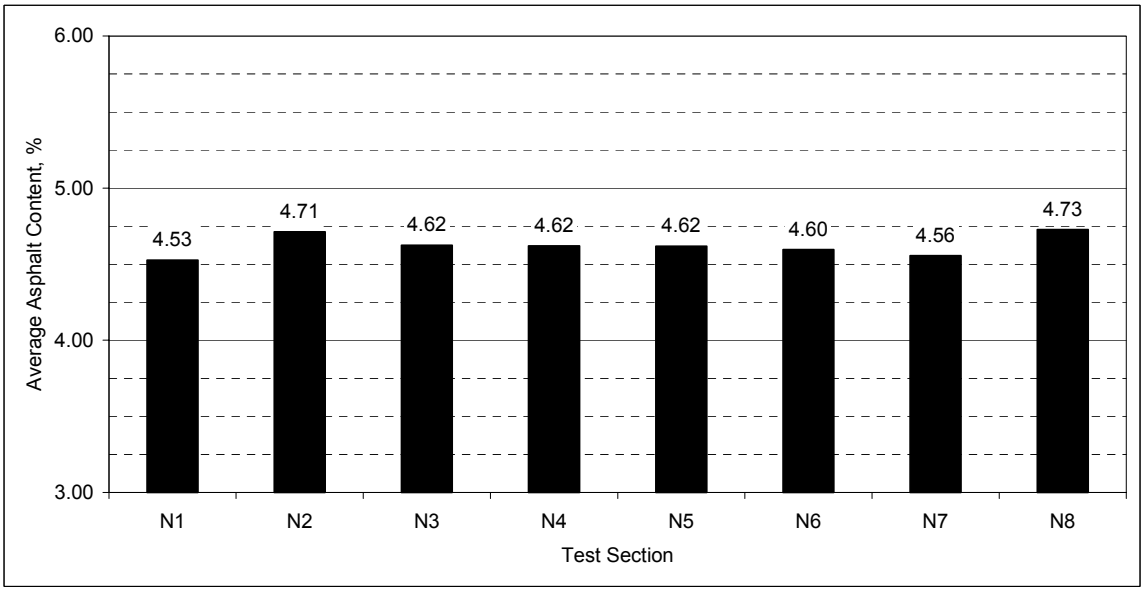

Figure 2.21 Average As-Built Asphalt Contents.

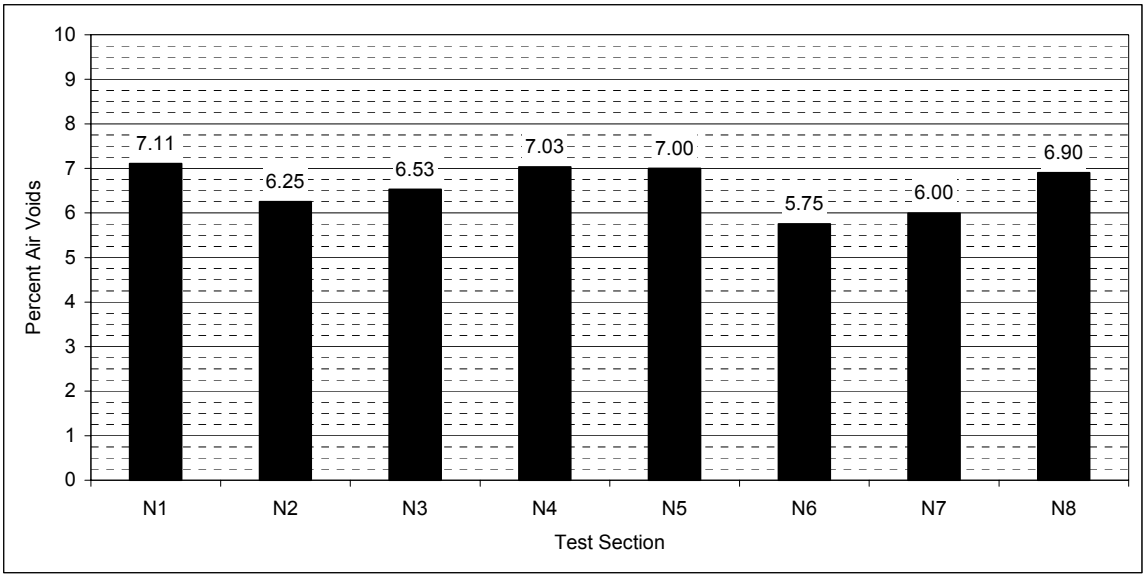

Figure 2.22 Average As-Built Air Void Content.

Figure 2.23 summarizes the thickness data from Figure 2.18 and also represents thickness along the length of the test section. The thicknesses were determined at three random locations and in the center of the gauge array in each section. Additionally, the data represent averages of the inside and outside wheelpath thickness at each random location. In general, the as-built thicknesses were close to the design thicknesses. Section N1, however, started thicker than designed and became thinner with increasing distance. This was due to tying the new test section into the preexisting section from the 2000 Test Track. The fact that the thickness varies significantly in section N1 is not necessarily a problem since it was documented, but highlights the need to have as-built thicknesses in addition to the design thickness.

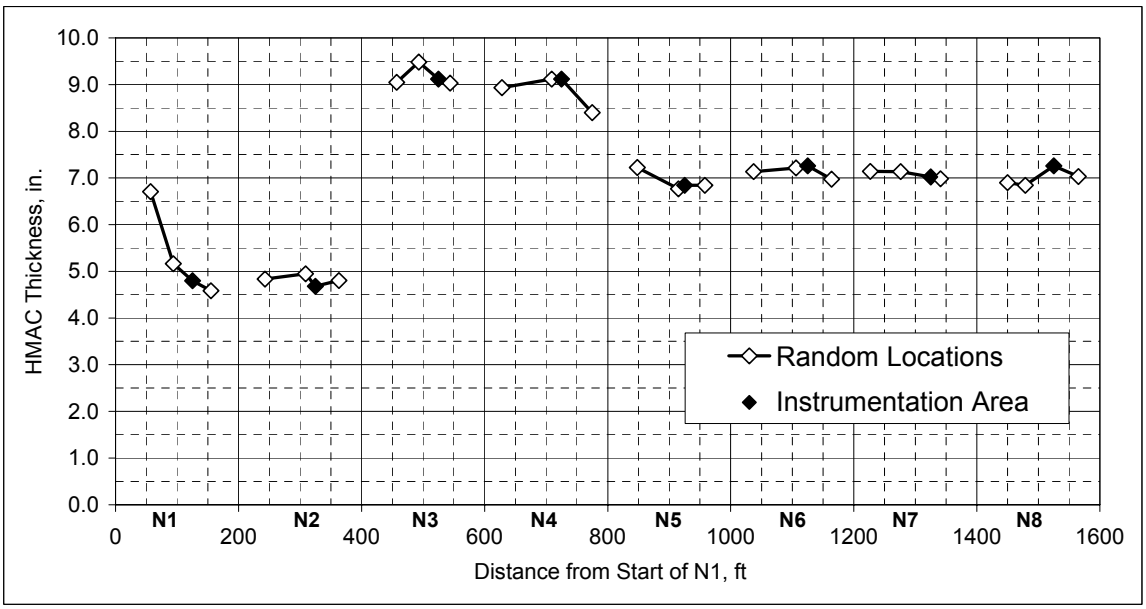

Figure 2.23 Test Section HMA Thickness.

SUMMARY

This chapter documented many of the individual pavement material properties used in the Structural Experiment, in addition to the general construction practices. The mechanistic properties presented in the following chapters are analyzed in the context of the parameters defined in this chapter.

CHAPTER 3 – LABORATORY MECHANISTIC PROPERTIES

INTRODUCTION

As part of the Structural Study, a series of tests were conducted in the laboratory to determine mechanistic properties of the respective materials. These tests, conducted by ALDOT and Purdue University, provide an important basis of comparison to the field-determined backcalculated stiffnesses obtained from the Test Track. The following sections detail the laboratory testing and results pertaining to the fill, base and HMA pavement layers.

FILL MATERIAL

The resilient modulus of the fill material was tested by ALDOT in accordance with AASHTO T307-99 (recompacted/thinwall tube samples). The test conditions, listed in Table 3.1, included three moisture contents, three confining pressures and five levels of cyclic stress (also known as deviator stress) ranging from 2 to 10 psi. It is important to understand the relationship between laboratory resilient modulus testing and material response under actual loads. In the laboratory, confining stresses are applied to simulate the surrounding material in a pavement structure. This confinement increases with increasing depth in the pavement. Thus, varying the confining pressure in a laboratory test simulates the material at different depths in the pavement. The cyclic (or deviator) stress in the laboratory represents applied wheel loads in the field that are transmitted through the HMA layers to the underlying unbound layers. Increasing the deviator stresses in the laboratory simulates increasing the applied load magnitude in the field.

Table 3.1 Fill Material Resilient Modulus Test Conditions

Parameter	Values
Gravimetric Moisture Content, %	7.2, 9.7, 20.1
Confining Pressure, psi	2, 4, 6
Cyclic (or deviator) Stress, psi	2 – 10
Maximum Dry Density, lb/ft^3	122.5
Average Compacted Dry Density as Tested, lb/ft^3	114.4

Figure 3.1 summarizes the results at the lowest moisture content, while Figure 3.2 shows the influence of moisture content. It is important to note, from Figure 3.1, the slight dependence of M_r on cyclic stress (S_c), while the level of confinement (S_3) has a stronger influence. This trend was noted at the other moisture contents as well. Further, the resilient modulus tended to range from 7,000 to 14,000 psi for the conditions tested. Figure 3.2 demonstrates the moderate decline in resilient modulus with increasing moisture content.

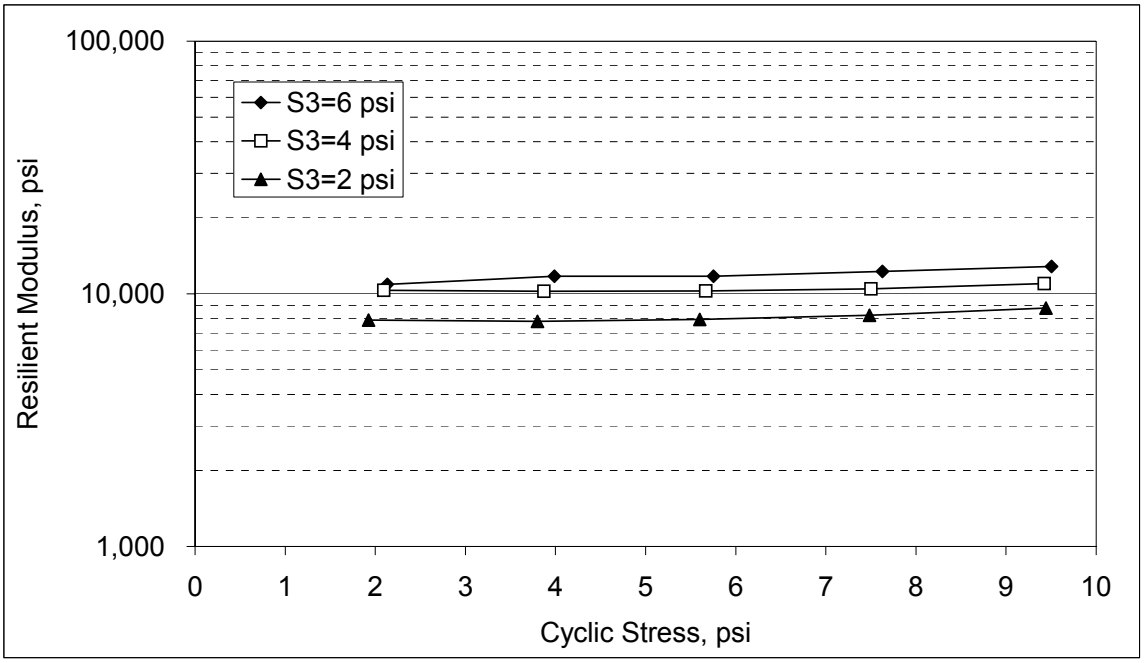

Figure 3.1 Fill Material Resilient Modulus at 7.2% Moisture Content.

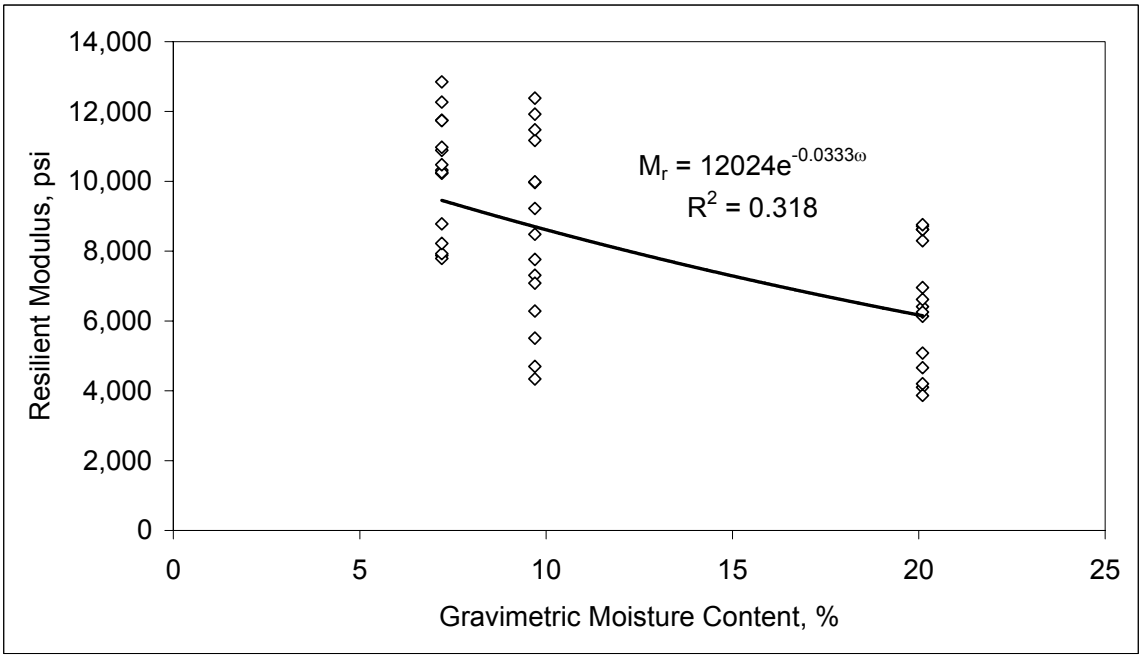

Figure 3.2 Influence of Moisture Content on Fill Material Resilient Modulus.

As part of the test reporting, ALDOT determined fitted model parameters, listed in Table 3.2, for the following equation:

$$M_r = k_1 S_c^{k_2} S_3^{k_3} \quad (3.1)$$

where:
M_r = resilient modulus, psi
S_c = applied cyclic stress, psi
S_3 = applied confining stress, psi
k_1, k_2, k_3 = fitted model parameters

Table 3.2 Fill Material Fitted Model Parameters

Moisture Content, %	k_1	k_2	k_3	R^2
7.2	5,780	0.06382	0.34686	0.97
9.7	2,443	0.21324	0.65770	0.97
20.1	2,518	0.07287	0.61171	0.97

As shown in Table 3.2, each model fit very well ($R^2 = 0.97$). However, it was desirable to also incorporate moisture content into a predictive equation. Therefore, a model incorporating the general trend observed in Figure 3.2 with the basic form of Equation 3.1 was developed as part of this investigation:

$$M_r = 5246.63 S_c^{0.1073} S_3^{0.502} e^{-0.0320\omega} \quad (R^2 = 0.921) \quad (3.2)$$

where:
ω = gravimetric moisture content, %

A summary of predicted versus measured resilient moduli is shown in Figure 3.3. The figure indicates very low residuals between the model and measured data, following the unity line, indicating that the model can be used to reasonably predict the resilient modulus of the fill material from a variety of test conditions.

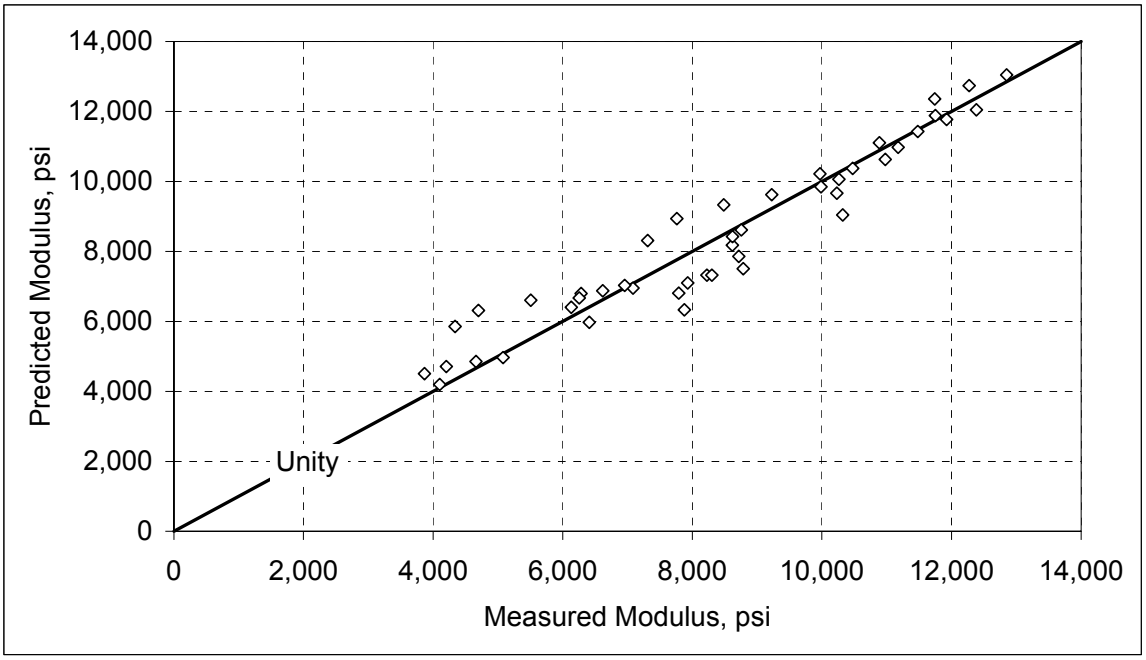

Figure 3.3 Fill Material Predicted versus Measured Modulus.

GRANULAR BASE

As with the fill material, the granular base was also tested by ALDOT for resilient modulus according to AASHTO T307-99 (subgrade protocol). A notable difference, as indicated in Table 3.3, was that only two moisture contents were tested.

Table 3.3 Granular Base Resilient Modulus Test Conditions

Parameter	Values
Gravimetric Moisture Content, %	5.3, 9.8
Confining Pressure, psi	2, 4, 6
Cyclic Stress, psi	2 – 10
Maximum Dry Density, lb/ft^3	138.1
Average Compacted Dry Density as Tested, lb/ft^3	128.6

Figure 3.4 shows the influence of confining stress and cyclic stress on the resilient modulus. Compared to the fill material (Figure 3.1), it appeared that the granular base resilient modulus was less dependent upon the applied cyclic stress which was probably due to the protocol and compacted density used during testing. This was further demonstrated by the k_2 model parameter, again provided by ALDOT, for the granular base material as listed in Table 3.4. Note that k_2 was lower for the granular base than the fill material, which indicated less of an influence of confining stress on resilient modulus. Also, it was observed that the range of moduli for the granular base were generally lower than that of the fill material. This observation will be further quantified below.

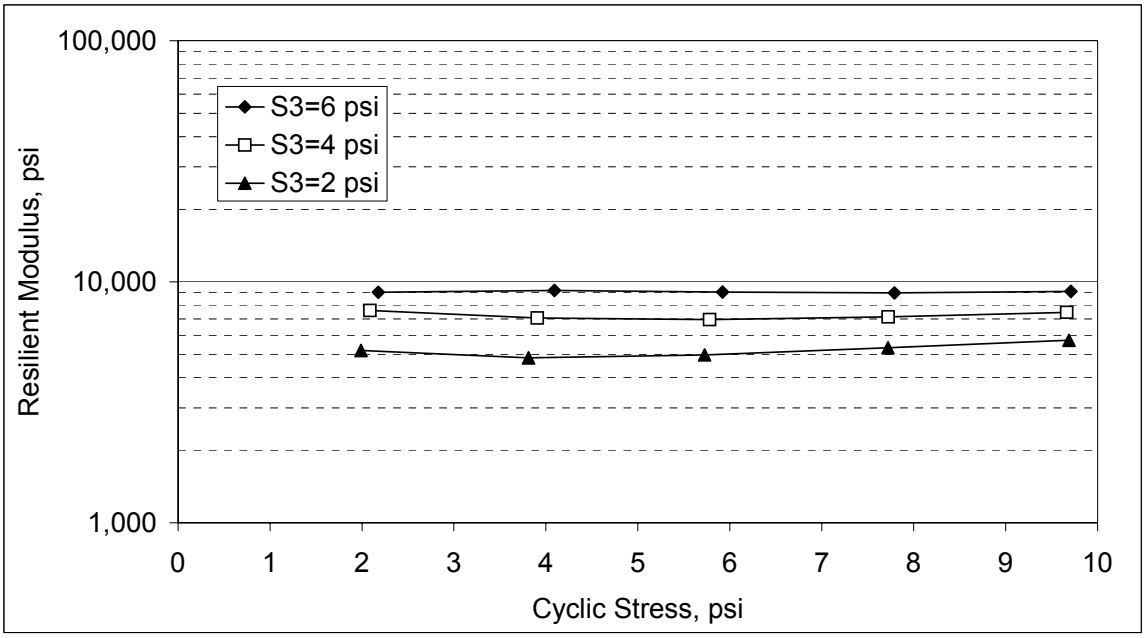

Figure 3.4 Granular Base Resilient Modulus at 5.3% Moisture Content.

Table 3.4 Granular Base Fitted Model Parameters

Moisture Content, %	k_1	k_2	k_3	R^2
5.3	3563	0.01407	0.50479	0.97
9.8	2678	0.03808	0.62483	0.97

As was done with the fill material, it was desirable to create a model incorporating moisture content to predict granular base resilient modulus from ALDOT test data. The resulting equation was:

$$M_r = 3529.09 S_c^{0.0109} S_3^{0.5678} e^{-0.0147\omega} \qquad (R^2 = 0.969) \qquad (3.3)$$

A plot of predicted versus measured granular base resilient moduli is shown in Figure 3.5. The residuals were again very small, and the equation can be used with good accuracy to predict granular base resilient modulus over the range of conditions used to establish this data set.

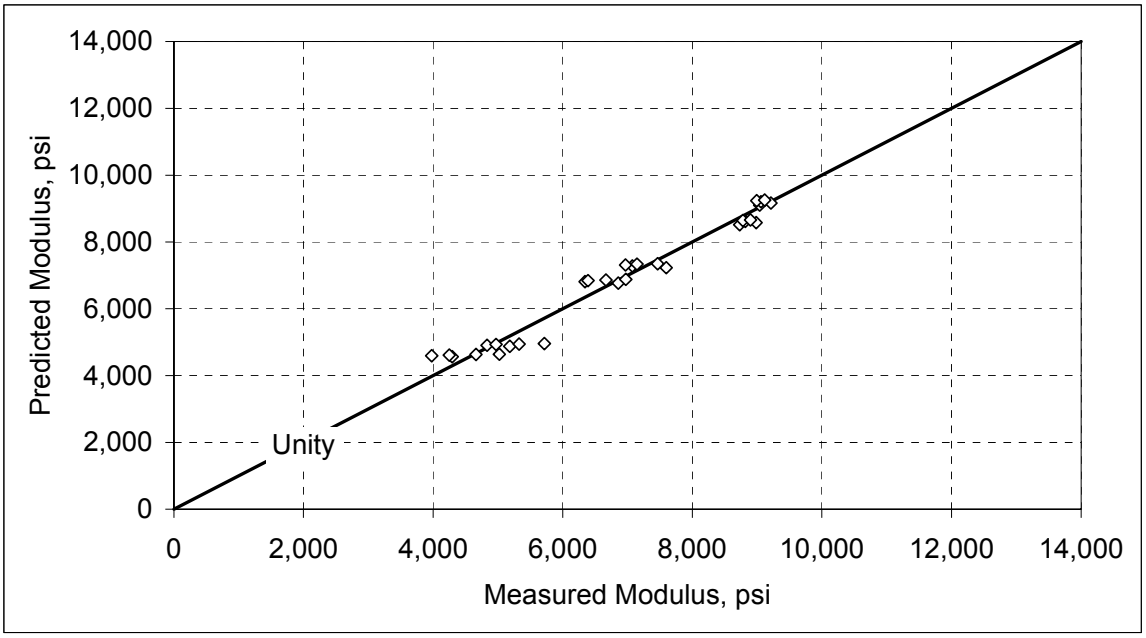

Figure 3.5 Granular Base Predicted versus Measured Modulus.

As mentioned above, it was generally observed that the granular base modulus was lower than the fill material. More specifically, Equation 3.2 can be divided by Equation 3.3:

$$Ratio = \frac{M_{r_{fill}}}{M_{r\,granular\ base}} = \frac{5246.63 S_c^{0.1073} S_3^{0.502} e^{-0.0320\omega}}{3529.09 S_c^{0.0109} S_3^{0.5678} e^{-0.0147\omega}} \tag{3.4}$$

which yields:

$$Ratio = 1.48 S_c^{0.0964} S_3^{-0.0658} e^{-0.0173\omega} \tag{3.5}$$

Equation 3.5, when considered within the range of test parameters used by ALDOT, generates ratios ranging from 1.18 to 1.62 with an average of 1.41. This means that, on average, the fill material modulus was approximately 41% higher than the granular base. This is important since it is commonly assumed that engineered granular base materials add significant structural capacity, through increased stiffness, to the overall pavement structure. However, the ALDOT laboratory data do not support this assumption. Also, the magnitude of the granular base resilient modulus was lower than what might be expected, ranging from 4,000 to 10,000 psi. However, recall from Table 3.3 that the tests were conducted on samples compacted to 128 lb/ft^3 dry density (93% of maximum). Therefore, the low stiffness values could be attributed to lower than desirable compaction.

Further laboratory testing was conducted by the granular base supplier, Vulcan Materials. Their testing protocol, also followed AASHTO T307-99, but used the protocol for base materials rather than subgrade. The base was evaluated at 5.5% moisture, a dry density of 134.5 lb/ft^3 and tested over a wider (and higher) range of stress conditions.

Specifically, the confining stress varied from 3 to 20 psi and the applied cyclic stress ranged from 3 to 40 psi. Vulcan Materials developed a bulk-stress model to predict resilient modulus and compared their data to that obtained by ALDOT. A summary of the results, including the bulk stress equations, are provided in Figure 3.6. It is very clear that the two data sets (ALDOT and Vulcan) do not match. As discussed above, this could be primarily due to the lower unit weight tested by ALDOT in addition to following the base material protocol. The equation provided by Vulcan will be evaluated relative to the FWD testing and backcalculation discussed in Chapter 5. For clarity, the Vulcan equation is:

$$M_r = 5677.2\theta^{0.4711} \quad (3.6)$$

where:

M_r = resilient modulus of base material, psi

θ = bulk stress applied to material, psi

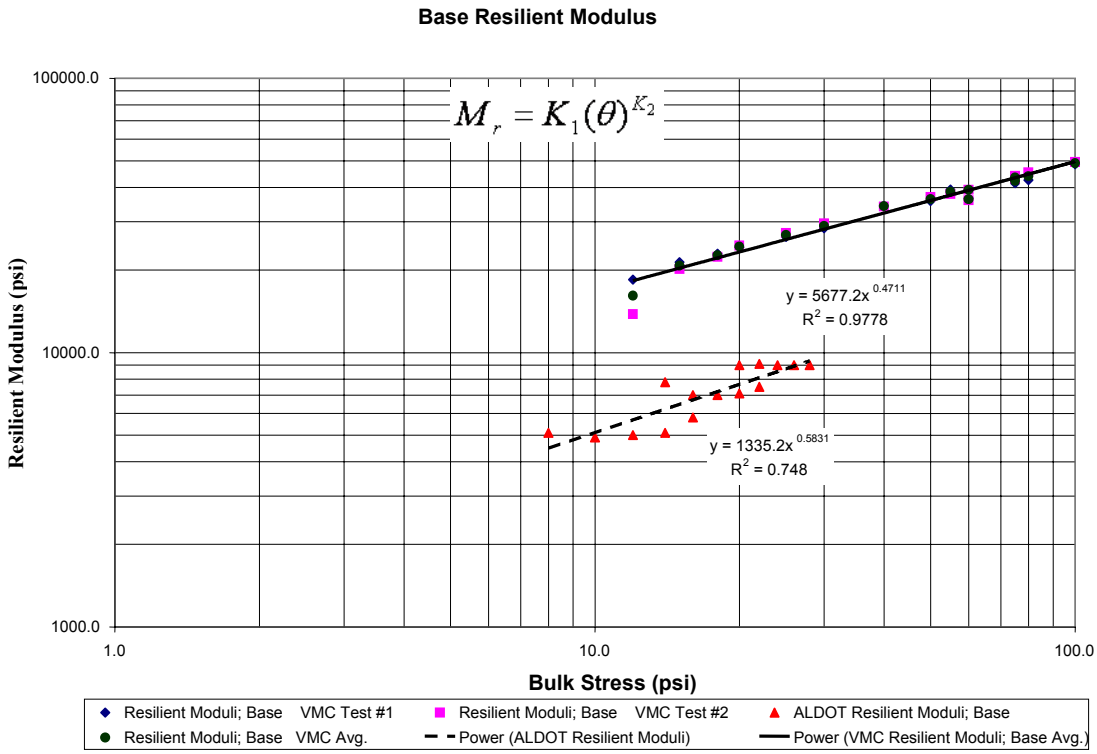

Figure 3.6 Granular Base Testing Provided by Vulcan Materials.

HOT-MIX ASPHALT

Dynamic modulus testing of the asphalt mixtures was conducted under the direction of Dr. Terhi Pellinen at Purdue University. This was in accordance with the research partnership between the Indiana Department of Transportation, Purdue University and NCAT. The materials were sampled from the delivery trucks during construction, shipped to Purdue University where they were compacted for testing with an average air void content of 7.2%. Each of the six mixtures used in the Structural Study, listed in

Table 3.5, were tested. Other details regarding the binder, aggregates and mix design were presented in Chapter 2. Tests were conducted at six different frequencies, five temperatures with four replicates per test condition.

Table 3.5 HMA Mixture Characteristics

Mixture	PG Binder Grade	Gradation
1	76-22	Wearing
2	76-22	Base
3	67-22	Wearing
4	67-22	Base
5	76-22	SMA
6	67-22 (optimum AC + 0.5%)	Base

Tables 3.6, 3.7 and 3.8 summarize the test results. As expected, it was generally observed that dynamic modulus increased with increased load frequency and decreased with increased temperature. This is demonstrated by Figures 3.7 and 3.8 which represent average dynamic modulus from mixtures 1 and 3 (combined) versus temperature and frequency, respectively. An examination of the variability for all the mixtures, in terms of coefficient of variation (COV = σ/μ), shows a range from 1.5% to 45.2% with an average of 15.4%. Other studies of resilient modulus of asphalt mixtures have found the coefficient of variation to range from 6% to 20% (Brown and Foo, 1991; Al-Sugair and Almudaiheem, 1992).

Dynamic Modulus Statistical Analysis

A series of analysis of variance (ANOVA) were conducted to test for differences among the six mixtures. Single factor tests, at a 95% confidence level, were executed on a selection of test conditions that included four temperatures and three load frequencies. The results are summarized in Table 3.9.

It was found that the average dynamic modulus for the six mixtures were not statistically different for test temperatures up to and including 70°F over the range of loading frequencies. Above 100°F, as shown in Table 3.9, the six mixtures were statistically distinguishable. Additional ANOVA tests were conducted by subdividing the mixtures into wearing course and SMA/base course mixtures. At 100°F, the two wearing mixtures (1 and 3) were not statistically different, while the remaining mixtures (2, 4, 5 and 6) fit into another group. At 130°F, the results were less clear. At the lowest frequency, mixes 1 and 3 were indistinguishable. However at 5 Hz and 25 Hz, mixture 1 was statistically higher than mixture 3. The opposite was true of mixtures 2, 4, 5 and 6. At the lowest frequency, the mixtures were statistically different while at 5 and 25 Hz, they not different.

When considering all the data together, the following statements can be made regarding the dynamic modulus of the various mixtures:

1. Binder grade and aggregate gradation make little difference in dynamic modulus at or below 70°F.

2. At higher temperatures, gradation becomes a controlling factor with the mixtures subdividing into fine and coarse groupings.
3. The binder grade appeared to influence the dynamic modulus only at the highest temperature tested in the higher frequency range for the fine gradation mixes.

Each of these factors, in addition to several other test parameters, were further investigated through regression analysis as described below.

Table 3.6 Dynamic Modulus of Wearing Mixtures

		Mixture #1			Mixture #3		
Temp, F	Freq, Hz	Avg E*, psi	StdDev E*, psi	COV, %	Avg E*, psi	StdDev E*, psi	COV, %
14	0.1	2,083,358	176,959	8.5%	2,029,222	285,773	14.1%
	0.5	2,468,142	213,917	8.7%	2,417,379	361,177	14.9%
	1	2,629,424	229,985	8.7%	2,581,816	397,024	15.4%
	5	2,985,601	272,947	9.1%	2,944,301	466,569	15.8%
	10	3,162,982	294,803	9.3%	3,101,703	506,310	16.3%
	25	3,344,061	330,664	9.9%	3,271,941	560,209	17.1%
40	0.1	974,980	147,835	15.2%	791,507	76,068	9.6%
	0.5	1,241,885	195,133	15.7%	1,031,399	78,291	7.6%
	1	1,362,085	217,755	16.0%	1,139,742	74,327	6.5%
	5	1,656,076	271,254	16.4%	1,432,827	55,933	3.9%
	10	1,793,318	281,201	15.7%	1,564,304	53,531	3.4%
	25	2,000,360	307,940	15.4%	1,723,628	25,969	1.5%
70	0.1	298,959	45,429	15.2%	288,879	88,673	30.7%
	0.5	436,418	74,327	17.0%	430,798	121,075	28.1%
	1	511,874	86,044	16.8%	508,140	136,706	26.9%
	5	732,658	121,717	16.6%	737,843	180,421	24.5%
	10	867,760	162,302	18.7%	859,820	195,207	22.7%
	25	1,029,622	182,845	17.8%	1,031,689	225,254	21.8%
100	0.1	85,463	14,807	17.3%	87,639	39,612	45.2%
	0.5	124,986	22,583	18.1%	123,391	50,665	41.1%
	1	147,902	27,601	18.7%	146,234	58,546	40.0%
	5	245,658	46,131	18.8%	235,505	78,348	33.3%
	10	310,272	59,041	19.0%	295,514	92,499	31.3%
	25	380,289	69,088	18.2%	382,066	128,806	33.7%
130	0.1	41,408	7,426	17.9%	31,256	6,074	19.4%
	0.5	55,332	10,510	19.0%	39,958	8,907	22.3%
	1	63,164	11,793	18.7%	45,397	10,321	22.7%
	5	99,387	18,474	18.6%	64,941	16,389	25.2%
	10	124,043	22,659	18.3%	77,414	19,433	25.1%
	25	152,833	25,922	17.0%	97,647	24,297	24.9%

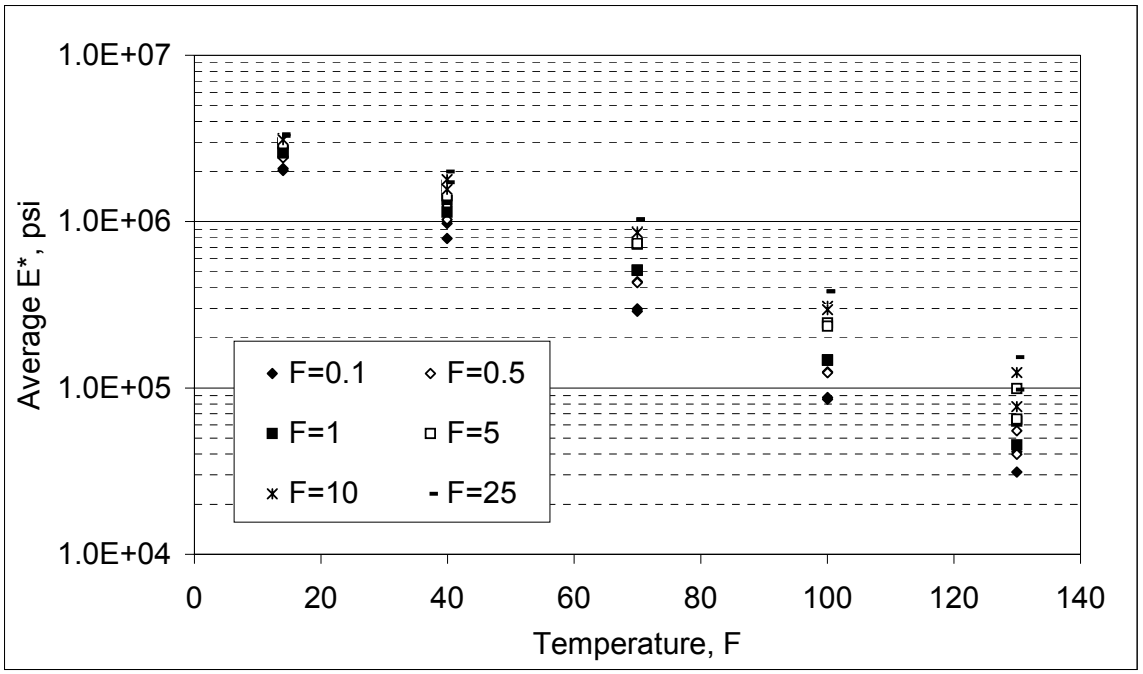

Figure 3.7 Dynamic Modulus versus Temperature (Mixtures 1 and 3 Combined).

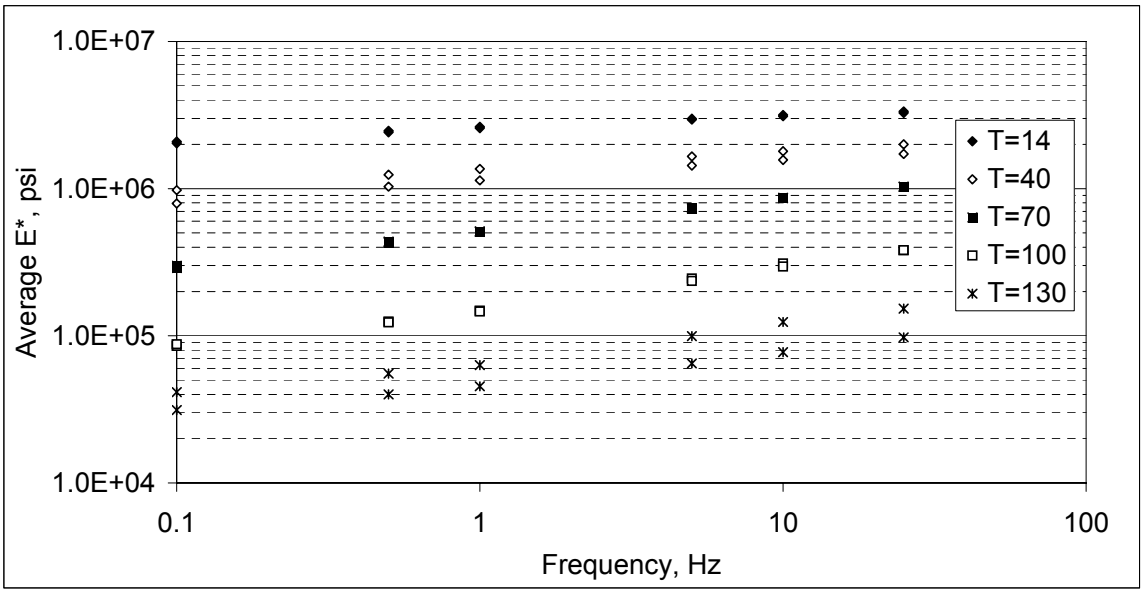

Figure 3.8 Dynamic Modulus versus Frequency (Mixtures 1 and 3 Combined).

Table 3.7 Dynamic Modulus of Base Mixtures

		Mixture #2			Mixture #4		
Temp, F	Freq, Hz	Avg E*, psi	StdDev E*, psi	COV, %	Avg E*, psi	StdDev E*, psi	COV, %
14	0.1	2,277,563	301,583	13.2%	2,298,485	192,823	8.4%
	0.5	2,725,367	337,116	12.4%	2,724,243	255,820	9.4%
	1	2,907,715	357,532	12.3%	2,897,164	276,114	9.5%
	5	3,304,176	410,690	12.4%	3,289,201	315,239	9.6%
	10	3,502,587	421,351	12.0%	3,421,801	320,689	9.4%
	25	3,689,759	450,429	12.2%	3,617,276	355,717	9.8%
40	0.1	1,153,195	203,310	17.6%	1,072,481	131,115	12.2%
	0.5	1,474,779	268,533	18.2%	1,395,625	157,677	11.3%
	1	1,623,189	300,838	18.5%	1,543,418	168,029	10.9%
	5	1,988,503	376,758	18.9%	1,920,335	188,822	9.8%
	10	2,148,479	421,027	19.6%	2,087,564	198,544	9.5%
	25	2,404,942	474,083	19.7%	2,327,093	210,715	9.1%
70	0.1	394,829	44,604	11.3%	378,875	67,659	17.9%
	0.5	565,357	71,916	12.7%	547,046	83,215	15.2%
	1	653,141	84,367	12.9%	643,423	88,274	13.7%
	5	913,955	125,840	13.8%	930,961	106,425	11.4%
	10	1,061,821	150,939	14.2%	1,064,722	116,677	11.0%
	25	1,243,734	184,064	14.8%	1,310,597	148,638	11.3%
100	0.1	151,383	15,348	10.1%	139,490	29,780	21.3%
	0.5	214,801	16,759	7.8%	197,650	38,716	19.6%
	1	254,106	17,495	6.9%	233,293	42,084	18.0%
	5	404,945	28,959	7.2%	359,657	57,351	15.9%
	10	507,342	34,227	6.7%	445,592	64,055	14.4%
	25	614,706	47,519	7.7%	574,095	105,440	18.4%
130	0.1	65,267	3,879	5.9%	63,055	6,364	10.1%
	0.5	83,832	5,467	6.5%	79,553	7,576	9.5%
	1	95,036	6,564	6.9%	89,815	9,182	10.2%
	5	142,898	4,857	3.4%	135,103	19,120	14.2%
	10	174,009	4,556	2.6%	167,845	25,931	15.4%
	25	218,137	16,623	7.6%	215,345	40,140	18.6%

Table 3.8 Dynamic Modulus of SMA and Rich Bottom Mixtures

		Mixture #5			Mixture #6		
Temp, F	Freq, Hz	Avg E*, psi	StdDev E*, psi	COV, %	Avg E*, psi	StdDev E*, psi	COV, %
14	0.1	2,501,030	709,921	28.4%	2,761,276	791,188	28.7%
	0.5	3,002,969	767,118	25.5%	3,333,933	882,942	26.5%
	1	3,219,256	773,388	24.0%	3,219,220	1,021,254	31.7%
	5	3,670,070	831,042	22.6%	3,974,323	915,088	23.0%
	10	3,851,331	846,562	22.0%	4,214,904	964,170	22.9%
	25	4,038,067	840,600	20.8%	4,448,777	986,368	22.2%
40	0.1	1,271,183	144,279	11.4%	1,157,219	154,357	13.3%
	0.5	1,639,905	193,115	11.8%	1,588,235	217,563	13.7%
	1	1,818,265	200,936	11.1%	1,796,618	250,586	13.9%
	5	2,239,708	232,291	10.4%	2,290,544	324,019	14.1%
	10	2,427,604	238,604	9.8%	2,514,047	366,069	14.6%
	25	2,700,312	230,373	8.5%	2,828,271	443,612	15.7%
70	0.1	378,222	50,509	13.4%	366,474	51,874	14.2%
	0.5	526,886	65,857	12.5%	537,292	71,363	13.3%
	1	602,668	75,084	12.5%	639,000	85,162	13.3%
	5	840,348	106,606	12.7%	954,565	148,350	15.5%
	10	962,434	113,358	11.8%	1,119,401	197,986	17.7%
	25	1,150,910	141,738	12.3%	1,364,623	240,230	17.6%
100	0.1	136,843	39,547	28.9%	127,959	14,246	11.1%
	0.5	192,356	42,286	22.0%	177,671	24,008	13.5%
	1	227,383	45,695	20.1%	209,543	31,258	14.9%
	5	354,291	50,810	14.3%	324,123	47,371	14.6%
	10	434,497	50,788	11.7%	403,205	59,116	14.7%
	25	536,096	66,932	12.5%	533,630	111,261	20.8%
130	0.1	54,679	4,679	8.6%	52,540	7,162	13.6%
	0.5	71,504	5,655	7.9%	66,536	8,734	13.1%
	1	82,128	5,733	7.0%	75,637	9,313	12.3%
	5	132,746	6,371	4.8%	116,139	13,273	11.4%
	10	166,975	6,324	3.8%	142,935	15,152	10.6%
	25	203,415	10,311	5.1%	180,318	16,116	8.9%

Table 3.9 Dynamic Modulus ANOVA Summary

Temp, F	Freq, Hz	Null	F Statistic	P-Value	F Critical	Accept Null?
14	0.1	u1=u2=u3=u4=u5=u6	1.250	0.330	2.810	Yes
	5	u1=u2=u3=u4=u5=u6	1.827	0.158	2.773	Yes
	25	u1=u2=u3=u4=u5=u6	1.943	0.137	2.773	Yes
70	0.1	u1=u2=u3=u4=u5=u6	2.263	0.092	2.773	Yes
	5	u1=u2=u3=u4=u5=u6	2.135	0.108	2.773	Yes
	25	u1=u2=u3=u4=u5=u6	2.207	0.099	2.773	Yes
100	0.1	u1=u2=u3=u4=u5=u6	4.042	0.012	2.773	No
	5	u1=u2=u3=u4=u5=u6	6.312	0.001	2.773	No
	25	u1=u2=u3=u4=u5=u6	4.581	0.007	2.773	No
100	0.1	u1=u3	0.011	0.921	5.987	Yes
	5	u1=u3	0.050	0.831	5.987	Yes
	25	u1=u3	0.001	0.981	5.987	Yes
100	0.1	u2=u4=u5=u6	0.517	0.678	3.490	Yes
	5	u2=u4=u5=u6	1.988	0.170	3.490	Yes
	25	u2=u4=u5=u6	0.771	0.532	3.490	Yes
130	0.1	u1=u2=u3=u4=u5=u6	18.389	0.000	2.773	No
	5	u1=u2=u3=u4=u5=u6	16.771	0.000	2.773	No
	25	u1=u2=u3=u4=u5=u6	14.672	0.000	2.773	No
130	0.1	u1=u3	4.480	0.079	5.987	Yes
	5	u1=u3	7.782	0.032	5.987	No
	25	u1=u3	9.651	0.021	5.987	No
130	0.1	u2=u4=u5=u6	4.809	0.020	3.490	No
	5	u2=u4=u5=u6	3.347	0.056	3.490	Yes
	25	u2=u4=u5=u6	2.105	0.153	3.490	Yes

Dynamic Modulus Regression Analysis

The raw dynamic modulus data provided by Purdue University were further investigated through non-linear regression analysis to determine the effects of the various test parameters. Listed in Table 3.10, the parameters included mix design and as-tested volumetric properties.

Table 3.10 Dynamic Modulus Regression Analysis Parameters

Parameter	Symbol
Temperature, ^{o}F	T
Frequency, Hz	F
Percent Passing #4 (4.75 mm) Sieve	$P_{4.75}$
Asphalt Content, %	AC
Air Void Content, %	VTM
PG Binder Grade	PG

Based upon observations from Figures 3.7 and 3.8, temperature and frequency were modeled as exponential and power functions, respectively. The remaining parameters were assumed to have a linear effect on dynamic modulus. The following regression model was developed from the data with fitted parameters listed in Table 3.10:

$$E^* = \left(c_1 e^{c_2 T}\right)\left(F^{c_3}\right) + c_4 + \left(c_5 * P_{4.75}\right) + \left(c_6 * AC\right) + \left(c_7 * VTM\right) + \left(c_8 * PG\right) \quad (3.7)$$

Table 3.11 Dynamic Modulus Model Parameters and Significance Levels

Variable	Value	P-value
c_1	4136196	0.00
c_2	-2.02E-02	0.00
c_3	9.28E-02	0.00
c_4	1436312	0.00
c_5	-6622.97	0.00
c_6	-1987.37	0.93
c_7	-198769	0.00
c_8	1961.02	0.49
R^2	0.9394	

It is important to note that while the model was a good fit ($R^2 = 0.94$) the coefficients for asphalt content and PG grade are not significant at a 95% confidence level as shown by the p-values in Table 3.11. Therefore, a truncated model was developed by eliminating PG grade and asphalt content. The model parameters, listed in Table 3.12, were fitted to:

$$E^* = \left(c_1 e^{c_2 T}\right)\left(F^{c_3}\right) + c_4 + \left(c_5 * P_{4.75}\right) + \left(c_7 * VTM\right) \quad (3.8)$$

This model resulted in a slightly better R^2, and all variables were significant. Figure 3.9 illustrates the model accuracy relative to the measured data. Though it appears that the model has poorer fit at the lower stiffness values, this is a distortion due to the log scale. For example, the increments between 1.0E+04 and 1.0E+05 are only 10,000 psi while the increments between 1.0E+05 and 1.0E+06 are 100,000 psi. So, what appear to be large differences at the lower stiffnesses are in effect "magnified" due to the smaller increments. In addition to the trends discussed above regarding the influence of temperature and frequency, it was found that dynamic modulus tended to decrease with the finer gradations (i.e., surface mixture). Also, increasing the air void content tended to decrease the dynamic modulus.

Table 3.12 Dynamic Modulus Truncated Model Parameters and Significance Levels

Variable	Value	P-value
c_1	4136275.9	0
c_2	-2.02E-02	0
c_3	9.28E-02	0
c_4	1522235.08	0
c_5	-6615.4	0
c_7	-193164.8	0
R^2	0.9398	

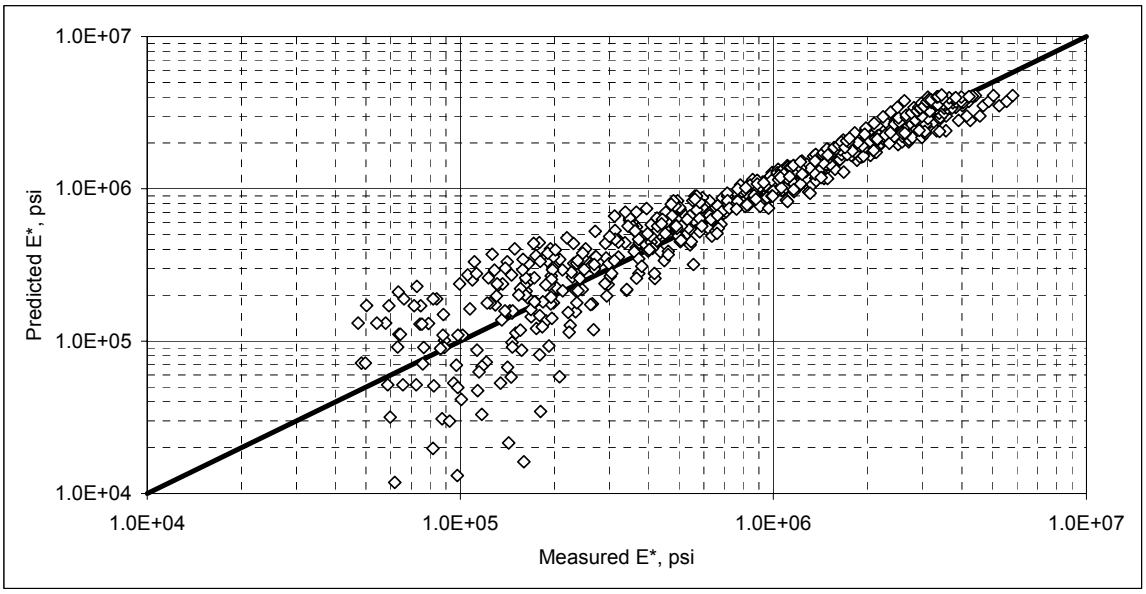

Figure 3.9 HMA Predicted versus Measured Dynamic Modulus.

The results of the regression analysis provided a reasonably accurate predictive equation that can be used in comparison to field data while also supporting the findings of the ANOVA analysis. Namely, that the binder grade did not significantly influence the dynamic modulus. It must also be remembered that dynamic modulus is *not* an all-encompassing property or performance predictor for asphalt mixtures. It is simply a characterization of the stiffness of the material under certain loading conditions which can be used to predict states of stress and strain in the material under load.

SUMMARY

This chapter detailed a number of laboratory investigations to characterize the stiffness of the component pavement layers in the Structural Study. In general, it was found that the fill material resilient modulus ranged from 4,000 to 14,000 psi and was slightly greater than the granular base resilient modulus. These values were considered low by typical granular base standards, and are further compared to field data in later chapters. Additional testing conducted by Vulcan Materials indicated values higher than those obtained by ALDOT. This was attributed to differences in density and applied stresses during testing. Very accurate regression models were developed to predict resilient modulus from confining stress, cyclic stress and moisture content.

Tests conducted on the asphalt mixtures indicated that the PG grade was not a significant factor in the dynamic modulus, while temperature, loading frequency, air void content and gradation were significant. A reasonably accurate non-linear regression equation was developed to predict dynamic modulus from the significant factors. This will be used to support the analysis of the field-determined moduli. It must be noted that the data and equations presented above were from a limited set of materials and may not be applicable to other sets of materials.

CHAPTER 4 – FWD TESTING AND BACKCALCULATION

INTRODUCTION

In the context of M-E design and analysis, field characterization of stiffness is important for a number of reasons. First, it characterizes the inherent variability of the pavement structure, in situ. This variability should be considered in any design or analysis approach. Second, the impact of environmental factors (i.e., temperature) can be investigated and quantified in terms of how the structure distributes loads under different conditions. Third, the effect of pavement damage on stiffness can be assessed.

To accomplish the field characterization, falling weight deflectometer (FWD) testing was conducted on a monthly basis at the Test Track. While the FWD testing approach is straightforward, backcalculation of the data to determine the pavement layer properties requires a great deal of care. The procedure requires a level of engineering judgment and understanding because a low error between predicted and measured deflections can be achieved from unreasonable moduli. This chapter details both the FWD testing scheme and the analyses conducted to determine the optimal backcalculation cross-section.

FWD APPARATUS AND TESTING SCHEME

ALDOT provided both the FWD and technical personnel for field testing. The FWD was a Dynatest 8000, pictured in Figure 4.1, with seven sensors spaced at 12 inches on center. The load plate, shown in Figure 4.2, had a radius of 5.91 in. and had a split configuration to ensure good seating on the pavement surface.

Figure 4.1 Dynatest 8000 Used at Test Track.

Figure 4.2 FWD Split Loading Plate.

Testing was conducted nearly every month once the test sections were opened to traffic. Table 4.1 lists the testing dates included with this report. It must be noted that due to scheduling conflicts and equipment problems, tests were not conducted in some months. Specifically, testing was not conducted in April/May/October 2004 and April/May/June 2005. Every effort should be made in future research cycles to ensure data are collected on a regular basis.

Table 4.1 FWD Testing Dates

Testing Dates
11/3/2003
12/15/2003
1/26/2004
2/23/2004
3/22/2004
6/14/2004
7/12/2004
8/2/2004
9/20/2004
11/1/2004
12/6/2004
1/10/2005
2/7/2005
3/21/2005
7/18/2005

For each date, tests were conducted at three random locations, listed in Table 4.2, in each test section. Recall from Chapter 2 that the thicknesses varied within each test section. This was taken into account during backcalculation by using the surveyed thickness at

each test location. Additionally, testing was to be conducted in both the inside and outside wheelpath at each random location. However, due to scheduling and equipment problems, both wheelpaths were not tested on every date. Each location was tested with two drops of an approximate 9,000 lb load.

Table 4.2 FWD Random Locations

Cell	Random Location	Distance from Start of Section, ft
N1	1	57
	2	94
	3	155
N2	1	43
	2	109
	3	163
N3	1	57
	2	93
	3	144
N4	1	28
	2	109
	3	175
N5	1	48
	2	115
	3	158
N6	1	37
	2	106
	3	164
N7	1	27
	2	76
	3	141
N8	1	50
	2	79
	3	165

Supplemental FWD testing was conducted on April 27, 2004 directly on top of embedded instrumentation in each test section. This was done, in part, to aid in determining the optimal cross-section for backcalculation. Pavement responses gathered under the FWD load were used as additional degrees of freedom in the backcalculation process which will be described later in the chapter. Within each test section, two drops of the 9,000 lb load were conducted on each pressure plate and two strain gauges (a longitudinal and transverse oriented gauge). Additional tests were conducted in sections N7 and N8 where there was instrumentation in both the inside and outside wheelpath. Figures 4.3 - 4.10 highlight the gauges subjected to the FWD load. While it was desirable to test in the center of the wheelpath, the selection of gauges was largely a function of which were operational at the time of testing. It is important to note that while the FWD load was dropped on top of individual gauges, responses were measured for the entire gauge array. This enabled strain and stress measurements at multiple offset distances from the center of the load. Further details regarding the instrumentation, and gauge labeling, has been documented elsewhere (Timm et al., 2004).

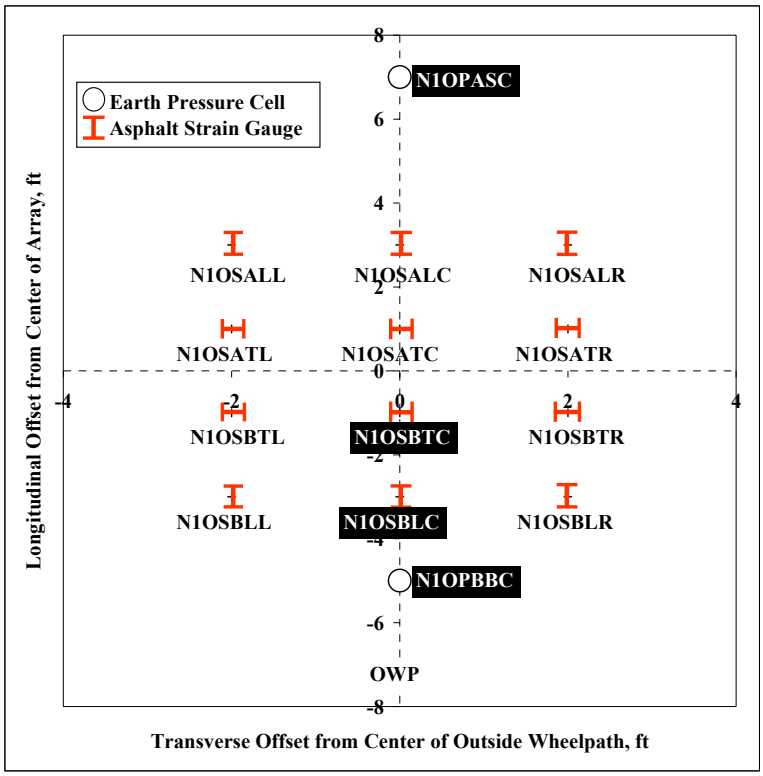

Figure 4.3 Section N1 FWD Test Locations.

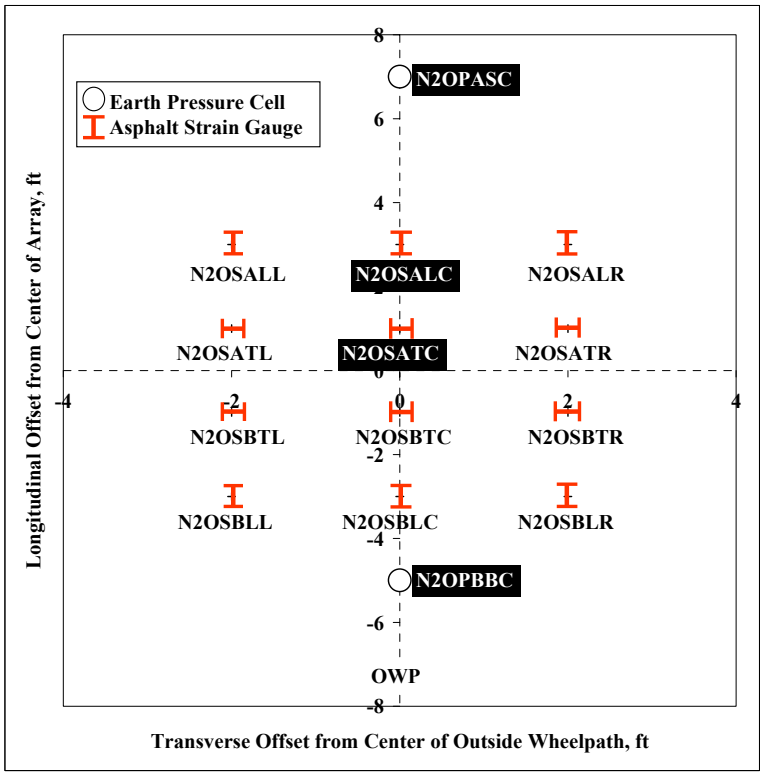

Figure 4.4 Section N2 FWD Test Locations.

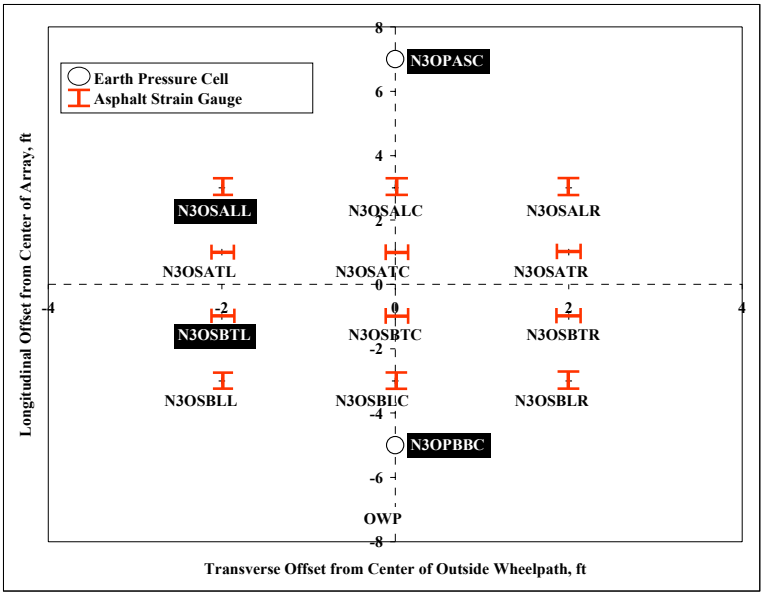

Figure 4.5 Section N3 FWD Test Locations.

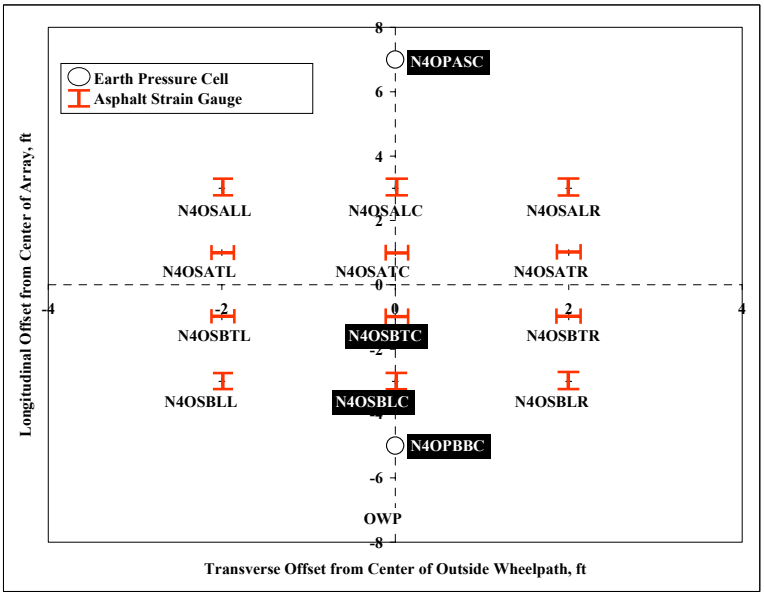

Figure 4.6 Section N4 FWD Test Locations.

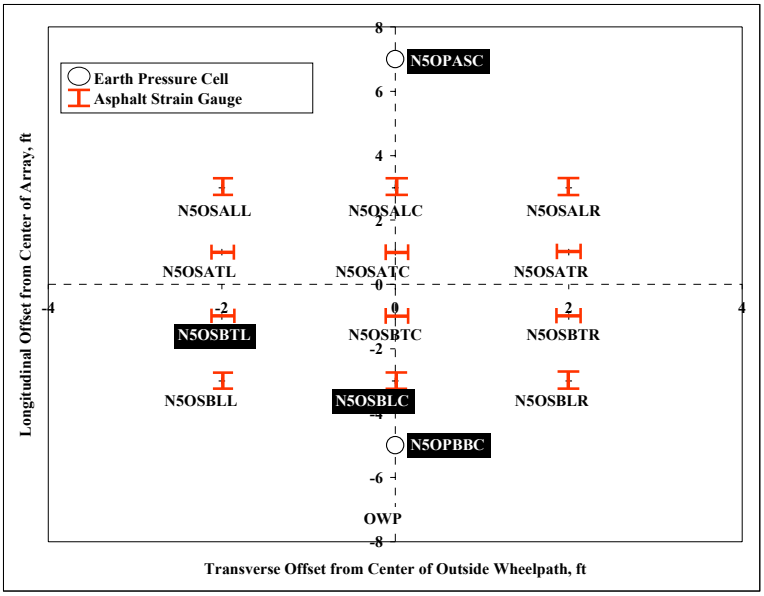

Figure 4.7 Section N5 FWD Test Locations.

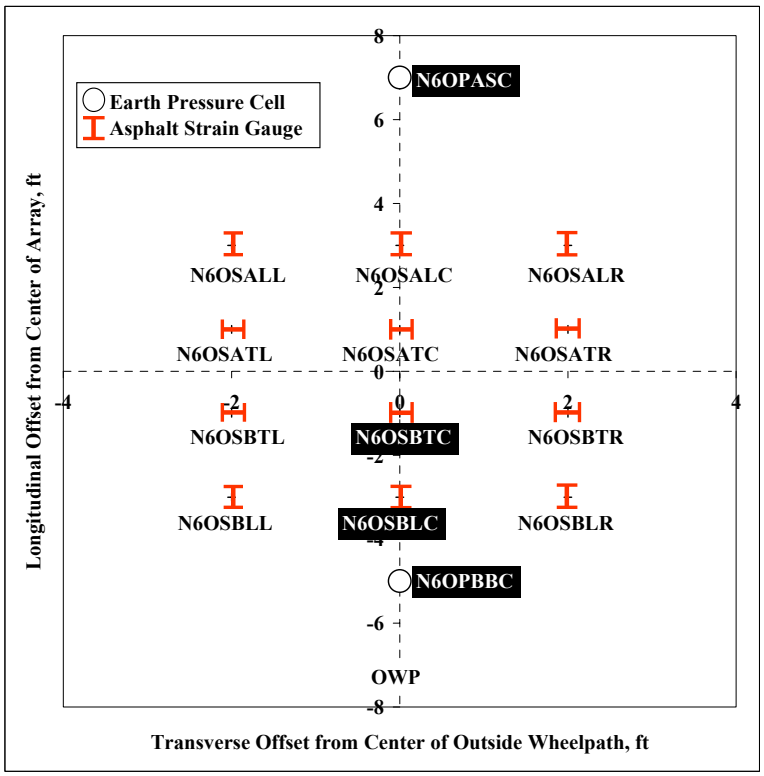

Figure 4.8 Section N6 FWD Test Locations.

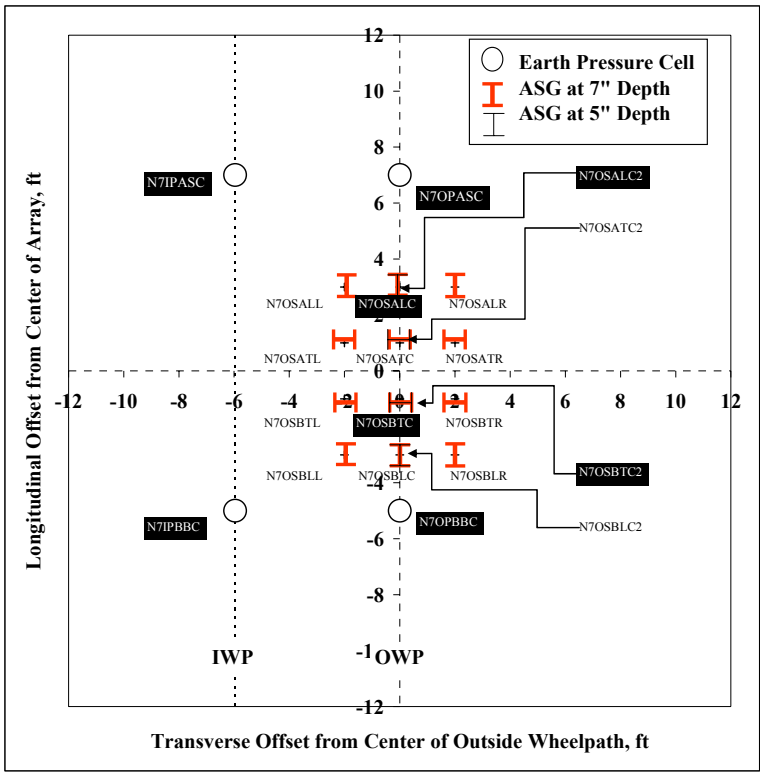

Figure 4.9 Section N7 FWD Test Locations.

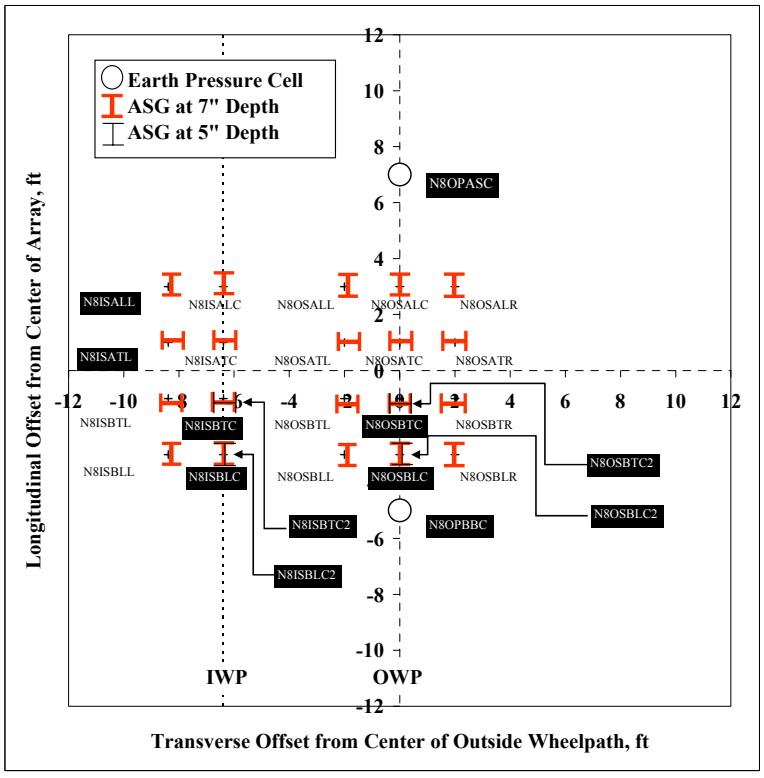

Figure 4.10 Section N8 FWD Test Locations.

DEVELOPMENT OF BACKCALCULATION CROSS-SECTION

As mentioned above, backcalculation of FWD data requires a great deal of care since erroneous layer stiffnesses can result from seemingly acceptable matches between predicted and measured surface deflections. Other issues surrounding backcalculation include difficulty in distinguishing layers with similar moduli and difficulty in distinguishing a thin layer from rest of structure.

With these issues in mind, a number of potential cross-sections were evaluated to determine the optimal cross-section for backcalculation. More specifically, four cross-sections were initially developed as trials for backcalculation in EVERCALC 5.0. The results from the different cross-sections were evaluated in terms of goodness of fit (root-mean-square of the error between measured and predicted deflections) and practical reasonableness. Data from the supplemental FWD testing on gauges were also used to determine the best cross-section. Potential cross-sections were eliminated based on a high degree of error or generation of results in conflict with other data sets. The details of this investigation are presented below.

The actual pavement cross-sections are illustrated in Figure 4.11. Notice that the sections have a varying HMA thickness followed by 6 in. of crushed granite granular base and fill material such that all the sections have the same total height. Further, all the sections were built on the same existing subgrade soil. From the actual cross-sections, a series of four trial cross-sections were developed. Pictured in Figure 4.12 and labeled X1 through X4, the four cross-sections represent different groupings of pavement layers. X1 is the closest match to the actual cross-section, with each of the component layers represented individually. X2 groups the granular base and fill into one layer, while X3 also groups these materials and considers a bedrock or stiff layer. Lastly, X4 groups the fill with the existing subgrade and considers the granular base as a separate layer.

Since the backcalculation process is very time and computationally intensive, it was decided to select only a few dates on which to determine the optimal cross-section. The dates were selected to represent a range of temperatures and are listed in Table 4.3. After the optimal cross-section was determined, backcalculation was conducted for all the testing dates listed in Table 4.1.

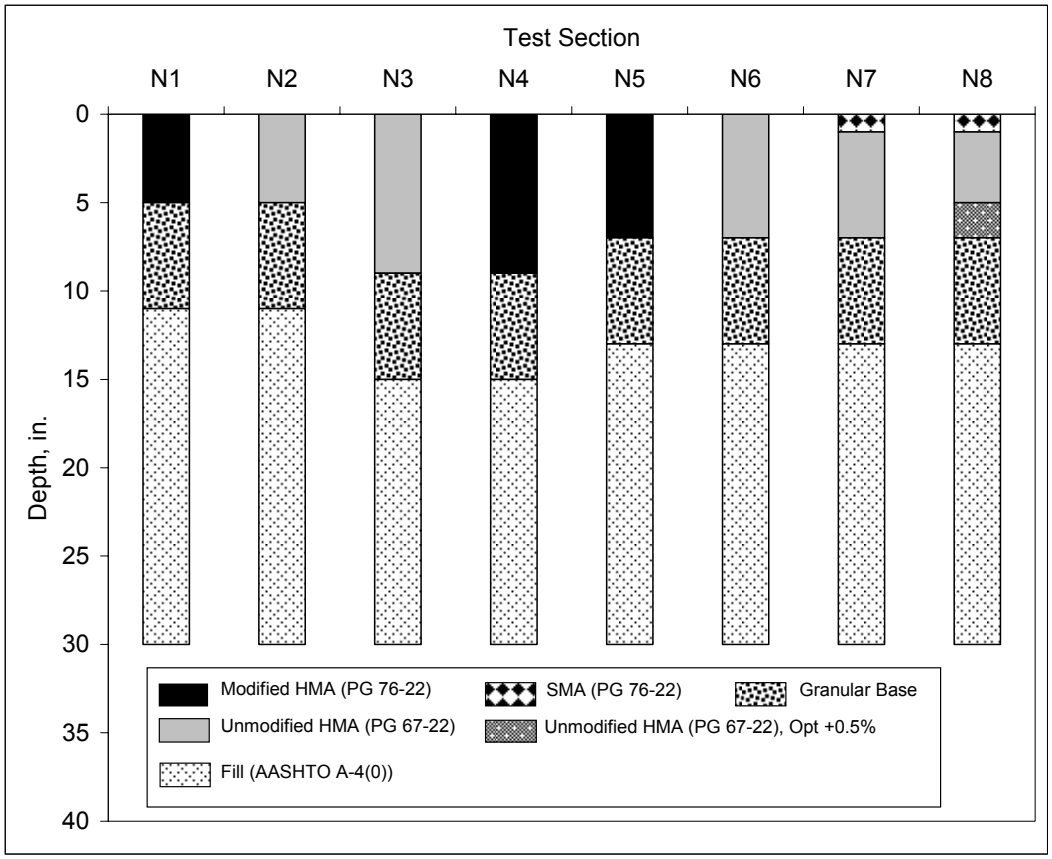

Figure 4.11 Actual Pavement Cross-sections.

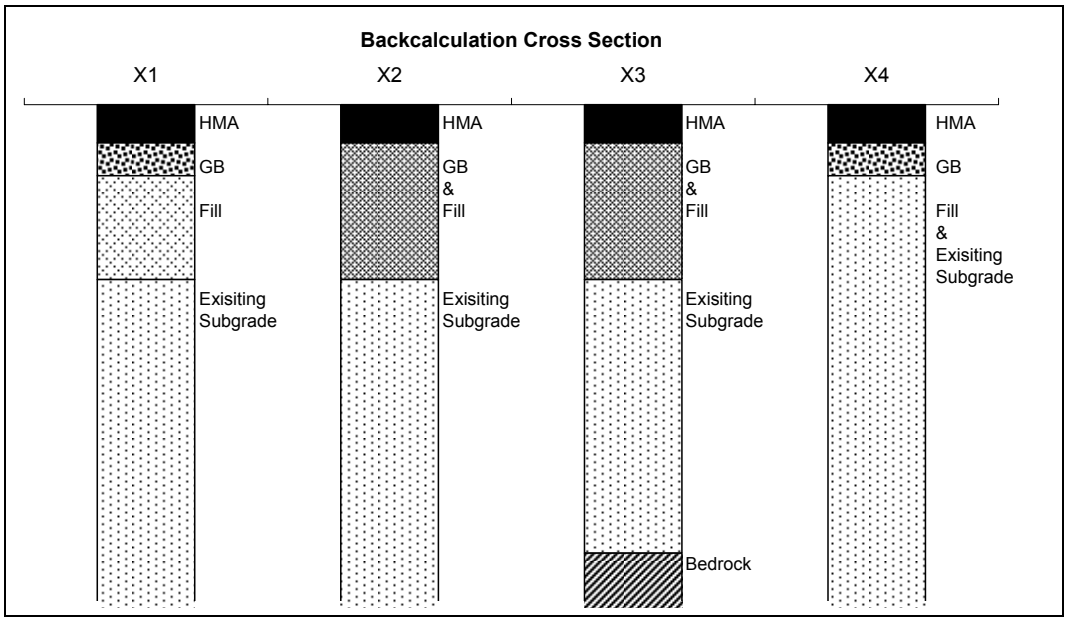

Figure 4.12 Backcalculation Trial Cross-sections.

Table 4.3 FWD Dates Used in Optimal Cross-Section Determination

FWD Dates
12/15/2003
3/22/2004
6/14/2004
9/20/2004

After conducting backcalculation on each of the eight test sections using all four of the potential cross-sections, the computed root mean square errors (RMSE) were tabulated. Figure 4.13 shows the cumulative distribution of the error for each cross-section. X3, which was the only cross-section with bedrock, showed by far the greatest error. Approximately 70% of the backcalculation solutions generated by the other three were below 5% RMSE, which is a common threshold for acceptance. The data shown in Figure 4.13 clearly eliminated X3 from the potential cross-sections due to the unacceptable error generated. However, the data presented did not distinguish between the other cross-sections. In addition, a conclusion regarding the optimal cross-section should not be made solely on the error produced.

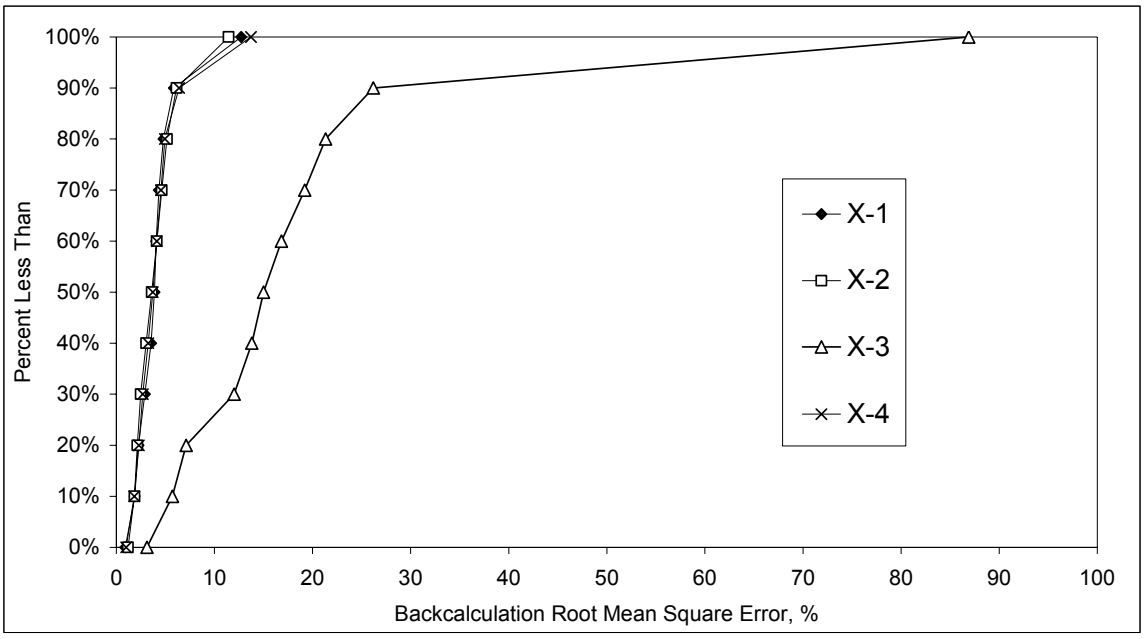

Figure 4.13 RMSE Range for Each Cross-section.

In further analysis, the computed HMA moduli were plotted against the recorded mid-depth temperature at the time of testing. Shown in Figure 4.14, X3 generates unreasonably low HMA moduli at higher temperatures. Considering the other three cross-sections, the moduli are very similar. Based upon the high error shown in Figure 4.13 and the unreasonable stiffness values in Figure 4.14, X3 was eliminated as a viable cross-section for backcalculation. Also, the north tangent at the Test Track was a fill section; therefore, it was unlikely that bedrock or some other stiff layer was present.

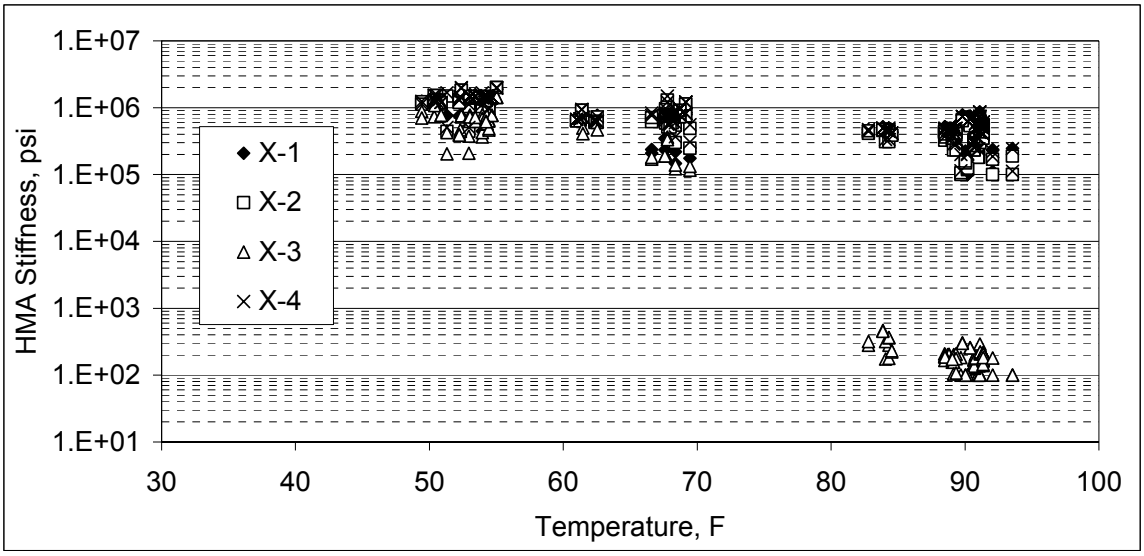

Figure 4.14 HMA Modulus versus Temperature.

The next phase of the investigation examined the calculated granular base, fill material and existing subgrade moduli for X1. The results are shown by section and date in Figures 4.15, 4.16 and 4.17 for the base, fill and subgrade, respectively. The subgrade moduli (Figure 4.17) appeared very consistent between test sections. The moduli ranged from 20,000 to 30,000 psi and were similar to the subgrade moduli obtained from the 2000 Test Track (Timm and Jess, 2005). However, the granular base and fill material moduli tended to fluctuate wildly and generated very low values for the granular base on the two latter dates. It must be noted that some approaches to backcalculation would fix a narrower limits for the material properties in backcalculation. For example, the granular base may be limited to a range of 20,000 to 40,000 psi. That was not done here since it artificially calculates backcalculated values in a pre-determined range. Rather, an approach was take to examine RMSE and the magnitude of the resulting layer properties in the context of reasonableness to arrive at a conclusion. The limits placed on the base layer were 1,000 psi to 50,000 psi which were considered extreme boundaries. That having been said, it appeared when examining Figures 4.15 and 4.16, that the granular base and fill material moduli were compensating for one another. The granular base modulus was higher for the first two dates, while the fill material was lower. The opposite was true for the second two dates. Recall from the laboratory data presented in Chapter 3, that the fill material and granular base moduli were somewhat similar with the fill modulus slightly greater than the granular base. Since the moduli are similar, it follows reason that trying to separate these layers in backcalculation could generate erratic results. It must also be noted, for sections N4 – N7 on 9/20/2004, that the fill material moduli reached the upper limit of 50,000 psi during backcalculation. Based upon these observations, X1 was eliminated as a viable cross-section.

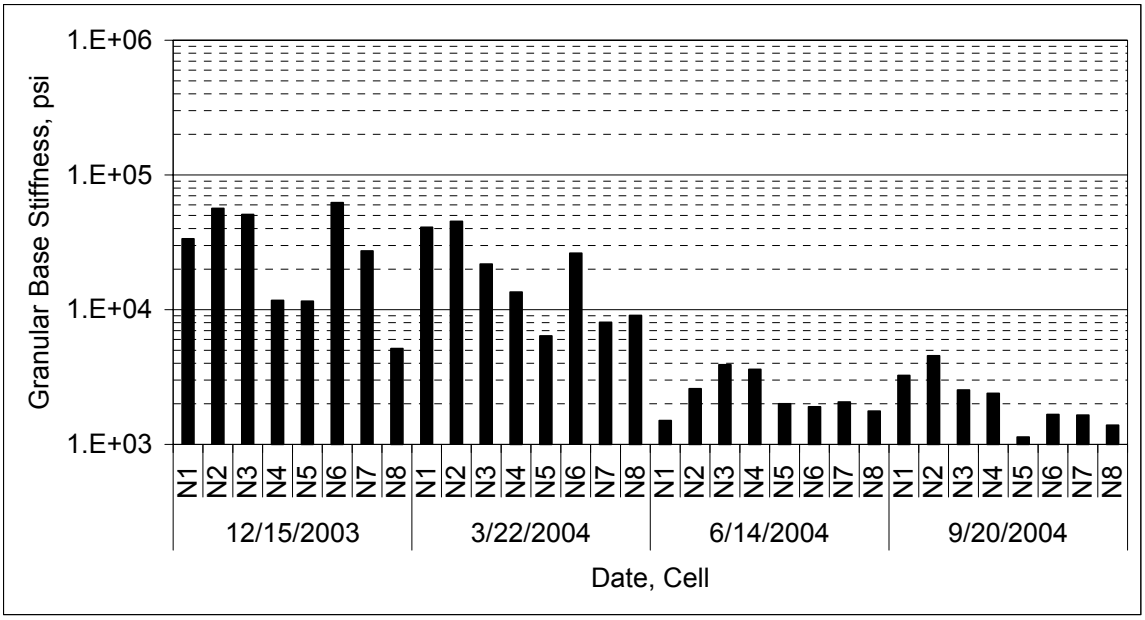

Figure 4.15 X1 Granular Base Modulus.

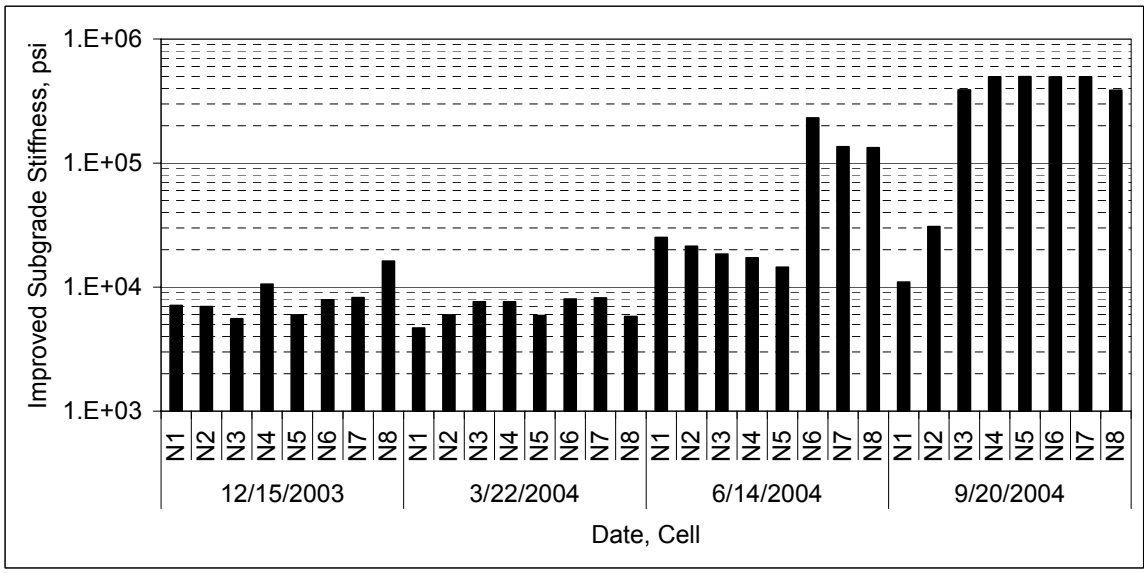

Figure 4.16 X1 Fill Material Modulus.

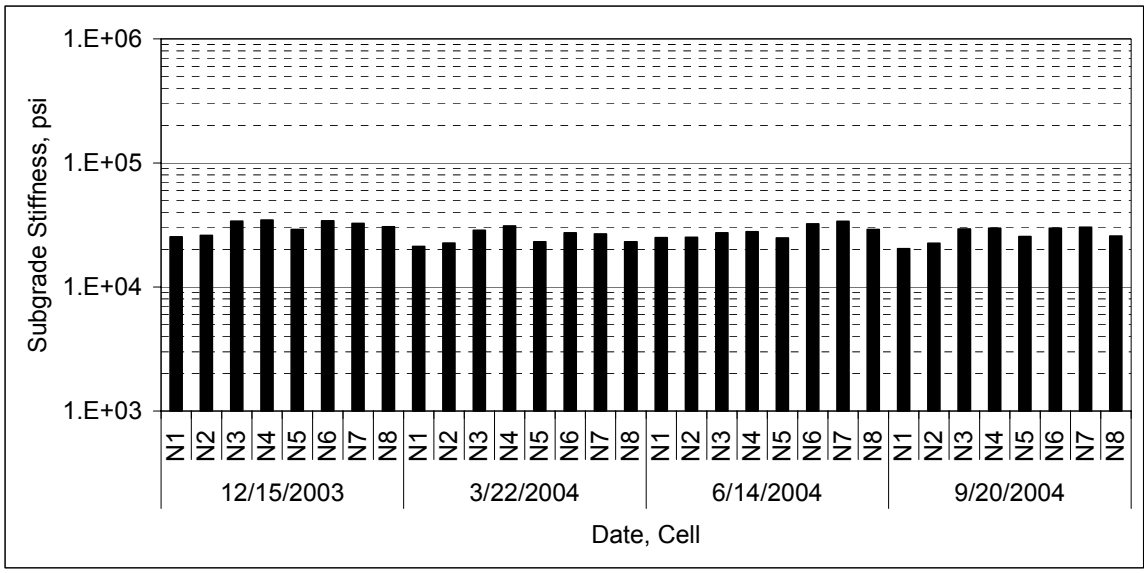

Figure 4.17 X1 Subgrade Modulus.

With cross-sections X1 and X3 removed from consideration, the investigation focused on X2 (granular base and fill combined) and X4 (fill and subgrade combined). As shown in Figure 4.13, there did not appear to be differences in the RMSE for the two cross-sections. In addition, Figure 4.14 indicated that there was not large difference in computed HMA stiffness either. Figure 4.18 compares the computed combined fill and subgrade stiffness from X4 against the subgrade stiffness from X2. The figure shows slightly higher moduli for X4 compared to X2. For practical purposes, the stiffness data sets were equivalent. The difference in X2 versus X4 lies in the layer above or combined granular base and fill layer from X2 versus the granular base layer from X4. The backcalculation results of these layers are summarized in Figures 4.19 and 4.20 and are discussed further below.

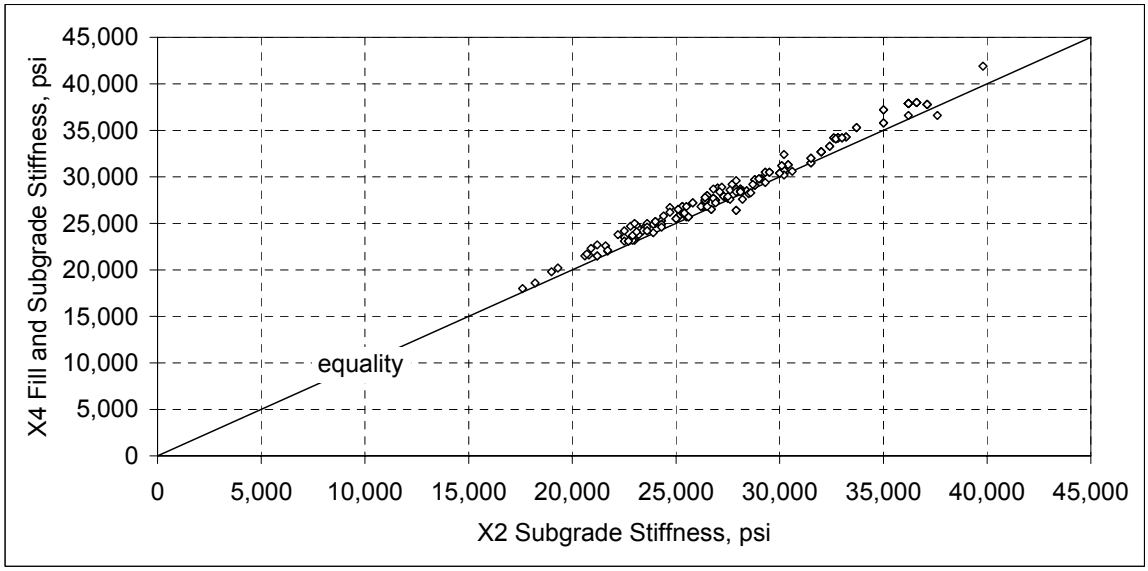

Figure 4.18 X4 and X2 Bottom Layer Stiffness Comparison.

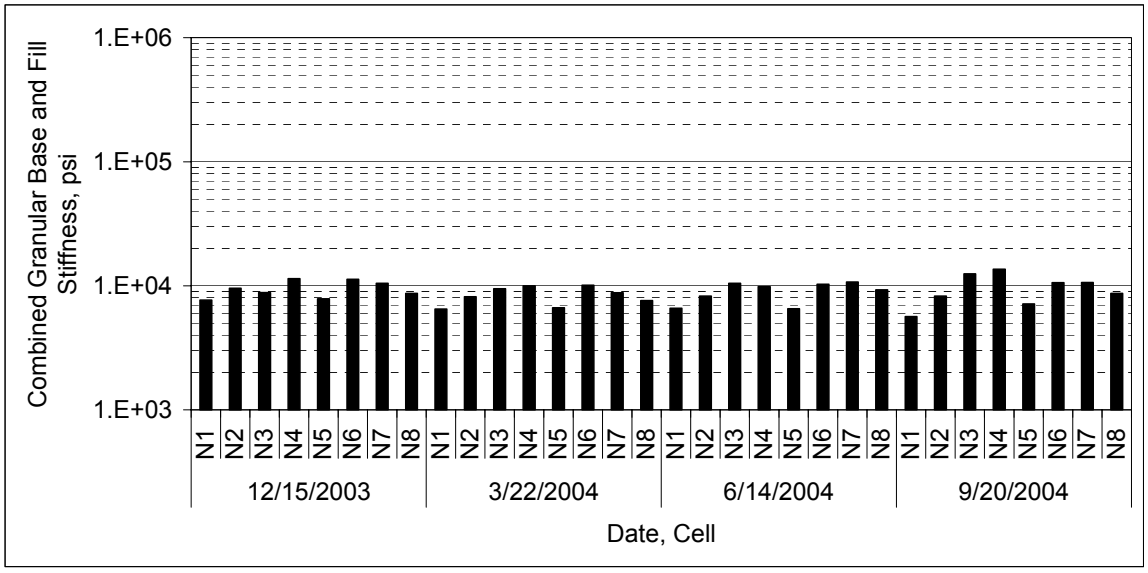

Figure 4.19 X2 Combined Granular Base and Fill Stiffness.

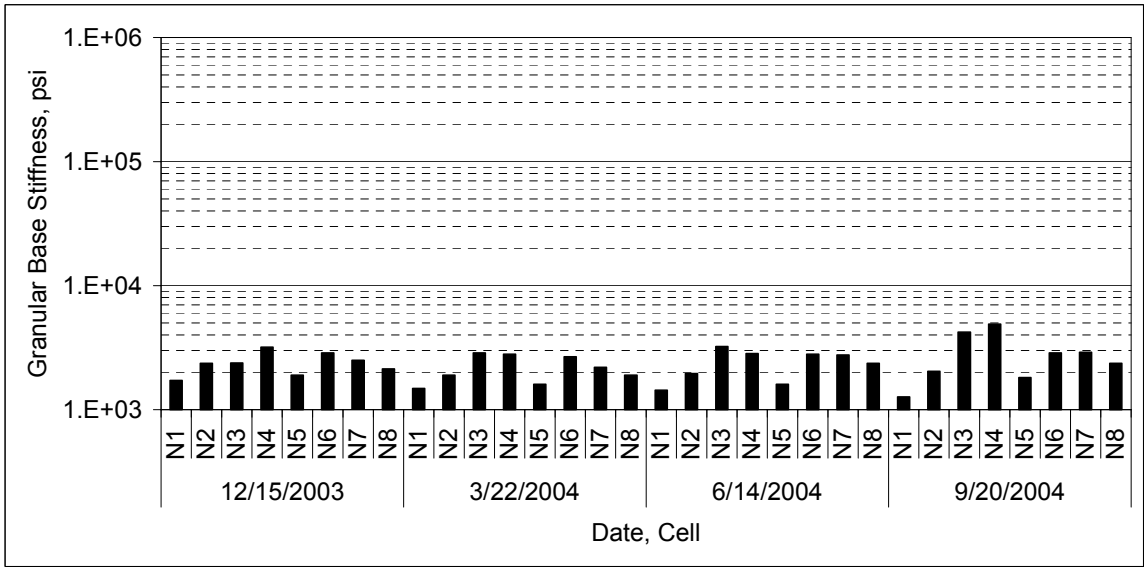

Figure 4.20 X4 Granular Base Stiffness.

A number of observations can be made regarding Figures 4.19 and 4.20. First, the granular base moduli from X4 (Figure 4.20) appear extremely low with nearly all the values below 3,000 psi. Recall from the ALDOT lab study described in Chapter 3, the resilient moduli for the granular base ranged from 4,000 to 9,000 psi (Figure 3.5). The lab values were not high by typical granular base standards, but they were certainly higher than the moduli presented in Figure 4.20. The Vulcan results were considerably higher. Second, the moduli presented in Figure 4.19 appear to agree more with the granular base laboratory data, ranging from 5,000 to 15,000 psi. Given these observations, cross-section X2 produced a base stiffness that agreed better with the

laboratory data than did X4. Further, because all else between X2 and X4 were essentially equal, X2 appeared to be the optimal cross-section for backcalculation. A final comparison of X2 and X4 was performed using data collected from the embedded instrumentation under the FWD load. This was done for two reasons. First, an additional check was needed to be certain X2 was a better representation of the actual pavement cross-section than X4. Second, the check served to validate the backcalculation procedure (i.e., it could have been that both X2 and X4 were equally incorrect).

Figure 4.21 illustrates an example of the strain response measurements made under the FWD load. The first peak of each trace indicates the primary FWD impact with residual peaks as the load settles onto the pavement. In this example, the load was dropped on the longitudinal gauge in the center of the wheelpath, noted by BLC. The other two traces represent another longitudinal gauge (BLR) 2 ft to the right of the load center and a transverse gauge in the wheelpath but 2 ft away from BLR (BTC). Strain readings were recorded from the baseline to the first peak of each trace.

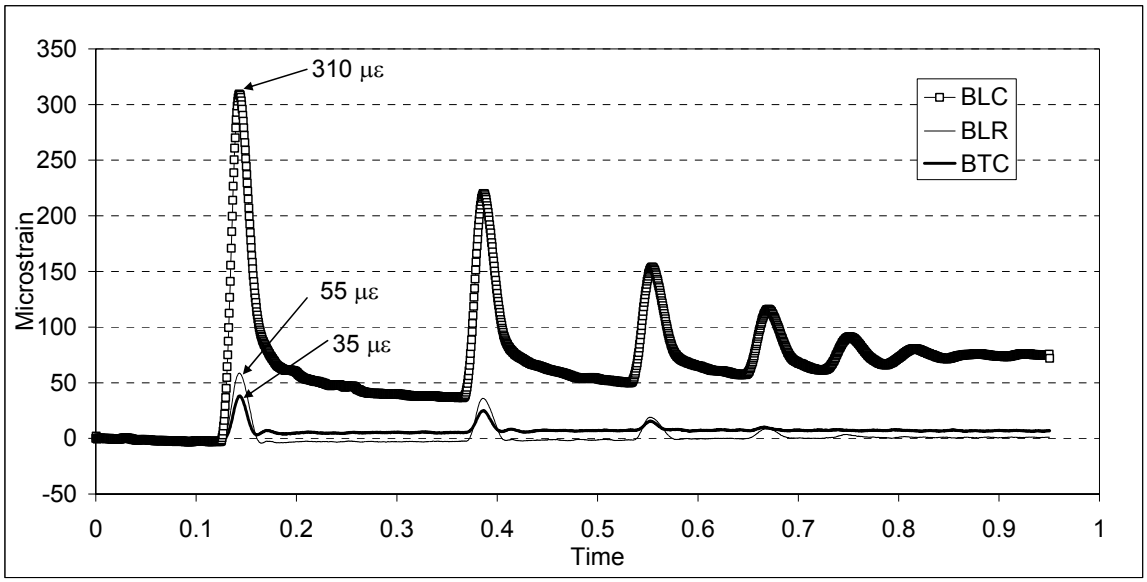

Figure 4.21 Example of Strain Response Under FWD Load.

For each drop of the FWD, backcalculated moduli were obtained for X2 and X4. The layer moduli and corresponding thicknesses were then input to WESLEA for Windows 3.0, a forward calculation layered elastic mechanistic pavement model. The contact pressure and impact load recorded by the FWD were also input to WESLEA. Finally, the coordinates of each active gauge in the array were entered as evaluation locations so that comparisons could be made between the measured pavement response from the strain gauges and the computed strain, using the backcalculated moduli, from WESLEA.

Figure 4.22 summarizes the results for X2 and X4 with respect to strain of the HMA layer. For both cross-sections, the predicted strain using the backcalculated layer moduli was very similar (within 20%) to the field-measured strain. Generally speaking, these results are very good and indicate that layered elastic analysis gives a reasonable approximation of the response of what is actually a pavement structure made up of

various and complex materials under dynamic loading. However, the results do not indicate which cross-section is more accurate. That issue is settled by examining the pressure responses, as discussed below.

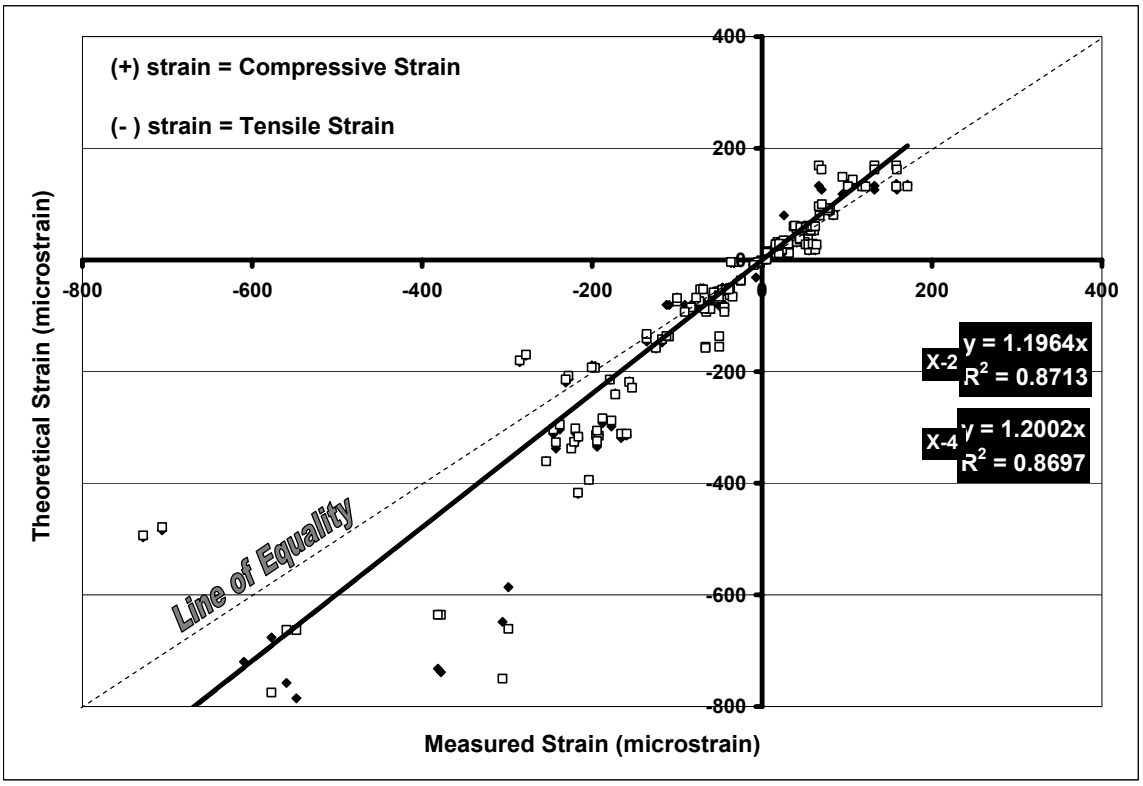

Figure 4.22 HMA Strain Comparison.

Figure 4.23 summarizes the vertical pressure prediction and measurement comparison for both X2 and X4. Additionally, the pressures pertain to both the top of the actual granular base and fill material layers, respectively. Clearly, X2 provides a better match between measured and theoretical responses. Considering all the data, X2 generates pressures within 30% of measured, which is tolerable. Based upon the data presented in Figure 4.23 and the fact that the X2 combined base/fill material moduli (Figure 4.19) are more consistent with laboratory determined base values, X2 was recommended as the optimal cross-section for further FWD analysis. The cross-section of X2 is presented again in Figure 4.24.

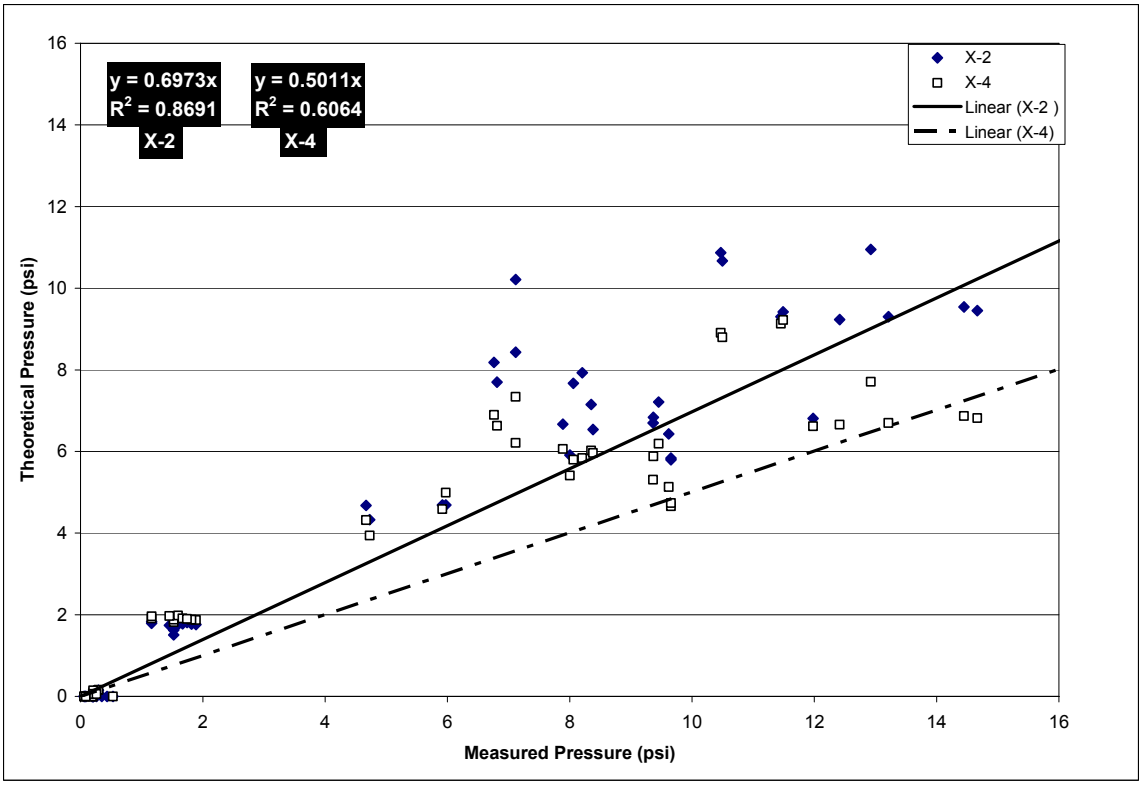

Figure 4.23 Vertical Pressure Comparison.

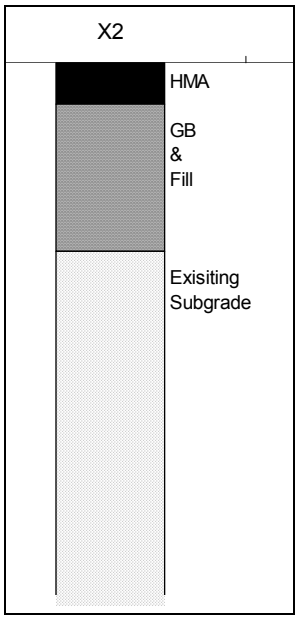

Figure 4.24 Recommended Backcalculation Cross-section.

SUMMARY

This chapter detailed the FWD testing scheme employed as part of the NCAT Test Track Structural Study. While the testing was straightforward, significant effort was put forth in determining the best cross-section to use in backcalculation. An assessment of the

solution error, comparisons to laboratory data, comparisons to measured pavement responses and engineering judgment were used to identify the best cross-section for the Structural Study. It was found that a three layer structure comprised of HMA over granular base/fill over the existing subgrade produced solutions with acceptably low error, the best match with field results and reasonable moduli. This cross-section, pictured in Figure 4.24, formed the basis for the extensive field characterization described in the next chapter.

CHAPTER 5 – FIELD CHARACTERIZATION OF STIFFNESS

INTRODUCTION

The FWD testing and backcalculation schemes were presented in the previous chapter, and it was shown that the best pavement cross section for backcalculation consisted of HMA over a combined granular base/fill layer on top of the existing subgrade. While the previous chapter examined FWD data from only four dates, this chapter presents the backcalculation results from all the testing dates to characterize seasonal trends in the stiffness of the pavement structure. Statistical analyses were conducted to look for differences among the sections and recommendations are made regarding overall characterization of the stiffness properties for each pavement layer.

SEASONAL AND CRACKING EFFECTS ON MODULI

Figures 5.1 through 5.3 illustrate the seasonal effects on HMA, granular base/fill and subgrade moduli, respectively. All the test locations (i.e., station and wheelpath) and FWD drops (i.e., two drops per location) are represented in these plots. Therefore, the plots illustrate each and every FWD test conducted as part of the structural experiment. Figures 5.4 through 5.6 are based on the same data sets, but data pertaining to testing dates after cracking was observed on individual sections were removed. Table 5.1 lists these cracking cut-off dates. From the data, the following observations were made.

The HMA was most affected by seasonal changes, which was expected since it is well known that HMA stiffness has a strong dependence upon temperature. The underlying pavement layers were not as severely affected by changes in season. This was especially the case for the existing subgrade, which maintained a modulus near 30,000 psi throughout the two-year research cycle.

There were no clear distinctions between test sections, based upon moduli, for any of the three pavement layers. This was expected for the granular base/fill and subgrade layers since they were made of the same materials and constructed according to the same specifications, though of varying thickness. This was also expected for the HMA because the results of dynamic modulus testing in the laboratory (Chapter 3) showed that the different mixtures were not statistically different except in the highest temperature ranges.

The effects of pavement damage on backcalculated moduli were clearly evident in the HMA and granular base/fill layers. For example, Figure 5.1 shows that the HMA stiffness was much lower for the latter testing dates in sections N1, N2 and N8. Figure 5.4, which removed the dates with cracking, shows a much more consistent seasonal trend. Once cracking was observed, the HMA layer was no longer intact, and thus registers a lower stiffness. In addition, the FWD testing is somewhat questionable on a cracked pavement because the load plate may not seat well and it is possible that a deflection sensor may lie on or very near a crack. A similar observation was noted in comparing the granular base/fill data between Figures 5.2 and 5.5; especially between July and October, 2004. The later dates also have lower stiffness values for the cracked

sections, but is not as apparent due to the log-scale. The lower values were due to the cracking in the HMA layer also adversely affecting the integrity of the underlying base/fill layer. It was observed that as the cracking progressed, water easily infiltrated into the base and caused pumping of the fines from the base/fill material. The existing subgrade was not so affected by cracking of the HMA because it was deep enough in the pavement structure. These observations highlight the need, in further studies, to conduct more testing prior to the application of traffic and ensuing pavement damage to firmly characterize the intact pavement structure. For example, the cut-off date for section N1 was the end of March (Table 5.1). Therefore, the spring and summer months were not accurately captured for that test section.

The above discussion characterized general seasonal trends, and the effects of cracking on the stiffness data. While this provides an overall view of the layer properties, further investigation into spatial variability and quantification of stiffness versus temperature are warranted. These topics are discussed in the following sections. It must also be clearly noted that all the following results and discussion pertain to backcalculated stiffnesses obtained from intact pavement sections.

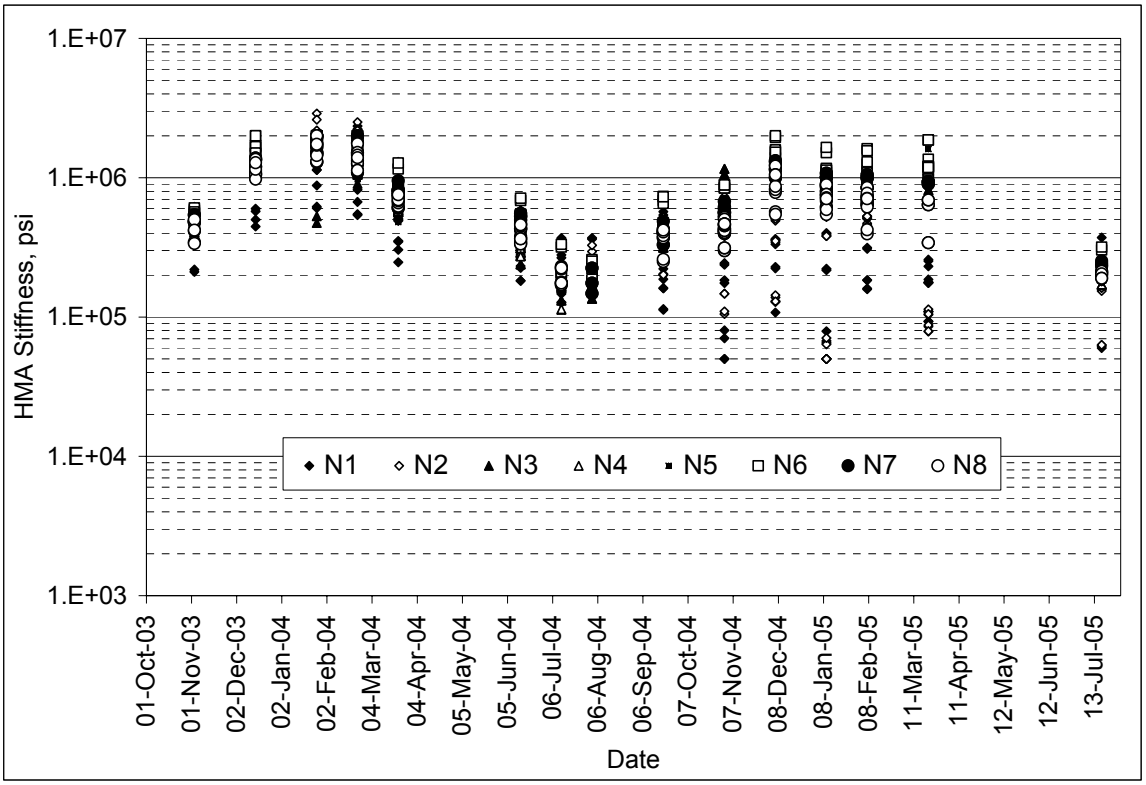

Figure 5.1 Backcalculated HMA Moduli versus Date.

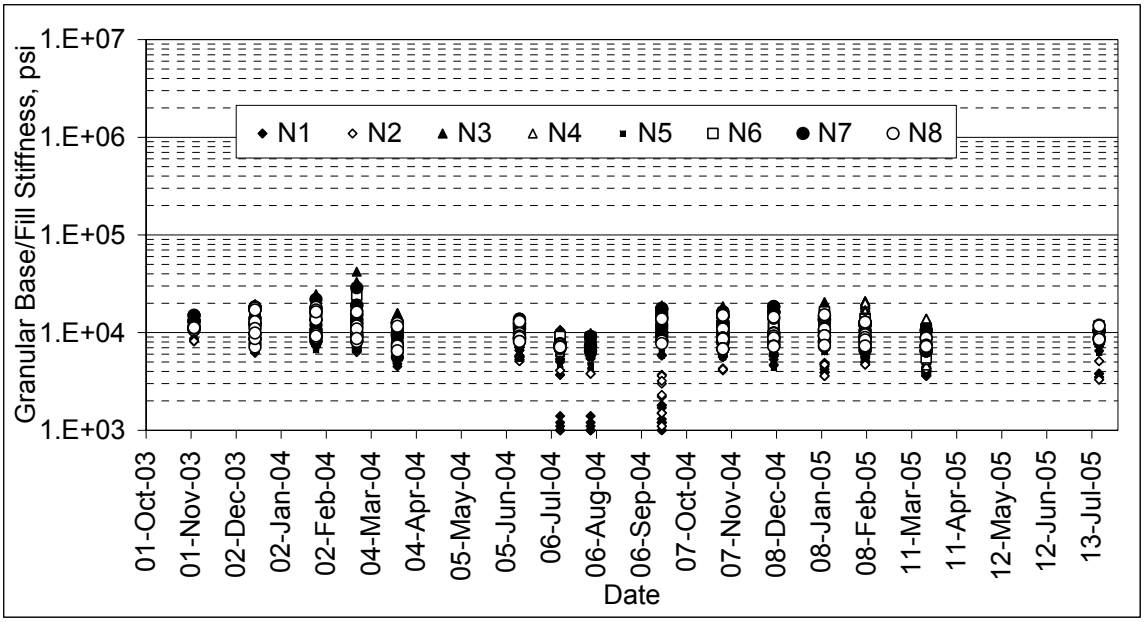

Figure 5.2 Backcalculated Granular Base/Fill Moduli versus Date.

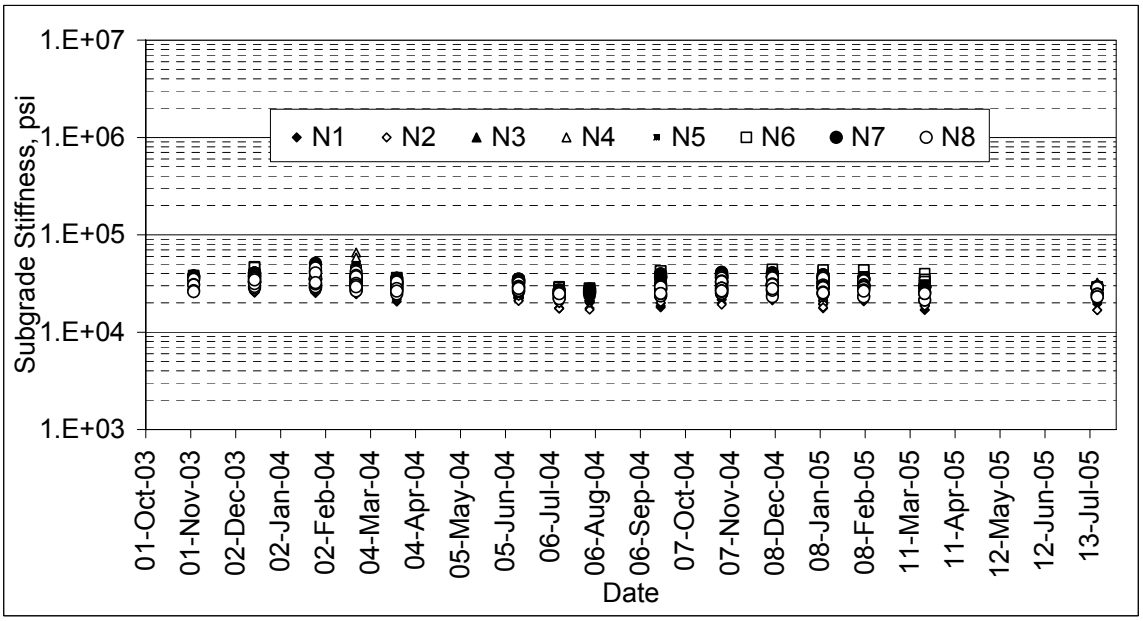

Figure 5.3 Backcalculated Existing Subgrade Moduli versus Date.

Table 5.1 FWD Cracking Cut-Off Dates.

Section	Last FWD Date with No Cracking
N1	3/22/2004
N2	6/14/2004
N3	Cracking not yet observed
N4	Cracking not yet observed
N5	2/7/2005
N6	2/7/2005
N7	2/7/2005
N8	7/12/2004

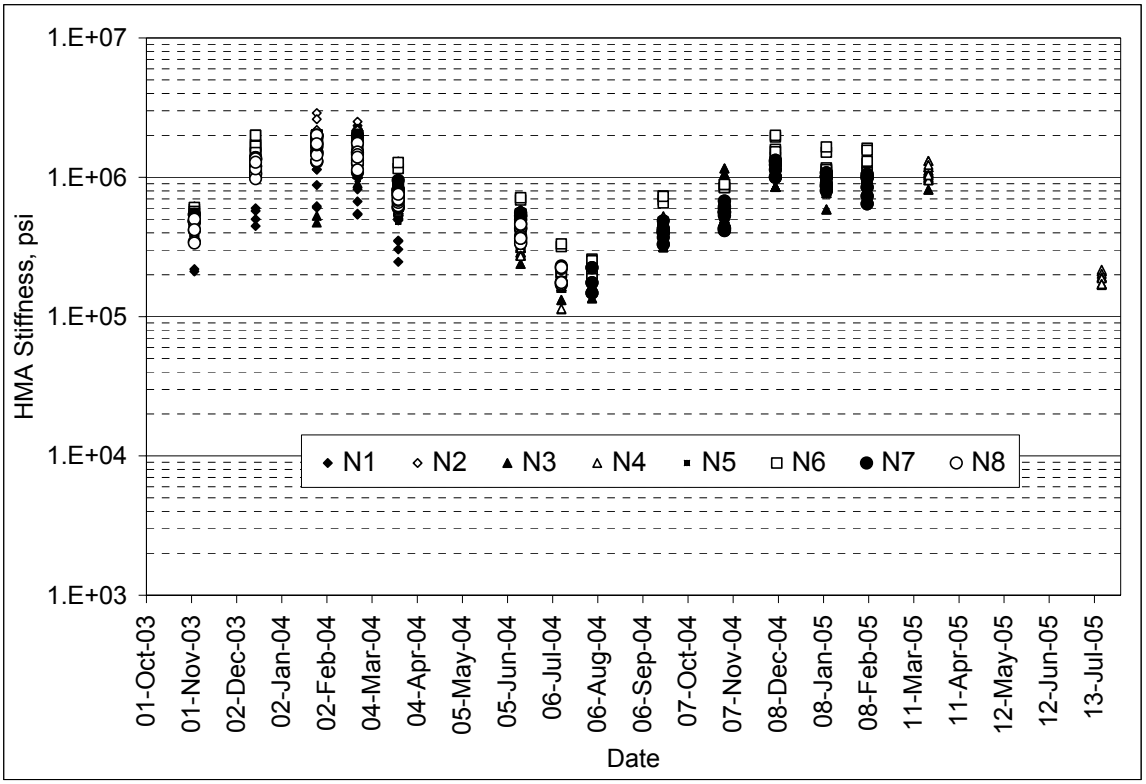

Figure 5.4 Backcalculated HMA Moduli versus Date (Dates with Cracking Removed).

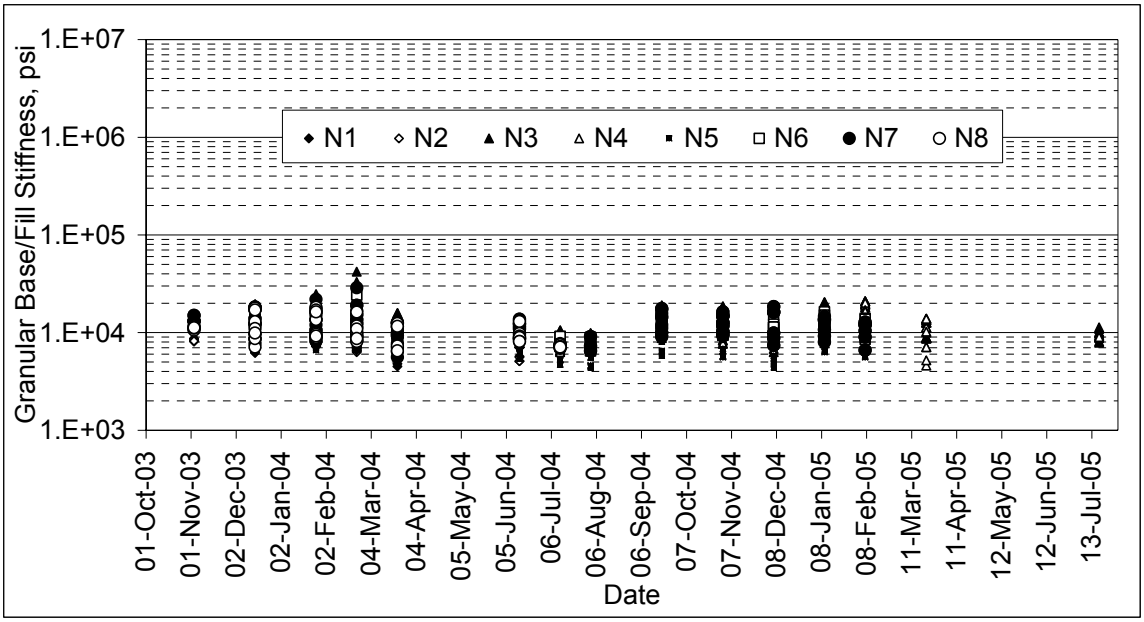

Figure 5.5 Backcalculated Granular Base/Fill Moduli versus Date (Dates with Cracking Removed).

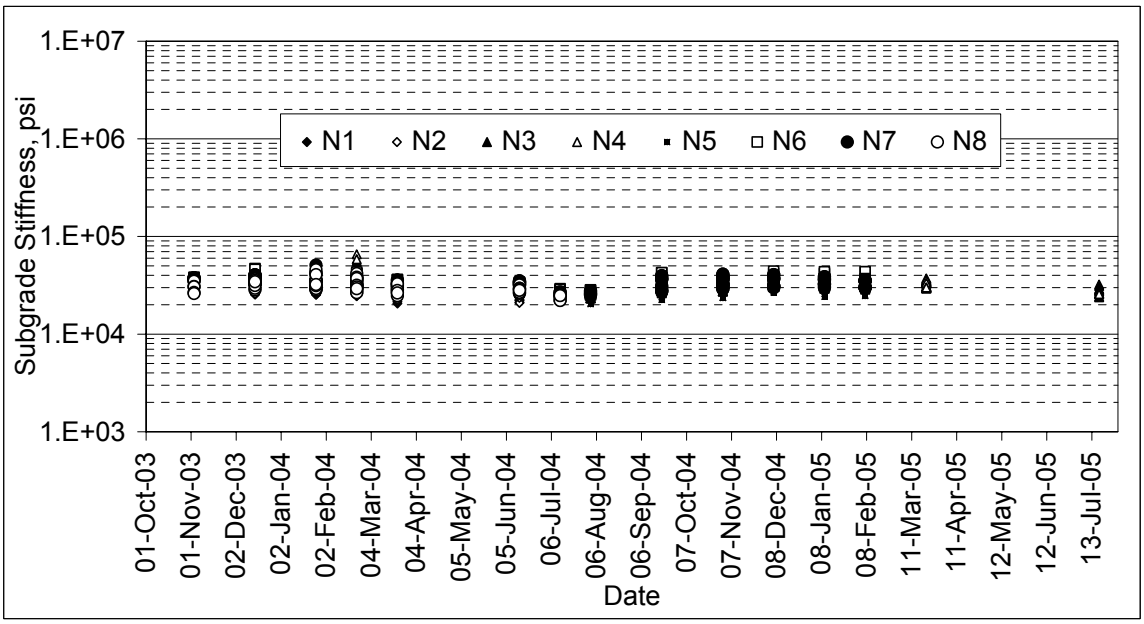

Figure 5.6 Backcalculated Existing Subgrade Moduli versus Date (Dates with Cracking Removed).

GRANULAR BASE/FILL LAYER CHARACTERIZATION

With regard to the granular base/fill layer stiffness, there were some key questions that required investigation. These included:

1. Are there significant differences between test sections?
2. Are there significant differences between testing dates, reflecting seasonal changes?
3. Are there significant differences between the inside and outside wheelpath?

Answering these questions will help develop a better understanding of the pavement sections themselves and provide guidance for other aspects of M-E design and analysis of the test sections.

Granular Base/Fill – Section Characterization

An ANOVA was conducted, at a 95% confidence level, to examine differences among the test sections in terms of granular base/fill modulus. Figure 5.7 illustrates the statistical data used in the ANOVA. While the null hypothesis was rejected that all sections were equivalent (F-statistic = 39.75), there did not appear to be obvious trends in the data. For example, the sections could not be statistically grouped into thin (N1-N2), medium (N5-N8) or thick (N3-N4). The differences, then, were simply attributed to natural spatial variability, not necessarily dependent upon particular pavement parameters. However, it is recommended that section-specific moduli be used for M-E analysis.

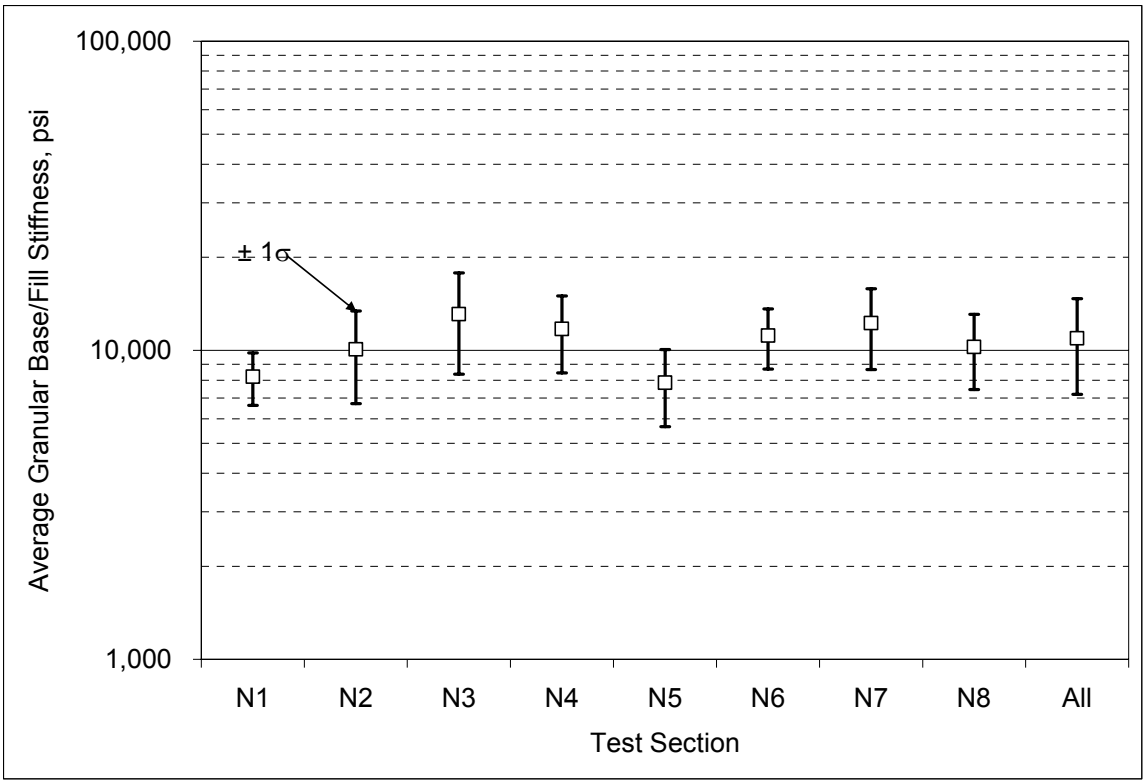

Figure 5.7 Backcalculated Granular Base/Fill Modulus – By Section.

Granular Base/Fill – Seasonal Characterization

Examination of the seasonal granular base/fill moduli with all sections grouped together, as shown in Figure 5.8, seemed to indicate a reduction in stiffness during the warmer parts of the year. ANOVA was again conducted and the differences between average moduli on each date were shown to be significant at the 95% confidence level (F-statistic = 10.57). During these warm periods, the HMA stiffness was also lower (Figure 5.4) which would correspond to a higher stress state in the underlying base/fill material. Recall from the laboratory study (Chapter 3) that higher stress states generally

corresponded to higher moduli in both the granular base and fill materials. Therefore, it was unexpected that the summertime moduli in the granular base/fill should be lower than other times of the year. However, the lower moduli can be explained as an artifact of the backcalculation process. Simply stated, it appears that EVERCALC attributed the increased deflection at warmer temperatures to slight reductions in granular base/fill modulus in addition to reductions in HMA modulus. A reasonable approach to mitigating these effects is to establish an annual average based upon testing at regular intervals.

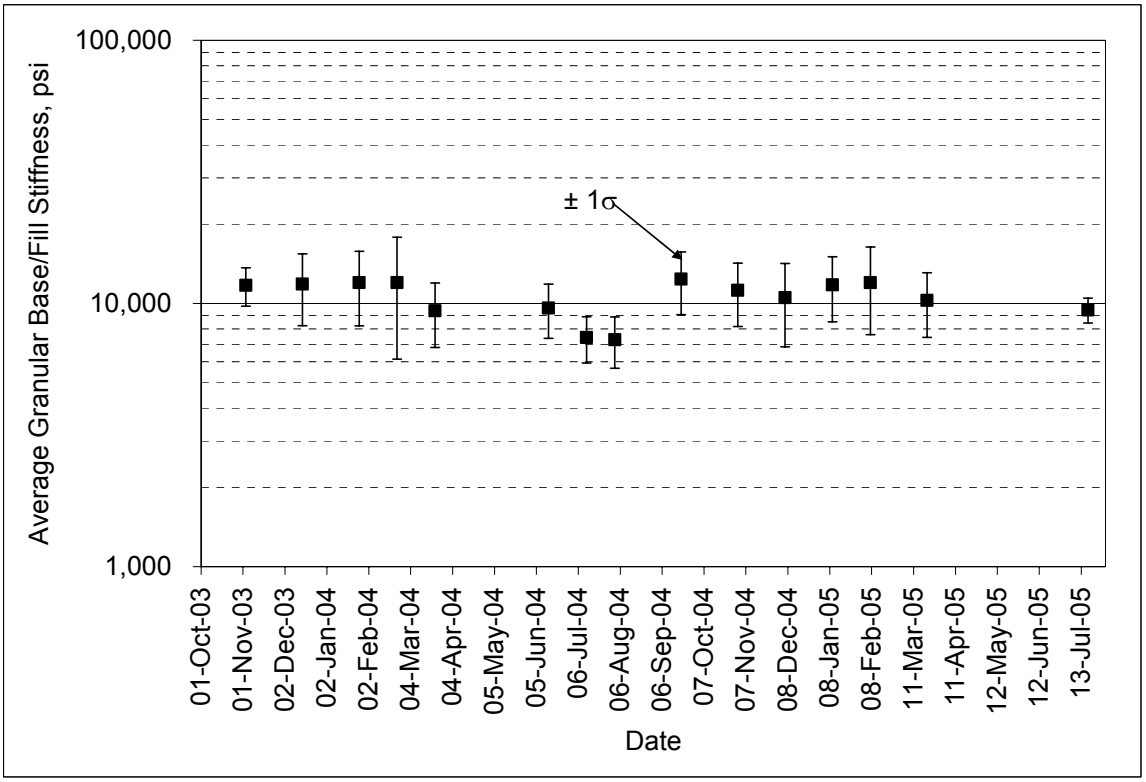

Figure 5.8 Backcalculated Granular Base/Fill Modulus – By Date.

Granular Base/Fill – Wheelpath Characterization

The granular base/fill moduli, divided into respective wheelpaths for all the sections, are presented in Figure 5.9. The ANOVA demonstrated that the inside wheelpath registered statistically significantly higher moduli values than the outside wheelpath (95% confidence level; F-statistic = 159.03). Though the actual difference in average stiffness between wheelpaths (approximately 3,000 psi) may not appear to be practically significant, it will be shown in the following sections that the outside wheelpath was consistently lower for each of the pavement layers. The reason for higher stiffnesses in the inside wheelpath were not immediately clear, but it was consistent with the field observation at the Test Track that the pavement distresses tended to be higher in the outside than the inside wheelpath. This is also the case for most open access facilities. Also, the inside lane which was left in place for the Structural Study could have affected the deflection testing in the inside wheelpath of the outside lane. For general M-E design and analysis, one would consider the two wheelpaths together. However, for the

Structural Study, it is recommended that the differences between the outside and inside wheelpaths be taken into account when considering the layer stiffnesses with respect to the embedded instrumentation.

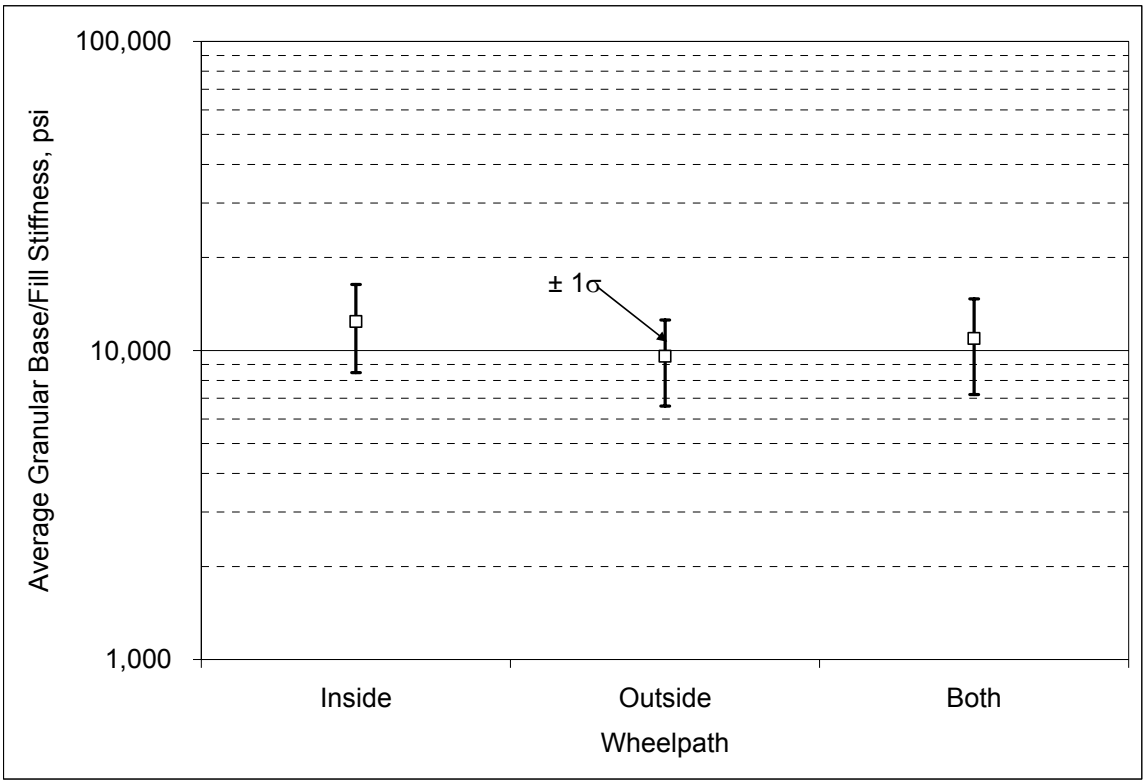

Figure 5.9 Backcalculated Granular Base/Fill Modulus – By Wheelpath.

SUBGRADE CHARACTERIZATION

Following the approach described above, the subgrade moduli were analyzed in terms of differences by section, by date and by wheelpath. The results are summarized and discussed below.

Subgrade – Section Characterization

The average subgrade modulus and standard deviation, for each test section, are shown in Figure 5.10. It is notable that these moduli are significantly higher than the granular base/fill layer (Figure 5.7). Specifically, the average subgrade stiffness between all sections was 32,000 psi while the average granular base/fill stiffness was 11,000 psi. Typically, one expects the granular base to have a higher stiffness than the underlying material. However, this was not the case at the Test Track. It must be recalled that the so-called "subgrade" in Sections N1-N8 is a constructed embankment left in place from the 2000 Test Track. Also, similar stiffnesses were determined for this material from FWD Testing during the 2000 study (Timm and Jess, 2005).

An ANOVA of the data in Figure 5.10 resulted in the sections having statistically different subgrade moduli (F-statistic = 32.39). However, as was found with the granular base/fill, there were no general trends that could be attributed to design characteristics of

the test sections. Rather, the differences were attributed to spatial variability and it is recommended that section-specific subgrade moduli be used for further analysis.

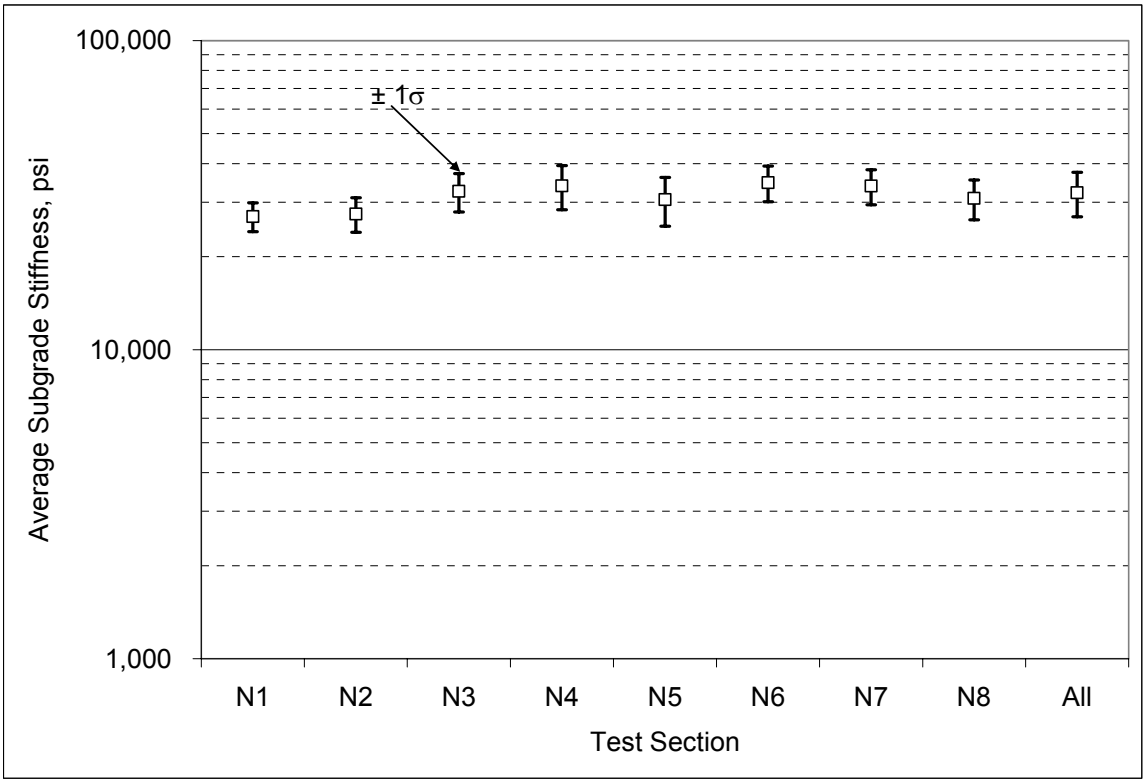

Figure 5.10 Backcalculated Subgrade Modulus – By Section.

Subgrade – Seasonal Characterization

From Figure 5.11, a similar observation was made regarding the subgrade modulus during the warmer times of the year as was made with the granular base/fill material. Namely, there appeared to be a small reduction in stiffness with increased temperature. This can again be attributed to an artifact of the backcalculation program and best mitigated by determining an annual average based upon FWD testing at frequent intervals.

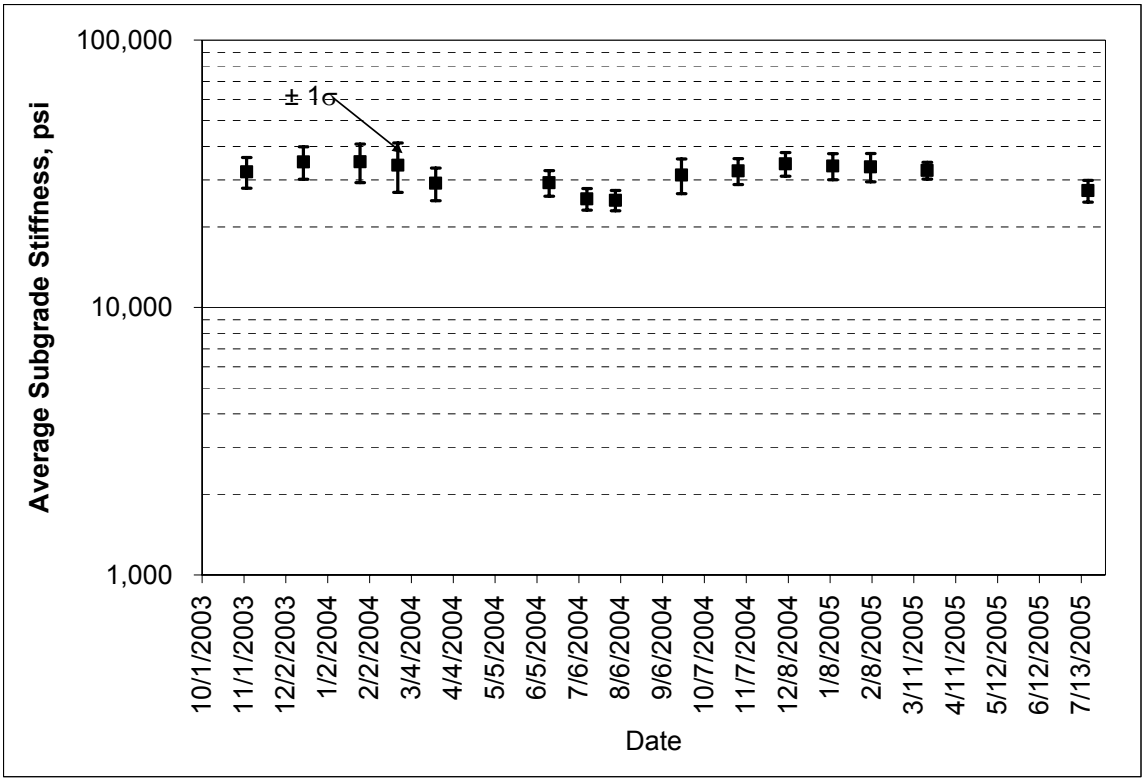

Figure 5.11 Backcalculated Subgrade Modulus – By Date.

Subgrade – Wheelpath Characterization

Again, the outside wheelpath subgrade moduli were higher than the inside wheelpath. Figure 5.12 illustrates the statistical data and an ANOVA clearly demonstrated the statistical differences between the inside and outside wheelpaths (F-statistic = 177.55). As discussed for the granular base/fill layer, the difference between wheelpaths (approximately 4,000 psi) may not have practical significance and would be considered together for general M-E design and analysis. However, it is recommended that wheelpath-specific moduli be used in conjunction with data from the embedded instrumentation in the test sections.

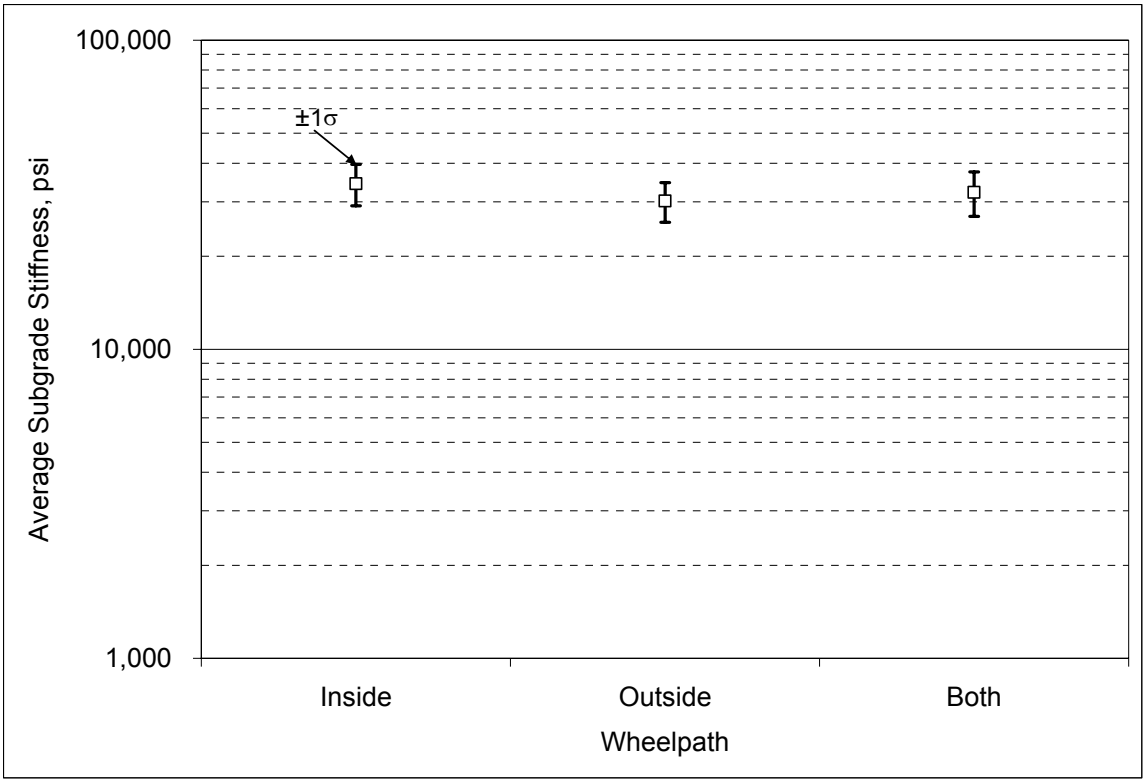

Figure 5.12 Backcalculated Subgrade Modulus – By Wheelpath.

HMA CHARACTERIZATION

Before closely examining the HMA stiffness – temperature relationship, it was decided to look for correlations between the various as-built mixture parameters, temperature and the backcalculated HMA stiffness. The as-built parameters were presented in Chapter 2, while the temperature presented in this discussion represents the interpolated mid-depth temperature at the time of the corresponding FWD test. The mid-depth temperature was calculated using data from the multi-depth thermistor bundle, assuming a linear temperature profile. Table 5.2 shows the correlations between the various parameters from which the following observations were made:

- As expected, temperature was highly negatively correlated to HMA modulus.
- The asphalt binder performance grade and asphalt content had the lowest correlations to the HMA stiffness at lower temperatures. This was not surprising given the laboratory study (Chapter 3) which showed that these parameters were also not significant in determining the dynamic modulus. Also, since the mixes were designed to similar asphalt contents using binders that were different by only one PG grade, one could expect the differences in stiffness to be correspondingly small.
- The asphalt binder performance grade and air voids are strongly positively correlated. This seems to indicate that the binder modification resulted in greater difficulty in compacting the mixture.
- The gradation parameter (percent passing the #4 sieve) showed correlations, as expected, to the other mixture parameters (binder grade, asphalt content and air void content).

Based upon the above observations, it was decided to first establish temperature-stiffness relationships and then more closely examine the effects of the other mixture parameters. Each of these analyses are presented below.

Table 5.2 HMA Correlations.

	Percent Passing #4 Sieve	Performance Grade	Air Voids	Asphalt Content	Mid-Depth HMA Temperature	HMA Stiffness
Percent Passing #4 Sieve	1.000					
Performance Grade	0.369	1.000				
Air Voids	0.226	0.807	1.000			
Asphalt Content	0.176	-0.043	0.320	1.000		
Mid-Depth HMA Temperature	-0.080	-0.027	-0.026	0.027	1.000	
HMA Stiffness	0.129	-0.061	-0.153	0.002	-0.793	1.000

HMA Modulus – Temperature Characterization

The backcalculated HMA moduli were plotted versus mid-depth HMA temperature (T) to establish stiffness-temperature relationships. Figure 5.13 illustrates the raw data best-fit regression lines for all the sections considered together. Further, Figures 5.14 through 5.16 show the data and regression for the data separated into the unmodified, modified and surface SMA sections. Though the SMA sections could have been grouped with the unmodified sections, they were separated for clarity in the graphs. The regression equation had the form:

$$E_{HMA} = k_1 e^{k_2 T} \tag{5.1}$$

and the regression parameters with corresponding R^2 values are listed by test section in Table 5.3. In general, the equations were good predictors of stiffness. The one exception was section N1 ($R^2 = 0.35$) which showed high variability in Figure 5.15. There could be a number of reasons for the higher variability. First, the section could simply have been built with greater variation (i.e., greater variation in asphalt content, density, etc.). Second, the fatigue cracking in N1 was first observed as fully interconnected cracks with pumping on April 8, 2004 (Figure 5.17). Though the cracking cut-off date was March 22, 2004, it could be that cracks not yet visible at the surface were present and contributed to higher moduli variability throughout the test section.

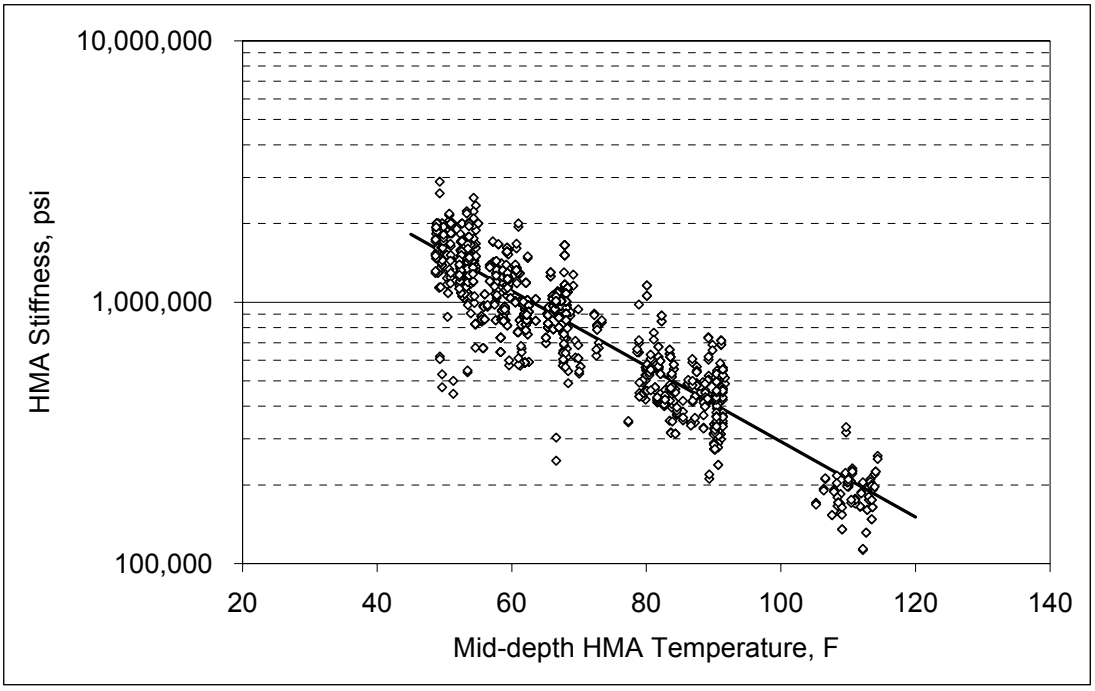

Figure 5.13 Backcalculated HMA Stiffness versus Temperature – All Sections.

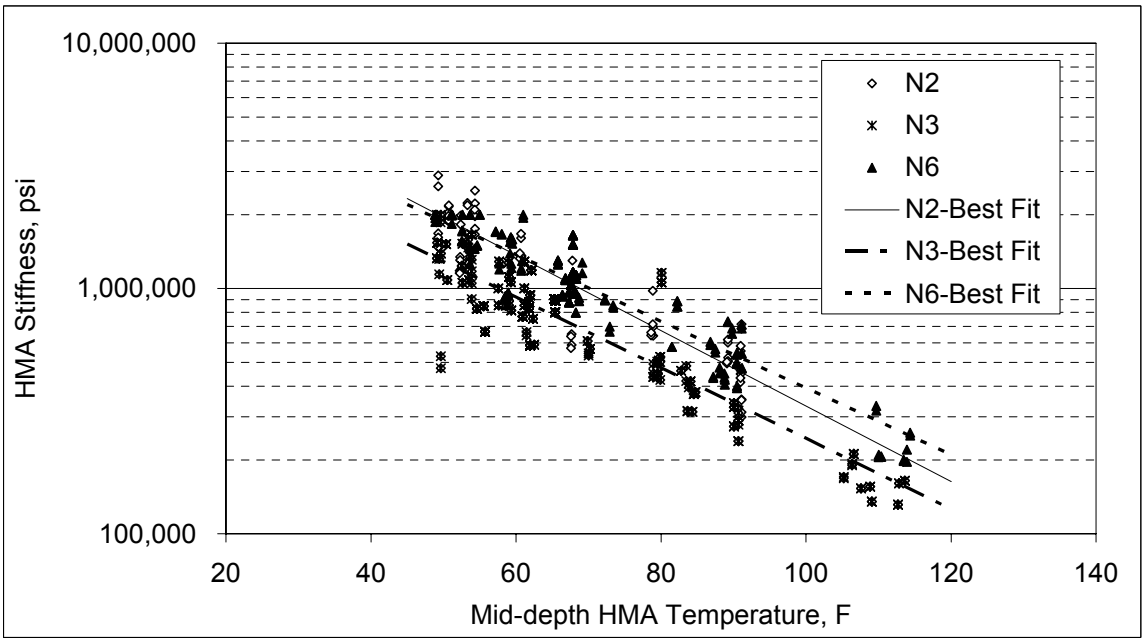

Figure 5.14 Backcalculated HMA Stiffness versus Temperature – Unmodified Sections.

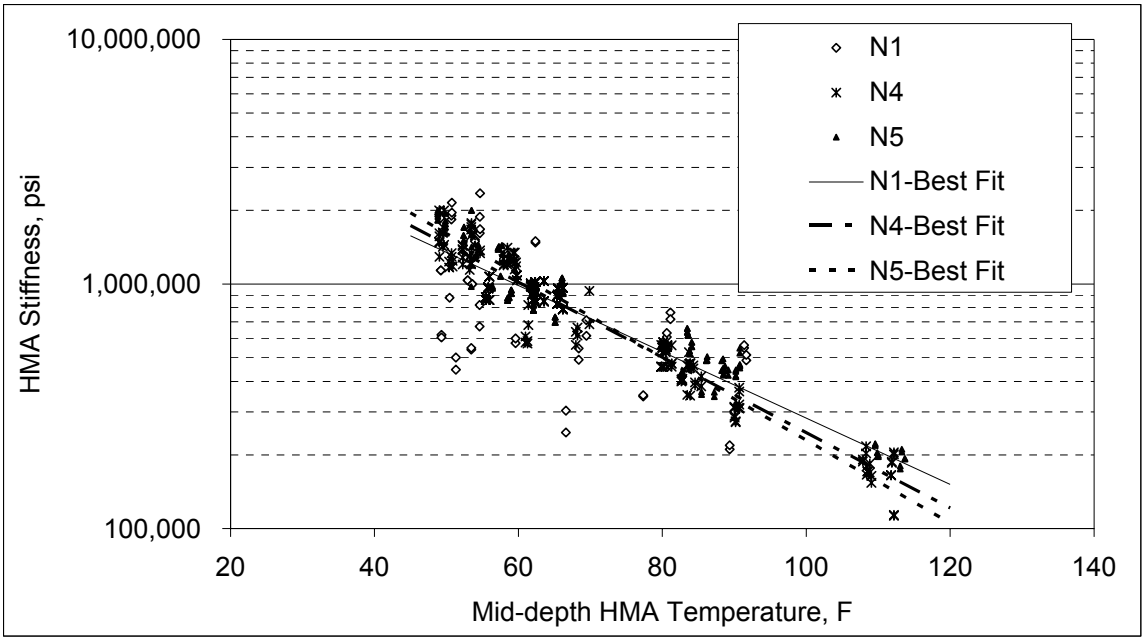

Figure 5.15 Backcalculated HMA Stiffness versus Temperature – Modified Sections.

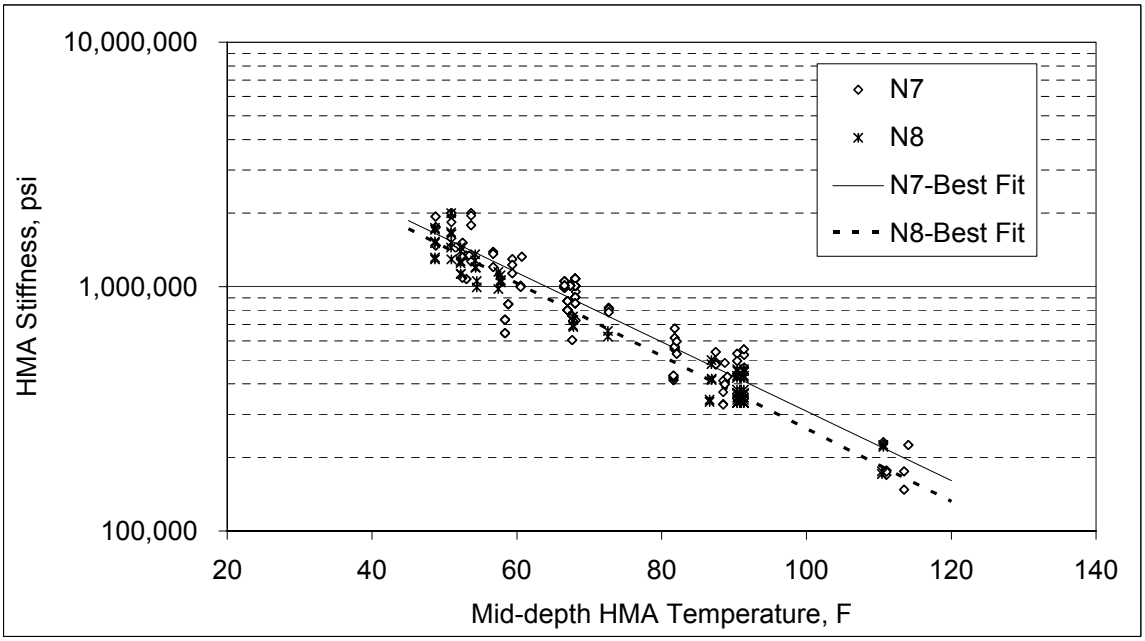

Figure 5.16 Backcalculated HMA Stiffness versus Temperature – SMA Sections.

Figure 5.17 First Observed Fatigue Cracking on Section N1.

Table 5.3 Backcalculated HMA Stiffness – Temperature Regression Parameters

Section	k_1	k_2	R^2
N1	6.427E+06	-0.0312	0.35
N2	1.145E+07	-0.0354	0.81
N3	6.776E+06	-0.0332	0.71
N4	8.561E+06	-0.0355	0.86
N5	1.126E+07	-0.0389	0.86
N6	8.987E+06	-0.0313	0.80
N7	8.088E+06	-0.0326	0.76
N8	8.046E+06	-0.0342	0.94
ALL	8.082E+06	-0.0332	0.68

HMA Mixture Parameter Characterization

To further examine the other parameters listed in Table 5.2, a temperature correction needed to be applied to adjust all the stiffness data to a single reference temperature. The reference temperature was set at 68^{o}F since it was near the middle of the temperature range presented in Figure 5.13 and also is used as the reference temperature in the current AASHTO Design Guide (1993). Correction factors (C) were established as a function of temperature, for each test section, according to:

$$C = \frac{E_T}{E_{68}} = \frac{k_1 e^{k_2 T}}{k_1 e^{k_2 68}} = e^{k_2 (T-68)} \tag{5.2}$$

The corrected stiffness (E_c) could then be computed from the uncorrected stiffness (E) by:

$$E_c = E \cdot C = E \cdot e^{k_2 (T-68)} \tag{5.3}$$

Figure 5.18 shows the effectiveness of the temperature correction scheme considering all the test sections, and Figure 5.19 shows the distribution of temperature-corrected HMA modulus for all the test sections combined. The average was approximately 850,000 psi, and the distribution appeared to be approximately log-normal with a 26% coefficient of variation. It must be noted that this level of variability for HMA stiffness is comparable to those found in other studies (Timm et al., 1999).

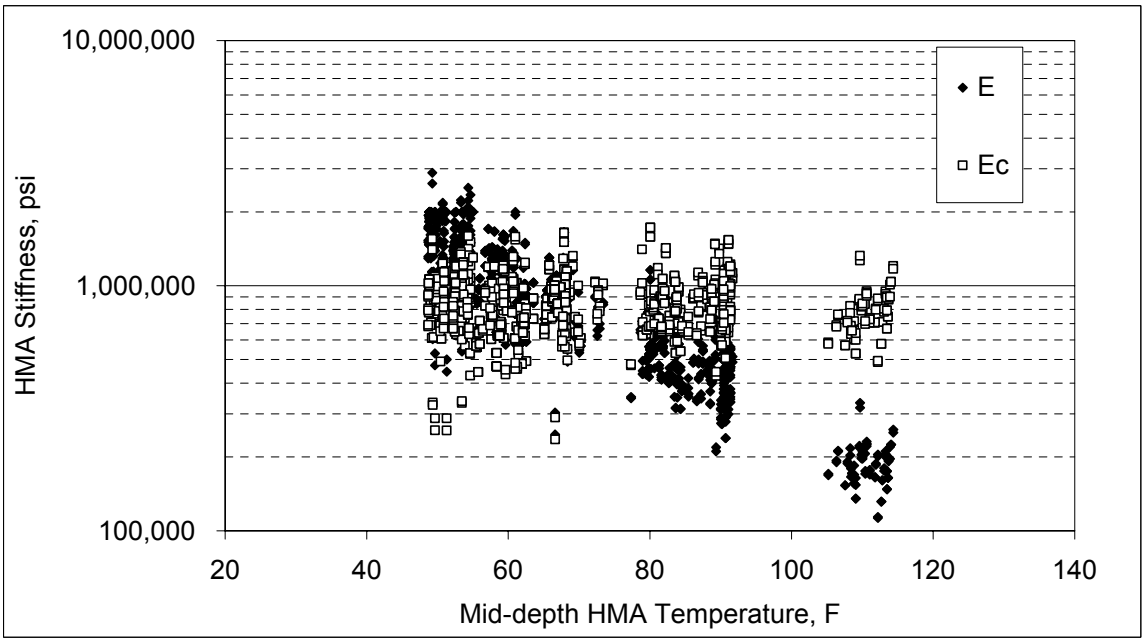

Figure 5.18 Effectiveness of Temperature Correction – All Sections.

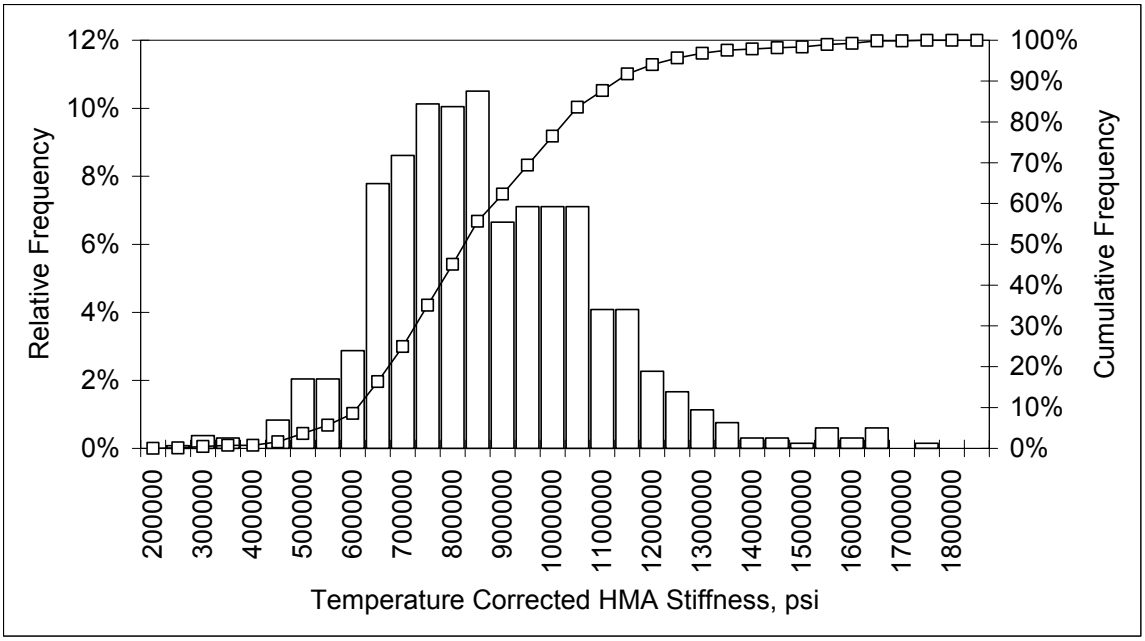

Figure 5.19 Backcalculated HMA Stiffness Variability – All Sections.

Figure 5.20 shows a sectional comparison of corrected HMA moduli, while Table 5.4 lists the values and coefficients of variation by test section. Note that section N1 was much more variable than the other test sections. An ANOVA was conducted on the test sections and the average stiffnesses were found to be statistically different at a 95% confidence level (F-statistic = 82.69). However, a Tukey comparison test, also conducted at the 95% confidence level, did not divide the sections into logical groups (i.e., modified, unmodified, SMA). For example, N1 (modified) was found to not be statistically different from N3 (unmodified), N4 (modified), N5 (modified) and N8 (SMA with rich bottom).

After the temperature effect was removed through the correction scheme, further regression analyses were conducted, similar to that presented in Chapter 3 for the laboratory dynamic moduli, to look for significant effects that could be attributed to asphalt content, air voids, and/or gradation. Figures 5.21 through 5.23 show the influence of these factors, respectively, on HMA stiffness. Only air void content (Figure 5.22) showed a slight effect, but the corresponding low R^2 value does not support a meaningful relationship. These results also correspond to the correlation coefficients listed in Table 5.2. As discussed above, the results are limited to the range of test parameters used in this investigation, which was relatively small. In future studies, larger variations in asphalt content and air voids, for example, may show greater changes in HMA stiffness.

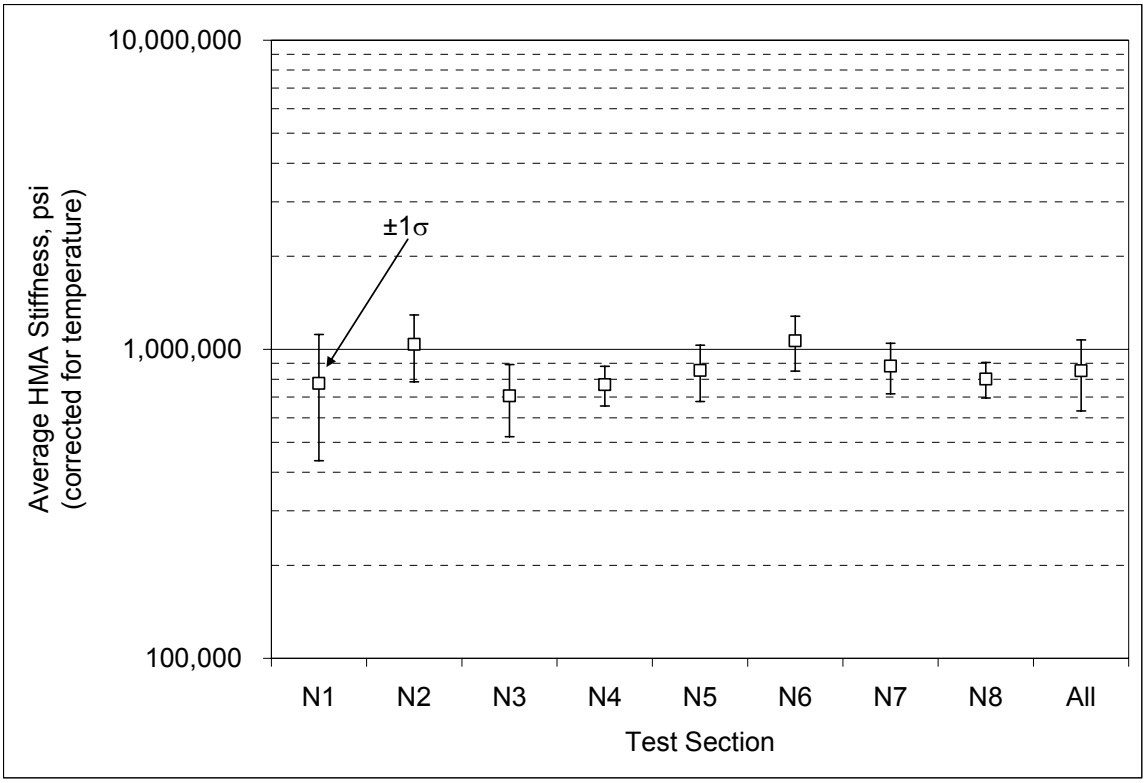

Figure 5.20 Backcalculated HMA Stiffness versus Section – Corrected for Temperature.

Table 5.4 Backcalculated HMA Stiffness versus Section–Corrected for Temperature

Section	Average, psi	Standard Deviation, psi	Coefficient of Variation
N1	776,190	340,185	44%
N2	1,037,764	253,385	24%
N3	707,303	185,870	26%
N4	767,759	112,144	15%
N5	854,371	177,249	21%
N6	1,064,386	214,964	20%
N7	881,303	164,059	19%
N8	800,680	105,294	13%
All	852,033	220,571	26%

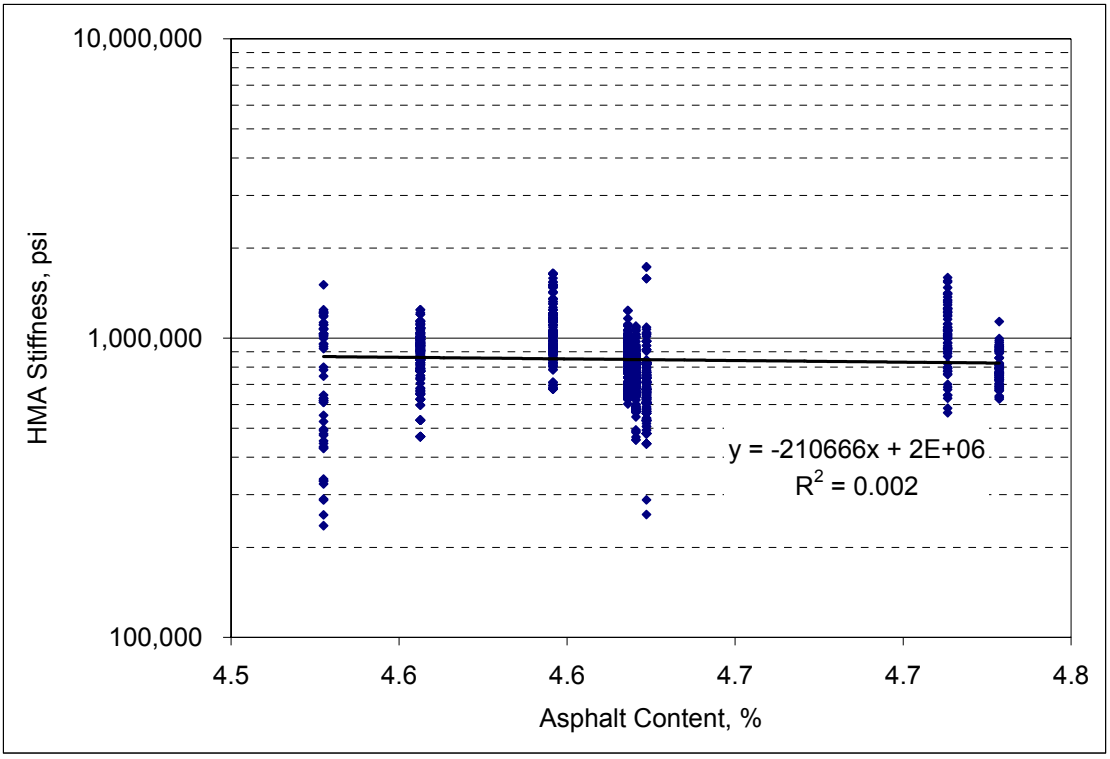

Figure 5.21 Backcalculated HMA Stiffness versus Asphalt Content – Corrected for Temperature.

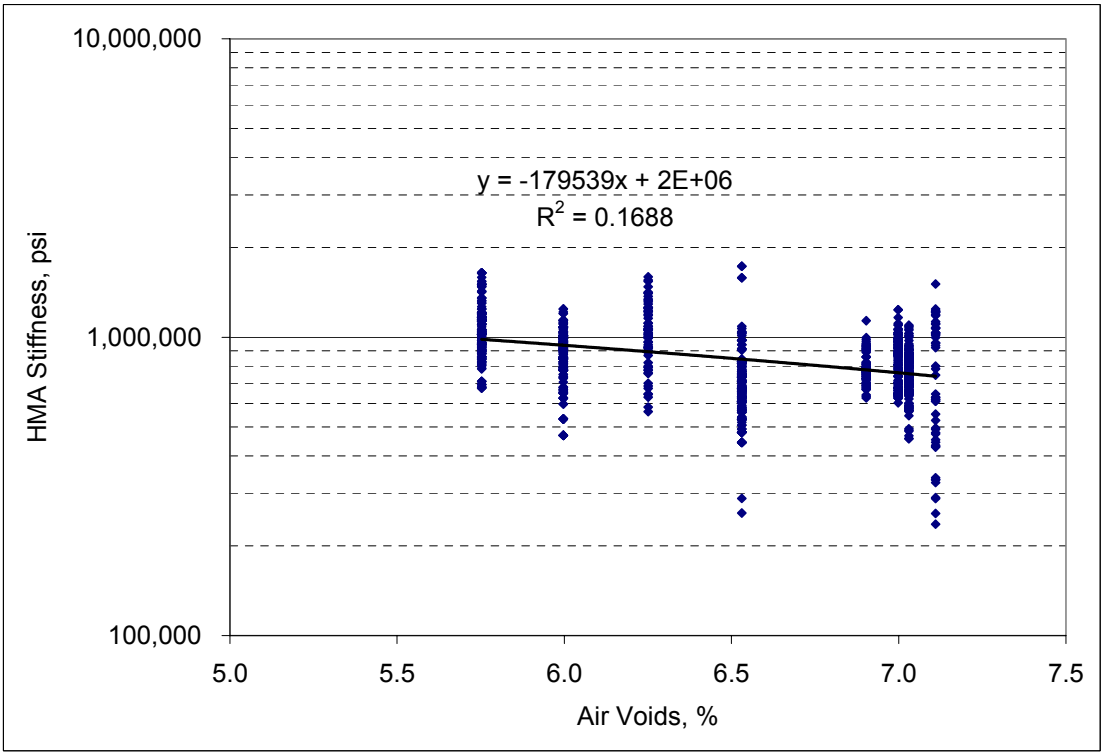

Figure 5.22 Backcalculated HMA Stiffness versus Air Voids – Corrected for Temperature.

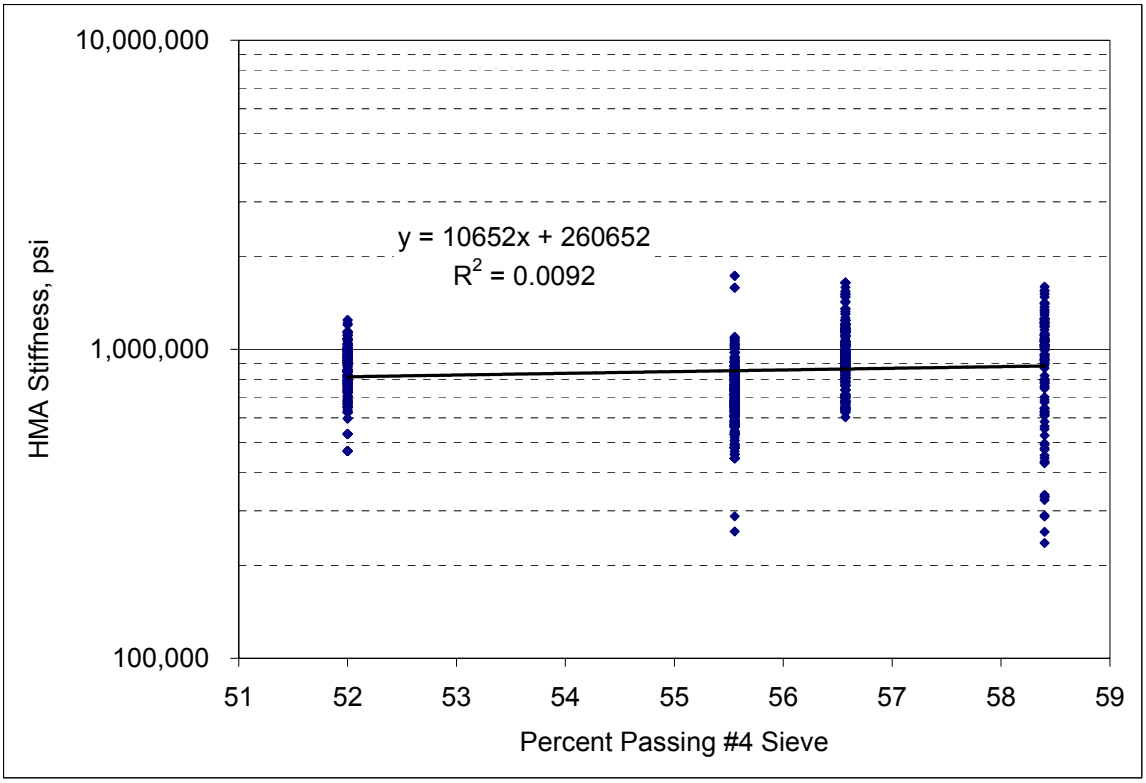

Figure 5.23 Backcalculated HMA Stiffness versus Gradation – Corrected for Temperature.

HMA – Wheelpath Characterization

As with the other pavement layers, the HMA stiffness was also evaluated with respect to wheelpath. Presented in Figure 5.24, the wheelpath was found significant through ANOVA at a 95% confidence level (F-statistic = 60.29). Similar to the granular base/fill and subgrade, the HMA stiffness was also higher in the inside than the outside wheelpath. Again, the issue of practical significance can be raised and for general M-E design and analysis, it makes sense to consider both wheelpaths together. In the context of the embedded instrumentation in the Structural Study, however, wheelpath-specific moduli should be used.

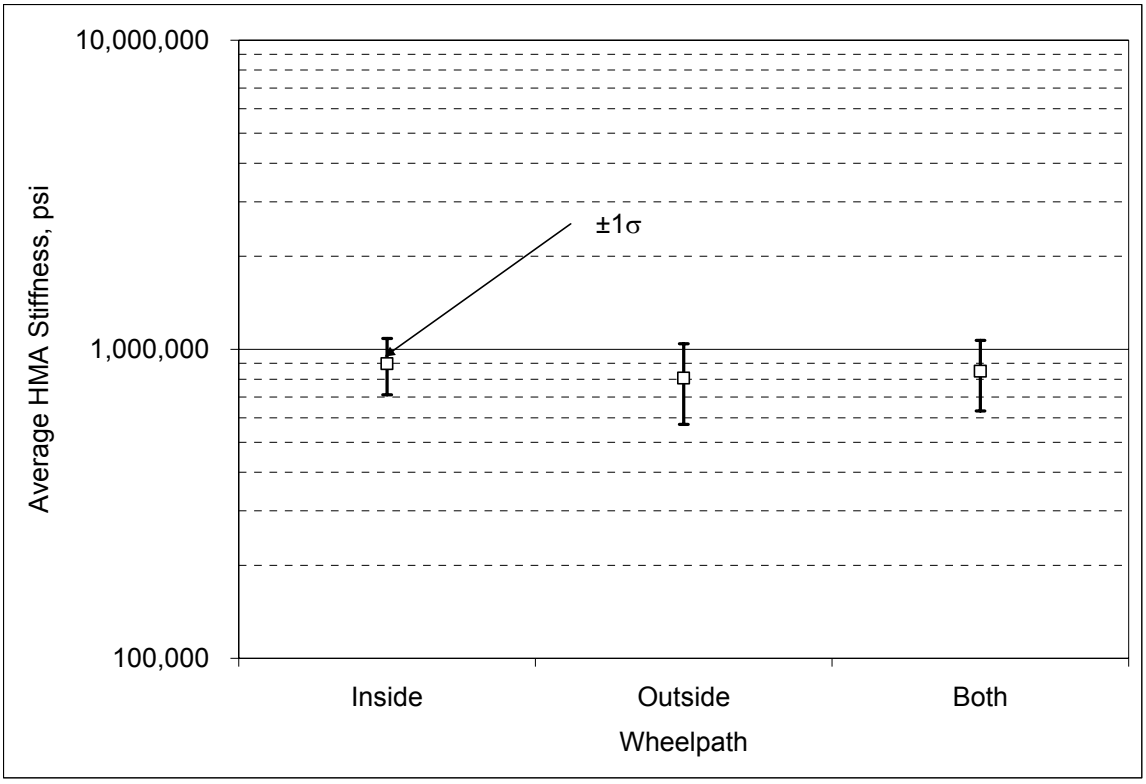

Figure 5.24 Backcalculated HMA Stiffness versus Wheelpath – Corrected for Temperature.

Based upon the results presented above, it is recommended that section and wheelpath specific moduli be used for mechanistic analysis. Also, the stiffness – temperature relationships presented in Table 5.4, can be used to characterize the seasonal changes in each test section. The other parameters were not found to have a meaningful or significant effect on HMA stiffness.

GRANULAR BASE/FILL – LABORATORY AND FIELD COMPARISON

As discussed previously in this report, there were some differences between ALDOT and Vulcan Materials laboratory testing of the granular base material. These were primarily attributed to differences in density and applied stress ranges during testing. Since the densities tested by Vulcan were much closer to the in-place densities, it was decided to compare the Vulcan-determined properties against those obtained from backcalculation.

To perform the comparison, FWD loads were simulated on the various cross sections with WESLEA for Windows and bulk stresses at the midpoint of the granular base/fill layer were computed. Figure 5.25 shows the relevant material properties and initial assumptions used in the simulations. The computed bulk stresses due to the applied load were added to the estimated geostatic bulk stress at the same point to obtain a total bulk stress. The total bulk stress was then used in the Vulcan-determined equation for the granular base material:

$$M_r = 5677.2\theta^{0.4711} \quad (5.4)$$

where:

M_r = resilient modulus of base material, psi

θ = bulk stress applied to material, psi

The resulting M_r, corresponding to the computed bulk stress, was re-entered into WESLEA to compute a new bulk stress. Iteration continued until M_r converged. Tables 5.5, 5.6 and 5.7 summarize the results. As a specific example, consider the data in Table 5.5 for the 5" section. The cross section, depicted in Figure 5.25, was simulated in WESLEA with a trial base/fill stiffness of 30,000 psi. The resulting bulk stress, which also included the geostatic stresses, was 10.28 psi. Equation 5.4 was then used to compute the resilient modulus, 17,020 psi, predicted by the Vulcan laboratory testing. This new value was used for the base/fill stiffness in the second iteration to obtain a new bulk stress and corresponding modulus. This procedure continued until convergence at 17,136 psi.

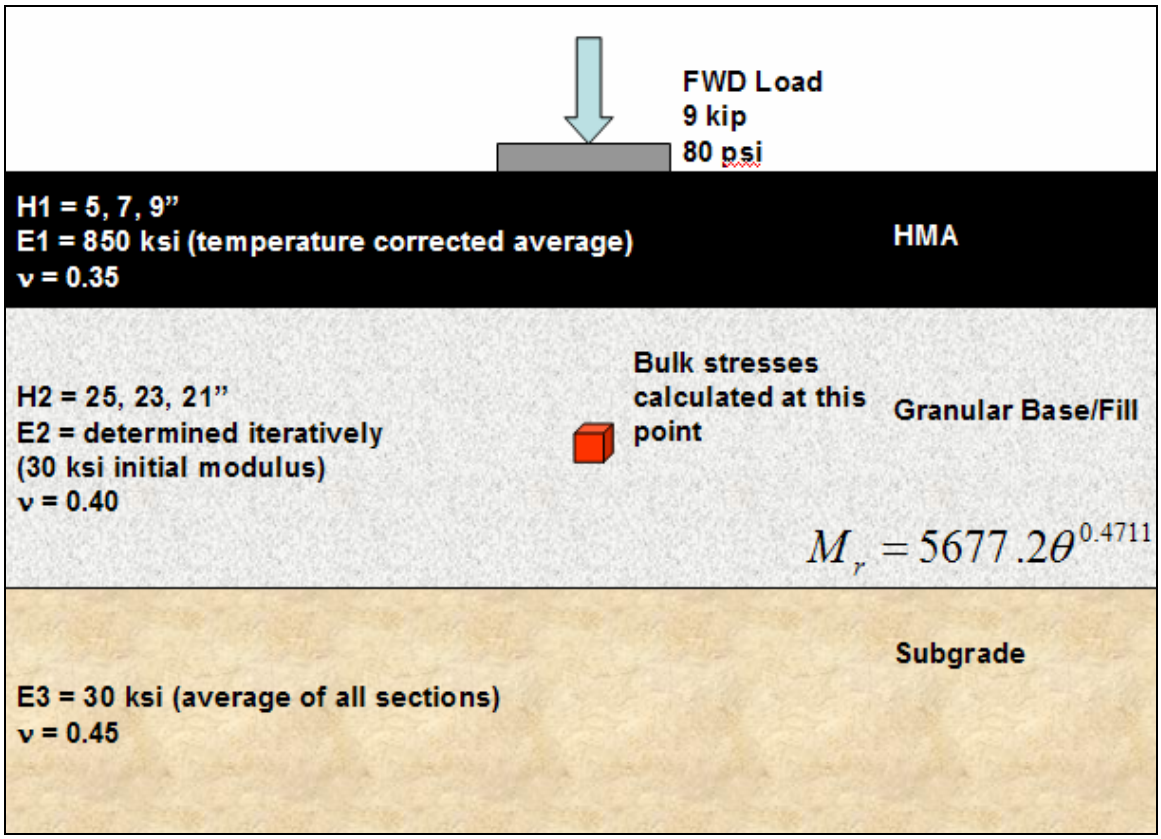

Figure 5.25 WESLEA Simulation of FWD Loading on Structural Sections.

Table 5.5 5" Section Simulation

Iteration	M_r Entered into WESLEA, psi	WESLEA-Computed Bulk Stress, psi	Computed M_r, psi
1	30,000	10.28	17,020
2	17,020	10.42	17,128
3	17,128	10.43	17,136
4	17,136	10.43	17,136

Table 5.6 7" Section Simulation

Iteration	M_r Entered into WESLEA, psi	WESLEA-Computed Bulk Stress, psi	Computed M_r, psi
1	30,000	8.68	15,714
2	15,714	8.84	15,849
3	15,849	8.83	15,841
4	15,841	8.85	15,858

Table 5.7 9" Section Simulation

Iteration	M_r Entered into WESLEA, psi	WESLEA-Computed Bulk Stress, psi	Computed M_r, psi
1	30,000	7.66	14,812
2	14,812	7.86	14,993
3	14,993	7.87	15,002
4	15,002	7.87	15,002

The average base/fill stiffness obtained from Tables 5.5-5.7 was superimposed on a distribution of backcalculated moduli obtained from the Test Track as shown in Figure 5.26. The laboratory-determined modulus is approximately the 90^{th}-percentile of the field-determined values. Given the inherant variability of construction, testing and natural variability of the material itself, the comparison demonstrates reasonable agreement between the two sets of data.

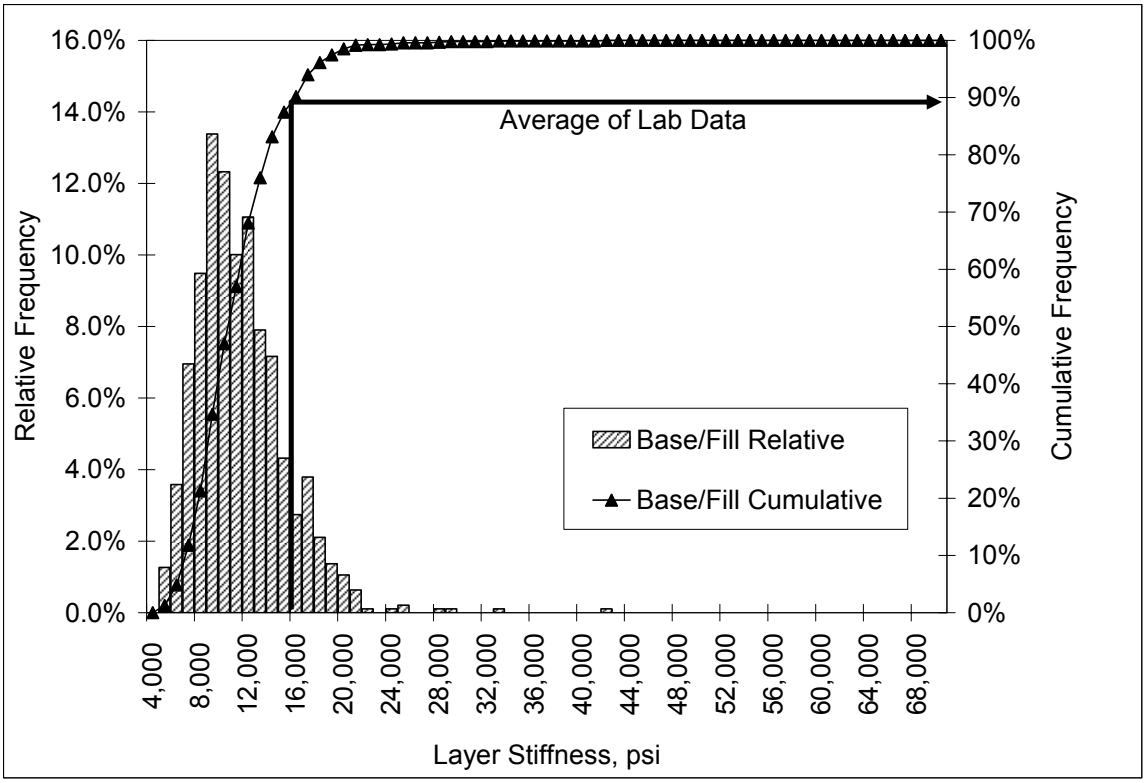

Figure 5.26 Comparison of Laboratory and Field-Determined Base/Fill Moduli.

SUMMARY

This chapter examined the backcalculated stiffnesses determined from FWD testing of the structural test sections. Seasonal trends, due to temperature changes, were most evident in the HMA layers. Slight changes in the granular base/fill and subgrade moduli were attributed to artifacts of backcalculation and it was recommended that seasonal data be averaged to account for these changes. Cracking had a significant impact on the backcalculated stiffnesses and dates with cracking were removed from the analysis.

The analysis of the unbound layers (granular base/fill and subgrade) found that the individual test sections were statistically different and was attributed to spatial variability. Further, the moduli determined from the inside wheelpath were statistically higher than the outside wheelpath and may have contributed to more rapid pavement deterioration in the outside wheelpath. The range of granular base/fill moduli were comparable to those determined in the laboratory by Vulcan Materials. No direct comparisons between lab and field-determined moduli of the existing subgrade could be made since the material was not tested in the laboratory. However, the backcalculated moduli were comparable to those obtained during the 2000 Test Track research cycle.

As expected, temperature was the overriding factor in the determination of the HMA stiffness. Again, spatial variability was important with the sections statistically different. However, other section-specific factors such as air voids, binder grade, gradation and asphalt content were not found to be highly significant, due mostly to their limited range in this study. The wheelpath was again a factor and it was recommended that section and

wheelpath-specific moduli be used for analysis in conjunction with the embedded instrumentation. For general M-E design and analysis, averaging the two wheelpaths is reasonable.

CHAPTER 6 – CONCLUSIONS AND RECOMMENDATIONS

The primary objective of this report was to document the properties of the materials used in the 2003 NCAT Test Track Structural Experiment. While emphasis was placed on characterizing the stiffness, in both the laboratory and field, other properties such as gradation, binder content and as-built densities were also presented. Based upon the results presented in this report, the following conclusions and recommendations can be made:

1. The resilient modulus, determined in the laboratory by ALDOT, was higher for the fill material than the granular base material under similar test conditions. Further testing provided by Vulcan Materials, at higher (and more realistic) density and over a wider range of applied stresses showed the fill material and base material to be comparable in terms of stiffness. It must be further understood that the fill material at the Test Track is considered extremely high quality for a material of its type rather than to assert that the granular base material is of poor quality. Further study of these materials is certainly warranted.
2. Laboratory dynamic modulus testing of the individual asphalt mixtures showed no statistical differences up to 70^{o}F. Above 100^{o}F, the differences in stiffness were primarily a function of gradation and air voids rather than binder grade. Further studies could be done using a wider range of binder grades, or alternative asphalt modifiers, to evaluate the extent of this observation.
3. Given the materials and structural cross sections used in this study, the best cross-section for backcalculation consisted of the HMA over the granular base/fill combined into a single layer over the existing subgrade. This cross-section is logical given the similarity of laboratory-determined moduli for the granular base and fill materials.
4. Layered elastic analysis is a reasonable approximation of actual pavement responses under load. Results from layered elastic back and forward-calculation compared well with measured pavement responses obtained under FWD loading. The greatest deviation between measured and predicted pavement responses occurred with vertical pressures above 8 psi. Further studies are warranted to examine the non-linearity of the materials and also make comparisons between responses under truck loads and predicted responses.
5. As expected, seasonal trends in pavement layer moduli were most evident in the HMA layer as a result of changes in temperature. The effects of cracking on moduli were also most evident in the HMA layer.
6. Sectional differences in the moduli of the granular base/fill and subgrade were found to be statistically significant. The stiffnesses were also statistically higher in the inside wheelpath compared to the outside wheelpath. It was recommended that section and wheelpath-specific moduli be used for analysis when considering the embedded instrumentation. Also, lower stiffnesses in the outside wheelpath correspond to higher distresses when compared to the inside wheelpath. While the stiffnesses were statistically different, it also must be noted that the level of variability observed amongst the test sections and wheelpaths was not uncommonly high.

7. The backcalculated HMA moduli confirmed the result of dynamic modulus testing in the laboratory where binder grade was not found to be significant to the HMA stiffness. Further studies could be done using more diverse materials to examine the effects of binder grade or modification on stiffness.
8. Sectional and wheelpath differences existed in terms of HMA stiffness. It was recommended that section and wheelpath-specific moduli be used for analysis in conjunction with embedded instrumentation and stiffness-temperature models were developed for each test section. It must also be noted that the observed variability, though resulting in statistical differences between test sections, was comparable to other studies and was not uncommonly high.
9. Comparisons were made between the Vulcan-determined base modulus and those obtained via backcalculation. The two data sets compared favorably and it is important to note that the base/fill average stiffness of approximately 11,000 psi corresponds to a bulk stress of approximately 10 psi in situ.

REFERENCES

1. --, "Thickness Design, Asphalt Pavements for Highways and Streets," MS-1, The Asphalt Institute, February 1991.
2. Al-Sugair, Faisal H. and Jamal A. Almudaiheem, "Variations in Measured Resilient Modulus of Asphalt Mixes," Journal of Materials in Civil Engineering, Vol. 4 No. 4, November 1992, pp. 343-352.
3. American Association of State Highway and Transportation Officials. *AASHTO Guide for Design of Pavement Structures*. Washington, D.C., 1993.
4. Barrett, W.E. and D.H. Timm, "Theoretical vs Measured Pavement Responses Under Dynamic Loading," 7th International Conference on the Bearing Capacity of Roads, Railways and Airfields, Trondheim, Norway, 2005.
5. Brown, E. R. and K. Y. Foo, "Evaluation of Variability in Resilient Modulus Test Results (ASTM D4123)", Journal of Testing and Evaluation, JTEVA, Vol. 19, No. 1, Jan. 1991, pp. 1-13.
6. Cedergren, H.R., J.A. Arman and K.H. O'Brien, "Guidelines for the Design of Subsurface Drainage Systems for Highway Pavement Structural Sections," Report No. FHWA-RD-72-30, Federal Highway Administration, 1972.
7. Chadbourn, B. A., Newcomb, D. E. and Timm, D. H., "Measured and Theoretical Comparisons of Traffic Loads and Pavement Response Distributions", Proceedings, Eighth International Conference on Asphalt Pavements, Seattle, WA, 1997, pp. 229-238.
8. Eres Consultants Division, "Guide For Mechanistic-Empirical Pavement Design of New and Rehabilitated Pavement Structures," Final Report, NCHRP 1-37A, 2004.
9. Highway Research Board, "The AASHO Road Test", Report 5, Pavement Research Special Report 61E, National Academy of Sciences – National Research Council, Washington, DC, 1962.
10. Miner, Milton A., "Estimation of Fatigue Life with Particular Emphasis on Cumulative Damage," Metal Fatigue, edited by Sines and Waisman, McGraw Hill, 1959, pp. 278-289.
11. Moulton, L.K., "Highway Subdrainage Design," Report No. FHWA-TS-80-224, Federal Highway Administration, 1980.
12. Powell, R. Buzz, "As-Built Properties of Experimental Sections on the 2003 NCAT Pavement Test Track," National Center for Asphalt Technology, 2004.
13. Theyse, H L., De Beer, M. and Rust, F. C., "Overview of South African Mechanistic Pavement Design Method," Transportation Research Record, No. 1539, Transportation Research Board, 1996, pp. 6 – 17.
14. Thompson, M., et al., "Calibrated Mechanistic Structural Analysis Procedures for Pavement," NCHRP Report 1-26, National Research Council, 1992.
15. Timm, D.H., Birgisson, B. and Newcomb, D. E., "Development of Mechanistic-Empirical Pavement Design in Minnesota," Transportation Research Record, No. 1629, Transportation Research Board, 1998, pp. 181-188.
16. Timm, D.H. and J.C. Jess, "Structural Coefficients for New Asphalt Mixtures," Alabama Department of Transportation, Montgomery, AL 2005 (in press).

17. Timm, D.H., D.E. Newcomb and B. Birgisson, "Mechanistic-Empirical Flexible Pavement Thickness Design: The Minnesota Method," Staff Paper, MN/RC-P99-10, Minnesota Department of Transportation, St. Paul, MN, 1999.
18. Timm, D.H., Priest, A.L. and McEwen, T.V., "Design and Instrumentation of the Structural Pavement Experiment at the NCAT Test Track," NCAT 04-01, National Center for Asphalt Technology, 2004.
19. Timm, D.H. and J. Young, "The Effects of Load Spectra and Variability on Perpetual Pavement Design," International Symposium on Design & Construction of Long Lasting Asphalt Pavements, International Society for Asphalt Pavements, Auburn, AL, 2004, pp. 131 – 152.
20. Van Cauwelaert, F.J., Alexander, D.R., White, T.D., and Barker, W.R., "Multilayer Elastic Program for Backcalculating Layer Moduli in Pavement Evaluation," Nondestructive Testing of Pavements and Backcalculation of Moduli, ASTM STP 1026, A.J. Bush III and G.Y. Baladi, Eds., American Society for Testing and Materials, Philadelphia, 1989, pp. 171-188.